EEG Characterization of Sensorimotor Networks: Implications in Stroke

Dylan Blake Snyder
Marquette University

EEG CHARACTERIZATION OF SENSORIMOTOR NETWORKS: IMPLICATIONS IN STROKE

By

Dylan B. Snyder, B.S.

A Dissertation submitted to the Faculty of the Graduate School,
Marquette University,
in Partial Fulfillment of the Requirements for
the Degree of Doctor of Philosophy

Milwaukee, Wisconsin

May 2020

ABSTRACT
EEG CHARACTERIZATION OF SENSORIMOTOR NETWORKS:
IMPLICATIONS IN STROKE

Dylan B. Snyder, B.S.

Marquette University, 2020

The purpose of this dissertation was to use electroencephalography (EEG) to characterize sensorimotor networks and examine the effects of stroke on sensorimotor networks. Sensorimotor networks play an essential role in completion of everyday tasks, and when damaged, as in stroke survivors, the successful completion of seemingly simple motor tasks becomes fantasy. When sensorimotor networks are impaired as a result of stroke, varying degrees of sensorimotor deficits emerge, most often including loss of sensation and difficulty generating upper extremity movements. Although sensory therapies, such as the application of tendon vibration, have been shown to reduce the sensorimotor deficits after stroke, the underlying sensorimotor mechanisms associated with such improvements are unknown. While sensorimotor networks have been studied extensively, unanswered questions still surround their role in basic control paradigms and how their role changes after stroke. EEG provides a way to probe the high-speed temporal dynamics of sensorimotor networks that other more common imaging modalities lack. Sensorimotor network function was examined in controls during a task designed to differentiate potential mechanisms of arm stabilization and determine to what degree the sensorimotor network is involved. After sensorimotor network function was characterized in controls, we examined the effect of stroke on the sensorimotor network during rest and described the reorganization that occurs. Lastly, we explored tendon vibration as a sensory therapy for stroke survivors and determined if sensorimotor network mechanisms underlie improvements in arm tracking performance due to wrist tendon vibration. We observed cortical activity and connectivity that suggests sensorimotor networks are involved in the control of arm stability, cortical networks reorganize to more asymmetric, local networks after stroke, and tendon vibration normalizes sensorimotor network activity and connectivity during motor control after stroke. This dissertation was among the first studies using EEG to characterize the high-speed temporal dynamics of sensorimotor networks following stroke. This new knowledge has led to a better understanding of how sensorimotor networks function under ordinary circumstances as well as extreme situations such as stroke and revealed previously unknown mechanisms by which tendon vibration improves motor control in stroke survivors, which will lead to better therapeutic approaches.

ACKNOWLEDGEMENTS

Dylan B. Snyder, B.S.

I would like to thank my dissertation advisors Dr. Brian Schmit and Dr. Scott Beardsley for their support, guidance and especially their ability to refocus my ideas when I inevitably wandered too far into the weeds of research.

Thank you to all my colleagues in the Integrative Neural Engineering and Rehabilitation Laboratory, the Integrative Neural Systems Laboratory and the biomedical engineering department at Marquette University. Dr. Allison Hyngstrom for performing the clinical assessments on each of my participants. Dr. Ryan McKindles and Dr. Joseph Lee for helping me traverse the complexities of EEG analyses as well as countless EEG preparations. My office mates, Dr. Alice Motovylyak, Miguel Sotelo and Wesley Richerson, for spit-balling ideas. Mrs. Wesley for her unwavering assistance with my numerous research requests.

I would also like to thank all the volunteers that sat through my long and sometimes sleep-inducing test sessions and experiments.

Lastly, I would like to thank my friends and family who provided love and support throughout my tenure as a graduate student. Especially, my fiancée, Danielle Bade, who piloted far too many of my experiments, although not without a few grumbles uttered. My parents, Dr. Larry Snyder Jr. and Renata Snyder, and my brother, Dalton Snyder, for supplying me with motivation with their persistent questions of “When are you graduating?”.

TABLE OF CONTENTS

LIST OF TABLES

LIST OF FIGURES

CHAPTER 1: INTRODUCTION AND BACKGROUND

1.1 Introduction

Sensorimotor networks play an essential role in completion of everyday tasks from reluctantly walking to work Monday morning to opening your favorite beverage Friday evening. Hidden beneath these often-unappreciated abilities is a complex system consisting of a primary controller, the brain's sensorimotor networks, which processes sensory information and generates motor plans, muscle actuators that set the plans into motion, sensory feedback elements that supply the sensorimotor networks with information about task execution, and neuronal tracts that act as communication pathways between components. If any one of these subsystems becomes corrupted, the successful completion of seemingly simple motor tasks becomes fantasy.

While sensorimotor networks have been studied extensively, unanswered questions still exist, such as, what is the sensorimotor network's role in basic control paradigms (e.g. upper extremity stabilization) and how are sensorimotor networks altered after an insult (e.g. stroke). When sensorimotor networks are impaired due to stroke, varying degrees of sensorimotor deficits emerge, most often including loss of sensation and difficulty generating upper extremity movements. Although sensory therapies, such as the application of tendon vibration, have been shown to reduce sensorimotor deficits after stroke, the underlying cortical mechanisms associated with such improvements are unknown (Conrad et al., 2011a, 2011b, 2015). The purpose of this dissertation was to characterize sensorimotor networks and examine the implications of stroke on sensorimotor networks; this knowledge will lead to an improved understanding of how

sensorimotor networks function and potentially open the door to improvements in stroke rehabilitation strategies.

We examined the activity and connectivity of sensorimotor networks in controls and stroke survivors using electroencephalography (EEG). First, we sought to understand how healthy sensorimotor networks function. To accomplish this, we examined sensorimotor networks in controls during upper extremity tasks designed to determine what degree the sensorimotor network is involved in arm stabilization. After normal sensorimotor network function was characterized in controls, we wanted to describe the effect that stroke has on sensorimotor networks in the most basic of states, rest (i.e. baseline). Once we had described the baseline cortical changes and reorganization that occurs to stroke sensorimotor networks during rest, we examined stroke survivors' sensorimotor networks during active states of control (i.e. tasks). During the tasks, we explored tendon vibration as a sensory therapy for stroke survivors and determined if sensorimotor network mechanisms underlie improvements in arm tracking performance seen in chronic stroke survivors due to wrist tendon vibration. This chapter provides an overview of sensorimotor networks in the brain, how they are believed to control upper extremity movements, how sensorimotor networks are disrupted and the effects of this disruption after a stroke, and current techniques used to examine sensorimotor networks.

1.2 Cortical Networks

1.2.1 Origins of Cortical Networks

Cortical networks are regions of the brain that pass information to and from each other to achieve an objective. The roles of cortical regions and how cortical regions

interact to achieve the cortical network's objective is a complicated question. In early experimental stimulation work investigating the location of sensation and motor function in the cerebral cortex, sensory and motor homunculi were defined (Jasper & Penfield, 1949; Penfield & Boldrey, 1937; Schott, 1993). The homunculi mapped the sensory and motor cortices to certain regions of the body with the medial portion near the longitudinal fissure representing the lower limbs, lateral portion near the temporal lobe representing facial features and the central regions representing the upper limbs (Jasper & Penfield, 1949; Penfield & Boldrey, 1937; Schott, 1993). Although this rough sensorimotor map of homunculi can be used as a general guideline for sensory and motor location in the sensorimotor cortices, more recent functional Magnetic Resonance Imaging (fMRI) research has revealed there exists no clear boundary between regions with activation patterns, suggesting a more distributed, overlapping representation than previously thought (Indovina & Sanes, 2001; Lotze et al., 2000; Schieber, 2001). As science and technology have advanced, it is becoming increasingly evident that the brain does not relegate tasks to individual cortical regions but instead uses a multitude of interacting cortical regions or cortical networks (Ashe & Georgopoulos, 1994; Bressler, 1995; Colebatch et al., 1991; Connolly et al., 2003; Corbetta, 1998; Demandt et al., 2012; Fortier et al., 1989; Mazoyer et al., 2001; Pfurtscheller & Lopes da Silva, 1999; Sukerkar, 2010).

Typically, cortical networks are defined as being either structurally connected, using methods such as diffusion tensor imaging to identify anatomical connections, or functionally connected, using imaging modalities such as functional magnetic resonance imaging (fMRI), electroencephalography (EEG) or magnetoencephalography (MEG) to

identify areas of the cortex that have similar activation time courses indicative of increased connectivity between regions (Berman et al., 2012; Cheng et al., 2012; Karamzadeh et al., 2013; O'Neill et al., 2017; Sun et al., 2004). While structural and functional connectivity define connectivity differently, they are intrinsically linked. Anatomical connections identified with structural connectivity lay out the foundational pathways that cortical regions use to communicate, ultimately resulting in similar activation patterns detected with functional connectivity techniques (Huang & Ding, 2016; Straathof et al., 2019). Investigations into structural cortical networks have identified areas of the brain (e.g. paracentral, posterior cingulate, precuneus and superior parietal gyri) that constitute a central core in the brain's structural pathways (Hagmann et al., 2008). The brain's central core consists of regions are that are densely connected locally and link modular regions of the cortex (Hagmann et al., 2008). Functional cortical network research has revealed that the brain utilizes varying cortical networks for different tasks such as memory consolidation, cognition, vision, and movement (Bressler, 1995; Corbetta, 1998; Mazoyer et al., 2001; Sukerkar, 2010).

1.2.2 Resting State Cortical Networks

Cortical networks are not limited to states of active cortical processing. Resting state networks are regions of the brain that are connected while the participant is at rest or in a relaxed state. It may seem counterintuitive to find any networks at all while at rest, but the brain is in fact constantly active. Using fMRI, Biswal and colleagues were the first to report the sensorimotor network in the absence of a task (Biswal et al., 1995). Following this groundbreaking study, research into resting state networks intensified with

the most commonly observed resting state network being the default mode network. The default mode network consists of nodes residing in the medial prefrontal gyrus, anterior cingulate, posterior cingulate and angular gyri and is thought to be associated with emotional processing, self-reference and remembering previous experiences (Damoiseaux et al., 2006; Muldoon et al., 2016; Raichle et al., 2001; Raichle, 2015). Other commonly reported resting state networks include the executive control network, mesial visual network, lateralized fronto-parietal networks, auditory networks, and temporo-parietal network (Aoki et al., 2015; Biswal et al., 1995; Brookes et al., 2011; Raichle, 2015; Rosazza & Minati, 2011). Historically, resting state network analysis has mainly been restricted to fMRI studies, with only a limited amount of research performed on resting state network analysis in other imaging modalities. Investigations using EEG and MEG have revealed resting state networks corresponding spatially to their fMRI counterparts, although the precise relationship between fMRI and EEG/MEG measures of brain activity is unknown (Barry et al., 2007; Brookes et al., 2011; Chen et al., 2008; Hipp et al., 2012; Qin et al., 2010).

1.2.3 Properties of Cortical Networks

Cortical network frequency characteristics as measured by EEG and MEG are determined by the size of the neuronal population within the network and the spatial extent of the network. Cortical networks containing a larger neuronal population or spatial extent oscillate at lower frequencies than networks with a smaller neuronal population or spatial extent (Bullock et al., 1995; Buzsáki & Draguhn, 2004; Eckhorn, 1994; Kopell et al., 2000; von Stein & Sarnthein, 2000). Nunez developed a theoretical

framework for the inverse relationship between frequency of activity and spatial scale of a network (Nunez, 2000). When examining the effect of spatial scale on cortical network frequency using EEG, von Stein and Sarnthein (2000) showed that local visual sensory integration (visual cortex) involves gamma (>30Hz) band activity, mid-range multimodal semantic integration (parietal and temporal cortex) involves upper alpha (8-12Hz) and lower beta (12-30Hz) band activity, while long rang interactions in a working memory paradigm (prefrontal and posterior association cortex) involves theta (4-8Hz) and alpha (8-12Hz) band activity (von Stein & Sarnthein, 2000). These cortical network frequency responses arise from the physical architecture of the networks, speed of communication due to axon conduction/synaptic delays and the number of synapses involved in the network path (Nunez, 1995; von Stein et al., 2000).

In addition to the frequency specific characteristics associated with cortical network architecture, analysis of cortical networks using graph theory metrics involving the network's clustering coefficient and path length between nodes has revealed that cortical networks tend to aggregate into structures known as small world topologies (Bassett & Bullmore, 2017; Bassett & Bullmore, 2006; Wang et al., 2010). Small world topologies are described as having a high degree of clustering or connections between neighboring nodes with few connections between distant nodes. On average, small world topologies have shorter path lengths between any two nodes of the network when compared to random network topologies, resulting in more efficient communication (Bassett & Bullmore, 2017; Bassett & Bullmore, 2006; Wang et al., 2010). The cortex might organize into these small world topologies due to the brain supporting both segregated (local) as well as distributed (long range) processing.

1.3 Cortical Control of the Arm

1.3.1 Cortical Control of Arm Movements

The cortical network primarily associated with the generation of movement, including movements of the arm, is the sensorimotor network and is comprised of regions located on the precentral and post central gyri. While the sensorimotor network is responsible for the generation of movement commands sent to the arm, it does not act alone to control arm movements. The brain is a dynamic system continuously sending commands to muscles and receiving sensory input. Information received about the state of the arm and environmental conditions from proprioceptive and visual receptors enable the sensorimotor control system to react and adapt to changing environments (Scheidt & Ghez, 2007; Scheidt & Stoeckmann, 2007). When either sensory modality is removed, an increase in the error of arm control is observed (Gordon et al., 1995). A complete model of cortical control of arm movements would not be complete without including brain areas associated with receiving, processing, and integrating feedback including the frontal cortex, somatosensory cortex, parietal cortex, occipital cortex, and cerebellum. Interactions between the sensorimotor cortex and these secondary regions play a central role in planning movements, completing movements, processing movement feedback, and movement error correction (Ashe & Georgopoulos, 1994; Colebatch et al., 1991; Connolly et al., 2003; Demandt et al., 2012; Fortier et al., 1989; Pfurtscheller & Lopes da Silva, 1999; Sukerkar, 2010).

While the complex networks of cortical areas involved in control of arm movement do receive feedback about arm movements, the accuracy of the feedback

received is often degraded by noise and delayed due to limited axonal conduction velocities (Mutha et al., 2008; Pruszynski et al., 2008). The lack of excessive error during arm movements implies that prediction, using some form of internal representation or model, might be utilized for control of the arm. A popular theory for a forward model involves the creation of a copy of efferent motor commands that is stored within the brain and used as an internal model to predict the resulting movement and corresponding sensory feedback (Bridgeman, 1995; Feinberg, 1978; Gauthier & Robinson, 1975; Shadmehr et al., 2010). When generating movements, the internal model is used to predict and then compare the planned movement with what the body is actually doing. Errors from this comparison are then used to calculate the next motor command update (Shadmehr et al., 2010).

1.3.2 Cortical Control of Arm Stabilization

While numerous motor control studies indicate cortical involvement in the control of arm movements (Ashe & Georgopoulos, 1994; Colebatch et al., 1991; Connolly et al., 2003; Demandt et al., 2012; Fortier et al., 1989; Pfurtscheller & Lopes da Silva, 1999), cortical involvement in the control of arm stabilization, at the end of the movement, is less clear. At least three possible mechanisms have been proposed for control of arm stabilization: 1) increased impedance of the arm through the co-contraction of antagonistic muscles (e.g. Franklin et al. 2004) 2) spinal or supraspinal reflex circuits to provide corrective muscle activity (Kurtzer et al., 2008) and/or 3) intermittent voluntary corrections to errors in position (Hasan, 2005). Although mentioned as separate mechanisms, co-contraction, reflex control, and voluntary corrections are not mutually

exclusive and most likely work together to provide robust stabilization of the arm. The first two mechanisms, co-contraction and spinal/supraspinal reflex activity, may require little to no cortical involvement during arm stabilization while the third mechanism would likely require robust cortical involvement via the sensorimotor network.

Co-contraction acts to stabilize the arm by activating antagonistic muscle pairs (Franklin et al., 2004). A lack of cortical activity during sustained contractions has been observed in sustained wrist contractions and isometric contractions of the lower limb (Alegre et al., 2003; Gwin & Ferris, 2012), suggesting the cortex may not be directly involved in arm stabilizing co-contractions. This phenomenon may arise from a lack of movement-related sensory feedback (Weiller et al., 1996), cortical oscillations maintaining the current motor state (Engel & Fries, 2010; Pfurtscheller & Lopes da Silva, 1999) or co-contraction mechanisms located at the spinal level. Cremoux and colleagues (2017) have observed increases in co-contraction after a spinal cord injury; possibly due to reduced cortical influence on spinal mechanisms that inhibit antagonist muscle activity (Cremoux et al., 2017).

The spinal/supraspinal reflex mechanism for stabilization works by tailoring the reflex responses of the motor system to resist perturbations to position (Kurtzer et al., 2008; Shemmell et al., 2009; Soechting et al., 1981). While the short latency reflex (~25ms) timing indicates responses driven by spinal cord mechanisms, long latency reflexes (40-100ms) may include cortical involvement (Crago et al., 1976; Marsden et al., 1983). Long latency, supraspinal reflex activity has been shown to be cortically modulated and to generate cortical activity (Abbruzzese et al., 1985; Cheney & Fetz, 1984; Pruszynski et al., 2011a; Pruszynski et al., 2008; Pruszynski et al., 2011b;

Shemmell et al., 2009). However, the cortical activity associated with long latency reflexes is not as extensive as volitional movements (Suminski et al., 2007). Further, long latency reflex activity is still present in spinalized cats and monkeys (Ghez & Shinoda, 1978; Tracey et al., 1980), raising questions about whether supraspinal structures are directly involved in the reflex response.

Cortically-driven intermittent voluntary corrections may also play a role in stabilization of the arm (Hasan, 2005). When using fMRI during a proprioceptive wrist stabilizing task, Suminski and colleagues observed cortical network activity (Suminski et al., 2007). The involvement of cortical networks during stabilization processes may arise due to limitations associated with co-contraction and spinal/supraspinal reflexes. Co-contraction is only useful for perturbations that can be subdued by joint and musculature properties, and spinal/supraspinal reflex amplitude modulation is limited with changing task goals (Mutha et al., 2008). Cortical involvement during stabilization can be beneficial due to the highly context-dependent responses generated as a result of proprioceptive and visual information arriving at the cortex. Hasan proposed that stability of a perturbed system is not guaranteed by continuous resistance but rather by later events, including voluntary corrections (Hasan, 2005). If cortically-driven intermittent voluntary corrections were involved in the process of arm stabilization, one might expect the cortical activity during arm stabilization to resemble sensorimotor network activity seen in voluntary goal directed movement.

1.4 Stroke

1.4.1 Incidence

Stroke is an event of massive cell death within the brain resulting in a rapid loss of neurological function due to a reduction of blood supply to the brain. Strokes are either classified as ischemic where the lack of blood supply is caused by a blockage such as a thrombosis or hemorrhage where the lack of blood supply results from a ruptured vessel. Each year approximately 800,000 US residents experience a stroke incident with around 600,000 of these being first time events (Mozaffarian et al., 2015). Stroke is one of the major causes of serious physical and cognitive long-term disabilities (Centers for Disease Control and Prevention (CDC), 2009) and prevents around 50% of stroke survivors from returning to work (Vestling et al., 2003).

1.4.2 Sensorimotor Deficits following Stroke

Motor dysfunctions such as abnormal muscle synergy patterns, spasticity and paresis (Brunnstrom, 1970; Gracies, 2005; Lance, 1980) as well as sensory dysfunctions including deficits in tactile, proprioceptive, pressure and thermal sense are common after stroke (Carey, 1995). These motor and sensory deficits ultimately result in a functionally corrupt motor control system that has trouble initiating and stopping movements; the movements that are produced are usually uncoordinated, slower, less smooth and have a reduced overall range of motion compared to the neurologically intact population (Beer et al., 2000; Cirstea & Levin, 2000; Fang et al., 2007; Kamper et al., 2002). Deficits in motor control may arise from the inability to generate appropriate motor commands

and/or to correctly process sensory feedback. Studies have reported that stroke patients with both sensory and motor deficits exhibit lower functional outcomes than those with motor deficits alone (Patel et al., 2000), and that sensory impairment is a strong predictor of length of recovery and long-term functional outcomes of stroke survivors (Carey, 1995; Tyson et al., 2008). This suggests sensory information plays an important role in motor control and has generated interest in exploring the use of sensory interventions to facilitate stroke rehabilitation.

1.4.3 Cortical Networks After Stroke

Immediately following a stroke, task-related brain activity in the ipsilesional and contralesional sensorimotor cortex during paretic finger movements is increased in the stroke population when compared to the neurologically intact population (Chollet et al., 1991; Weiller et al., 1992). As stroke survivors recover over time, decreases in abnormally increased cortical activity correlate with improved functional recovery (Ward, 2003). Patients who display poor recovery, retain higher levels of cortical activity outside the primary sensorimotor areas while well recovered patients have normal levels of activity resembling controls (Ward et al., 2003).

Many fMRI studies have examined the effect of stroke on cortical networks in sensorimotor task-based paradigms. The most common findings include increased activity in both hemispheres (excluding the lesioned region) and decreased connectivity within and between hemispheres (Carey et al., 2002; Grefkes et al., 2008; Mintzopoulos et al., 2009; Rossini et al., 1998; Ward et al., 2003). EEG and MEG measures of sensorimotor activity in task-based studies have shown impairment specific changes in

cortical activity following stroke. These include a decrease in activity above the lesion, increased cortical asymmetries between hemispheres and connectivity increases within the lesioned motor networks of well recovered stroke participants (Bönstrup et al., 2018; Platz et al., 2000; Rossiter et al., 2014; Stępień et al., 2011; Strens et al., 2004). After stroke, decreases in functional connectivity occur throughout the brain, but mainly in the lesioned hemisphere (Crofts et al., 2011; Crofts & Higham, 2009; De Vico Fallani et al., 2009; Tuladhar et al., 2013). Changes in fMRI and EEG/MEG network activity/connectivity relate to functional/behavioral outcomes, and both indicate that brain networks normalize with recovery (Bönstrup et al., 2018; Grefkes et al., 2008; Grefkes & Fink, 2014; Strens et al., 2004; Ward et al., 2003).

The abnormal increases in cortical activity outside of the primary sensorimotor areas, abnormal connectivity patterns and increased asymmetries after stroke may indicate a redistribution of neurological functions to healthier tissue as a potential recovery mechanism (Cicinelli et al., 1997; Delvaux et al., 2003; Johansen-Berg et al., 2002; Platz et al., 2000; Rossini et al., 1998; Wang et al., 2010). Random growth of new axonal connections might also contribute to network re-organization after stroke (Carmichael, 2006, 2008; Wang et al., 2010). James and colleagues showed that asymmetric reorganization can facilitate recovery rather that a return to symmetry (James et al., 2009). Further, Johansen-Berg and colleagues used disruptive transcranial magnetic stimulation (TMS) applied to the contralesional motor cortex to demonstrate that motor networks can be redistributed after stroke (Johansen-Berg et al., 2002). The redistribution/re-organization of cortical networks after stroke might lead to a shift in the frequency of cortical communication. Specifically, cortical networks might have a higher

reliance on local network (high frequency) activity due to less efficient long-range pathways or dysfunctional hubs in global (low frequency) networks.

1.4.4 Tendon Vibration as a Therapeutic Intervention

Sensory feedback is a key component of closed loop systems, e.g. human motor control. Depending on how the feedback is altered, the system might produce a better or worse output. The application of an extraneous vibration to the neurologically-intact population has been shown to improve motor learning and motor control (Conrad et al., 2011a, 2011b, 2015; Priplata et al., 2003; Rosenkranz & Rothwell, 2012). Extraneous stimuli such as vibration and somatosensory electrical stimulation applied to people with stroke improve spasticity, balance control, arm tracking, arm stabilization, hand function, and reduce the magnitude of stretch reflexes (Celnik et al., 2007; Conrad et al., 2011a, 2011b, 2015; Dewald et al., 1995; Levin & Hui-Chan, 1992; Priplata et al., 2006; Wu et al., 2006). The mechanisms underlying these changes in sensorimotor control are unclear. When vibration is applied to wrist flexor tendons during a motor task, improvements in muscular function are not isolated to the wrist but are seen throughout the arm (Conrad et al., 2011a, 2011b, 2015). This observation suggests that vibration enhances not only cortical function of the stimulated area but also areas not directly associated with stimulation, possibly by way of improved cortical network function.

Non-invasive stimulation techniques alter cortical activity and connectivity. The application of external stimuli to the cortex using transcranial direct current stimulation and repetitive transcranial magnetic stimulation in the neurologically intact and stroke populations increases not only the functional connectivity of the stimulation site, but also

the connectivity of regions distant from the site of stimulation (Bestmann et al., 2005; Grefkes et al., 2010; Grefkes & Fink, 2011; Polanía et al., 2011). A transcranial magnetic stimulation study found that vibration at the muscle can modulate the excitability of the motor cortical circuits and increase motor evoked potentials (Rosenkranz & Rothwell, 2003), furthering the idea that vibration induces supraspinal changes during motor control. The possibility that an enhanced sensory signal excites widespread cortical networks is an exciting prospect for functional rehabilitation in stroke.

Tendon vibration is thought to increase proprioceptive sensory information by activating Ia-afferent neurons (Cordo et al., 1995; Roll et al., 1989); however, tendon vibration also affects Golgi tendon organs and muscle spindle secondaries (Burke et al., 1976; Fallon & Macefield, 2007). The flow of additional proprioceptive information via tendon vibration might help to boost task-relevant proprioceptive signals of the limb through a stochastic resonance process, and help the system overcome the sensory deficits typically seen in people with stroke (Connell et al., 2008).

1.5 Electroencephalography

1.5.1 Physiological Origins

EEG is a recording of the brain's electrical potential at the scalp. Even though all neurons may play a small role in the generation of EEG, pyramidal neurons in the gyri and sulci of the cortex are the primary contributors to EEG due to their regular anatomical organization, proximity to the scalp, and their orientation perpendicular to the cortical surface. The inputs to the pyramidal neurons, post synaptic potentials, generate neuronal current flow toward the soma (cell body) of the neuron that can be well

characterized as an electrical dipole (Murakami & Okada, 2006; Sanei & Chambers, 2007). When large populations of pyramidal cells, typically macro columns consisting of 1000s of neurons, are active at the same time, their dipole activity synchronizes and sums together to produce the electrical potentials measured on the scalp by EEG (Baillet et al., 2001; Hari & Salmelin, 1997; Misulis & Head, 2003). Due to noninvasive nature of EEG, i.e. being recorded at the scalp, the cortical signal must pass through the pia matter, arachnoid membrane, dura matter, skull, periosteum, and skin before being recorded at the electrode; this process attenuates and effectively low pass filters the brain's electrical signal giving the EEG a bandwidth of about 100Hz (Cooper et al., 1965). The soft tissues and skull also create a smearing effect that, along with the limited number of EEG electrodes, causes the signal's spatial resolution to be on the order of centimeters (Michel et al., 2004). However, the temporal resolution of EEG (millisecond range) is much finer than other neuroimaging techniques such as fMRI, which measures hemodynamic responses, because it is a direct measurement of neuronal activation (Logothetis, 2002, 2003; Nunez & Srinivasan, 2006).

1.5.2 EEG Challenges

Recording EEG is not a straight-forward process and presents many challenges. During the recording process, EEG data can become contaminated with artifacts due to muscle activity (face, neck, jaw, eyes), eye blinks, head movements, impedance changes over time and electrical line noise. Advances in EEG hardware such as active electrodes, which amplify EEG signals at the scalp to minimize line noise and any movement artifacts, have improved the quality of neural signals measured from the cortex. Filtering,

template subtraction and blind source separation techniques such as independent component analysis (ICA) have also been employed in post-processing to remove EEG signal artifacts (Correa et al., 2007; Jervis et al., 1989; Mognon et al., 2011). ICA decomposes data into statistically independent components which can then be examined for distinct artefactual characteristics in space and time and can then be removed (Delorme et al., 2012; Makeig et al., 2004; Mognon et al., 2011; Puce & Hämäläinen, 2017; Stone, 2004).

1.5.3 EEG Analysis

Early research using EEG mainly examined evoked or event related potentials at the electrode level, which indicate a measure of cortical processing of underlying areas and provide information about the time course of EEG activity (Luck & Kappenman, 2011). Evoked potentials are phase locked to an event, such as a movement cue or sensory response, and are typically averaged across many trials to increase the signal to noise ratio of the cortical signal. However, interpreting the underlying cortical areas responsible for the activity can be difficult due to the signal smearing effect (i.e. volume conduction). Volume conduction is generated by the spatial blurring of cortical point sources measured at the scalp. Source localization techniques have allowed for more accurate localization of neuronal activation patterns on the cortical surface and help reduce the effect of volume conduction by including estimates of tissue properties in the forward model (Baillet, 2011; Grech et al., 2008).

More recently, the analysis of induced responses by way of time-frequency analysis has been used to examine cortical activity. Induced responses are not phase

locked to an event and are thought to arise from higher order processes described as ‘binding’ or neural synchronization (David et al., 2006; Singer, 1995). When examining induced responses, trials are typically transformed to the frequency domain and averaged to improve the signal to noise ratio, after which modulations of frequency band power can be observed (Kilavik et al., 2013; Pfurtscheller et al., 1996; Pfurtscheller & Lopes da Silva, 1999; Pfurtscheller et al., 1998). Generally, there are five defined categories in the frequency domain know as EEG frequency bands: delta (0-4Hz), theta (4-8Hz), alpha (8-12Hz), beta (12-30Hz) and gamma (>30Hz). Time-frequency analysis of EEG has led to the discovery of beta band (12-30Hz) power fluctuations above the sensorimotor cortex during movement referred to as event related desynchronization (decrease in power during movement, ERD) and event related synchronization (increase in power following movement, ERS) (Pfurtscheller et al., 1999; Pfurtscheller & Lopes da Silva, 1999). ERD is generally thought to indicate cortical activation whereas ERS is thought to indicate the resetting or end of cortical processing (Pfurtscheller & Lopes da Silva, 1999; Steriade et al., 1990). When an area of the cortex becomes active, neuronal activity within the active region de-phases, due to local information processing, from the baseline oscillatory state of the cortex resulting in a decrease in power (Pfurtscheller et al., 1999; Pfurtscheller & Lopes da Silva, 1999; Steriade et al., 1990).

In addition to the analysis of cortical activity, an exciting area of EEG research involves connectivity analyses to identify the interactions between brain regions associated with cortical networks (Siegel et al., 2012). Numerous connectivity measures exist (e.g. Granger causality, coherence, correlation, dynamic causal modeling, etc.) to examine how cortical regions interact. Functional connectivity measures quantify

dependencies between cortical signals while effective connectivity measures quantify the directed influence of one cortical region on another (Sakkalis, 2011; Schoffelen & Gross, 2009). Two of the more common functional connectivity techniques examine the correlations between amplitude changes in signals over time and the phase coherence between signals (Brookes et al., 2011; Hipp et al., 2012; Rappelsberger, 1989; Siegel et al., 2012; Stam et al., 2009). Coherence is the frequency domain analog to cross-correlation of signals in the time domain and gives an estimate of frequency power accounted for between two signals of interest (Schoffelen & Gross, 2009). Coherence values are defined across all frequencies between the two signals and can range from 0 to 1. A value of 1 means the two signals are perfectly coherent at that frequency with a constant phase difference while a value of 0 means the signals are not coherent at that frequency with a randomly changing phase difference.

While many EEG connectivity measures exist, they all suffer from the effects of volume conduction. Volume conduction is theorized to propagate instantaneously and results in significant spatial correlation between EEG electrodes that can extend over distances larger than 8cm (Nunez et al., 1997) even if the cortical regions immediately below the electrodes are not functionally connected. Source localization techniques can help reduce the effect of volume conduction on connectivity analyses (Baillet, 2011; Grech et al., 2008). However, current source localization techniques require a re-referencing of EEG signals to a common average reference, which may alter true connectivity patterns (Essl & Rappelsberger, 1998; Nunez et al., 1999; Rappelsberger, 1989; Zaveri et al., 2000). More recently, imaginary coherence (Nolte et al., 2004), orthogonalization techniques (Brookes et al., 2012; Hipp et al., 2012) and other phase

metrics excluding zero lag connectivity (Nolte et al., 2008) have been used to mitigate this issue.

1.6 Specific Aims

The purpose of this dissertation was to characterize sensorimotor networks and examine the implications of stroke on sensorimotor networks. We examined the activity and connectivity of sensorimotor networks in stroke survivors and controls using EEG. Sensorimotor network function was examined in controls during upper extremity tasks designed to differentiate potential mechanisms of arm stabilization and determine to what degree the sensorimotor network is involved in arm stabilization. After basic sensorimotor network function was characterized in controls, we examined the effect of stroke on the sensorimotor network at baseline (rest) and described the reorganization that occurs. Lastly, we explored tendon vibration as a sensory therapy for stroke survivors and determined if sensorimotor network mechanisms underlie improvements in arm tracking performance seen in chronic stroke survivors due to wrist tendon vibration.

1.6.1 Aim 1: Determine if Cortical Networks Are Involved in Visuomotor Control of Arm Stability

To test this aim, EEG data were recorded from young healthy participants while they completed tasks designed to differentiate three potential mechanisms for control of arm stability: 1) increased impedance of the arm through co-contraction of antagonistic muscles 2) corrective muscle activity via spinal/supraspinal reflex circuits and/or 3) intermittent voluntary corrections to errors in position. EEG beta band power fluctuations were used as indicators of brain activity and coherence between EEG electrodes was used

as a measure of functional connectivity between brain regions. If cortical error correction networks are being utilized during stabilization, we would expect the cortical activity during control of arm stability would mimic voluntary goal directed movement. *We hypothesized that cortical error correction networks contribute to arm stabilization.*

1.6.2 Aim 2: Characterize the Reorganization of Resting State Cortical Networks After Stroke Using EEG

To test this aim, EEG data were collected from chronic stroke and neurologically-intact participants while they were in a relaxed, resting state. EEG power was used as an indicator of network activity and correlations of orthogonalized EEG band envelope activity were used as a measure of functional connectivity between cortical regions. We expected cortical networks after stroke to have a higher reliance on local network activity with less efficient pathways connecting local regions, resulting in a shift to higher frequency. *We hypothesized that cortical networks are more asymmetric after stroke and that there is a shift in the frequency due to changes in cortical communication after stroke.*

1.6.3 Aim 3: Determine if Cortical Network Mechanisms Underlie Improved Arm Tracking Performance in Chronic Stroke Survivors Due to Wrist Tendon Vibration

To test this aim, EEG data were collected from chronic stroke and neurologically-intact participants while they completed a series of figure-8 tracking tasks. Brain activity (EEG beta band power fluctuations), functional connectivity between brain regions (spatially correlated coherence), and arm tracking performance were compared before, during, and after tendon vibration. If cortical mechanisms underlie stroke survivors'

improved arm tracking performance with the application of tendon vibration, we would expect stroke survivors' cortical activity and connectivity to approach that seen in controls when tendon vibration is applied. *We hypothesized that application of tendon vibration to the wrist forearm flexor tendons causes tracking improvements in the paretic arm by increasing the cortical activity and connectivity in the regions displaying cortical deficits after stroke.*

CHAPTER 2: THE ROLE OF THE CORTEX IN VISUOMOTOR CONTROL OF ARM STABILITY

2.1 Introduction

Visuomotor control of arm posture might involve cortical structures that provide motor commands to correct errors in position. During movement, agonist muscles are activated to move the limb toward the target, which is followed by antagonist muscle activation to provide braking. While numerous motor control theories describe the control of arm trajectory during a reach (Feldman, 1986; Flash & Hogan, 1985; Houk et al., 2000; Kalaska et al., 1997; Latash et al., 2010; Todorov & Jordan, 2002), the control of the stabilization phase after the end of the movement is less clear. At least three possible mechanisms have been proposed for visuomotor control of arm posture: 1) increased impedance of the arm through the co-contraction of antagonistic muscles (e.g. Franklin et al. 2004) 2) spinal or supraspinal reflex circuits to provide corrective muscle activity (Kurtzer et al., 2008) and/or 3) intermittent voluntary corrections to errors in position (Hasan, 2005). In this study, we examined electroencephalography (EEG) data during a series of arm stabilization tasks to test the hypothesis that cortical error correction networks are involved in visuomotor control of arm posture.

Each of the proposed mechanisms of arm stabilization has potential advantages and limitations. Co-contraction acts to stabilize the arm by activating antagonistic muscle pairs (Franklin et al., 2004). This mechanism is beneficial because it increases joint stiffness without the necessity for a complex motor control network to respond continuously to perturbations and appears to be the preferred method of stabilization when a dynamic force field is present (Franklin et al., 2003a; Franklin et al., 2003b).

Increasing the co-contraction of the arm during arm movements and postural maintenance tasks results in better movement accuracy and less positional error respectively, providing increased stability to the limb during reach (Franklin et al., 2003a; Franklin et al., 2003b; Gribble et al., 2003; Scheidt & Ghez, 2007). A limitation of co-contraction for postural control of the arm is that it is thought to be metabolically inefficient (Gribble et al., 2003; N. Hogan, 1984), because increased muscle activity is related to an increase in metabolic costs (Foley & Meyer, 1993; Hogan et al., 1996; Sih & Stuhmiller, 2003). Co-contraction is also only useful for perturbations that can be subdued by joint and musculature properties. The stiffness of the joint cannot exceed the physical properties of the tissues and tendons being used to stabilize the joint. Some joints, such as the ankle, have such low stiffness that they fall short of the of the minimum required for stability, which may also occur in the joints of the arm if strong perturbations are encountered (Hof, 1998; Morasso & Sanguineti, 2002; Morasso & Schieppati, 1999).

The spinal/supraspinal reflex mechanism for stabilization works by tailoring the reflex responses of the motor system to resist perturbations to position (Kurtzer et al., 2008; Shemmell et al., 2009; Soechting et al., 1981). Both short latency (~25ms) and long latency reflexes (40-100ms) are observed in response to muscle stretch; reflex regulation may be beneficial for stabilization because of the speed of the correction and limited need for higher level processing (Crago et al., 1976; Marsden et al., 1983). Short latency reflexes can modulate their response depending on the underlying muscle activity (Mortimer et al., 1981; Soechting et al., 1981), providing a generic response to muscle stretch that may not account for task context. On the other hand, long latency reflex

mechanisms can modulate their responses to muscle stretch and perturbations in a task specific manner, acting as an intermediary between short latency reflexes and volitional responses (Mutha et al., 2008; J. Pruszynski et al., 2008; Shemmell et al., 2009; Soechting et al., 1981). While long latency reflexes are able to modulate the direction and amplitude of their responses when prior knowledge of the task is known (Pruszynski et al., 2008), Mutha and colleagues showed that the amplitude modulation of long latency reflexes is limited during movements with changing task goals (Mutha et al., 2008). Modeling studies have suggested that the cyclic response of reflex activity coupled to a viscoelastic system could lead to unbounded amplification of an initial perturbation and even resemble spastic clonus due to reflex delays (Baratta et al., 1998; Hidler & Rymer, 1999). The absence of clonic activity during visuomotor control of arm posture suggests that reflex gains may be limited under normal circumstances, reducing this instability issue.

Cortically-driven intermittent voluntary corrections could also provide visuomotor control of arm posture (Hasan, 2005). Cortical involvement during stabilization can be beneficial due to the highly context dependent responses generated as a result of the proprioceptive and visual information arriving at the cortex. However, cortically-driven corrections of arm posture are limited by the long delays (150-200ms) associated with sensory feedback and generation of corrective responses (Mutha et al., 2008; Pruszynski et al., 2008), as well as a larger computational load associated with the use of higher-level motor control mechanisms to achieve stabilization goals without excessive cumulative errors. The lack of excessive error implies that prediction using

some form of internal representation or model may be utilized for visuomotor control of arm posture (Shadmehr et al., 2010).

Co-contraction, spinal/supraspinal reflex and cortically-driven voluntary correction mechanisms of arm stabilization are not mutually exclusive and are most likely all employed during stabilization tasks. Experiments involving arm movement tasks have shown co-contraction decreases over time, possibly indicating a shift from a co-contraction mechanism, which provides greater accuracy in the absence of a fully formed internal model, towards internal representations of the movement and feedforward control after practice (Franklin et al., 2003b; Gribble et al., 2003). Co-contraction also shares a relationship with short latency reflexes. In unstable environments, as the level of co-contraction increases the magnitude of the reflex response also increases suggesting both are used to compensate for perturbations (Akazawa et al., 1983; Soechting et al., 1981). Research investigating the disruption of cortical activity using transcranial magnetic stimulation or disconnect between the cortex and the spinal cord in the people with spinal cord injury have shown that reflex activity is lowered and the baseline level of co-contraction is increased respectively when cortical drive is reduced (Shemmell et al., 2009). When investigating balance of an inverted pendulum with the ankles, Loram and Lakie (Loram & Lakie, 2002) showed that stability requires not only intrinsic ankle stiffness but also anticipatory neural modulation of ankle torque. Further, intersegmental interactions during brief force perturbations show electromyography (EMG) responses in segments downstream from the perturbed segment that exacerbate instead of resist perturbations (Koshland et al., 1991; Lacquaniti & Soechting, 1984, 1986). It has been suggested that this unexpected response cannot be completely explained by reflex activity

and may arise from a repertoire of voluntary movements (Koshland et al., 1991; Latash, 2000). Although co-contraction and spinal/supraspinal reflex activity both contribute to stabilization, there also appears to be a cortical component. Hasan proposed that stability of a perturbed system is not guaranteed by continuous resistance but rather by later events, including voluntary corrections (Hasan, 2005).

In this study, we set out to identify the cortical mechanisms of visuomotor control of arm posture. We collected EMG, kinematic, and electroencephalography (EEG) data across four different experimental tasks designed to differentiate potential stabilization mechanisms and determine which are involved in stabilization of arm posture. Our approach used a reach and hold paradigm to place the arm at a target position where the mechanisms of visuomotor control of arm posture were tested during the ensuing hold period. We used a position control task with minimal arm stabilization requirements, a co-contraction task with pure arm co-contraction, a voluntary task with pure volitional arm movement and a perturbation task consisting of a force field in which participants were asked to stabilize their arm. EEG beta band (13-26Hz) power fluctuations during stabilization were used as indicators of brain activity associated with motor function (Pfurtscheller & Lopes da Silva, 1999; Pfurtscheller & Lopes da Silva, 1999; Steriade et al., 1990), and the coherence between EEG electrodes was used to measure functional connectivity between cortical areas (Rappelsberger et al., 1993). We tested the hypothesis that cortical error correction networks contribute to arm stabilization. Due to the involvement of co-contraction during stabilization of reach, we anticipated that perturbations during postural stabilization of the arm would show signs of increased EMG co-contraction. If cortical error correction networks are being utilized during

stabilization, we would expect the cortical activity during visuomotor control of arm posture would mimic voluntary goal directed movement. Further, we postulated that invoking cortical visuomotor control networks would result in higher connectivity between the sensory regions interpreting the error and the motor regions correcting posture.

2.2 Methods

2.2.1 Participants

A sample of 10 right-handed healthy participants (age 21-34 years, 6 male) participated in the study. All participants gave written informed consent, and all procedures were approved by the Marquette University Institutional Review Board in accordance with the Declaration of Helsinki. Inclusion criteria required that the participants be healthy with no known neurological disease or injury.

2.2.2 Test Apparatus

The study was conducted using a custom-built mechanical linkage (Figure 2-1A) (APPENDIX A: MANIPULANDUM). The linkage constrained movement to the horizontal plane and provided measurements of end-point trajectory using optical encoders (Celesco Transducer Products, Inc., Chatsworth, California; BEI Sensors, Goleta, California) located at each joint. The device frame was constructed using 2.5x2.5cm extruded aluminum (80/20 Inc., Columbia City, Indiana) and contained three rotational joints to allow unrestricted movement in the horizontal plane. While seated at the device, the participant's forearm was secured to an Ultra High Molecular Weight

Polyethylene tray located at the end of the manipulandum. An overhead projector displayed hand position and target location on an opaque screen (80x60cm) directly above the plane of hand motion. The device was interfaced with LabVIEW (National Instruments Corporation, Austin, Texas) in order to control the projector display, record (1 kHz sampling rate) kinematic data, and generate digital pulses used to synchronize the timing of movement and EMG/EEG data collection.

2.2.3 Experimental Protocol

Before testing, EMG data were recorded from each participant as they sat in a chair and performed maximum voluntary isometric contractions (MVCs) for the 6 muscles analyzed in this study. Each MVC was sustained for around 5s. Anterior and posterior deltoid MVC data were collected as participants tried to internally or externally rotate the arm against resistance while the shoulder was abducted 90^{o} in plane of scapula and elbow flexed 90^{o}. Biceps and lateral head of the triceps MVC data were collected as participants tried to flex or extend the elbow against resistance while the shoulder was abducted 45^{o} in plane of scapula and elbow flexed at 90^{o}. Flexor carpi radialis and extensor carpi ulnaris MVC data were collected as participants tried to flex and extend the wrist against resistance while the shoulder was in a neutral position and the elbow was flexed 90^{o}. These measurements were used later for normalization of EMG data obtained during the experimental trials.

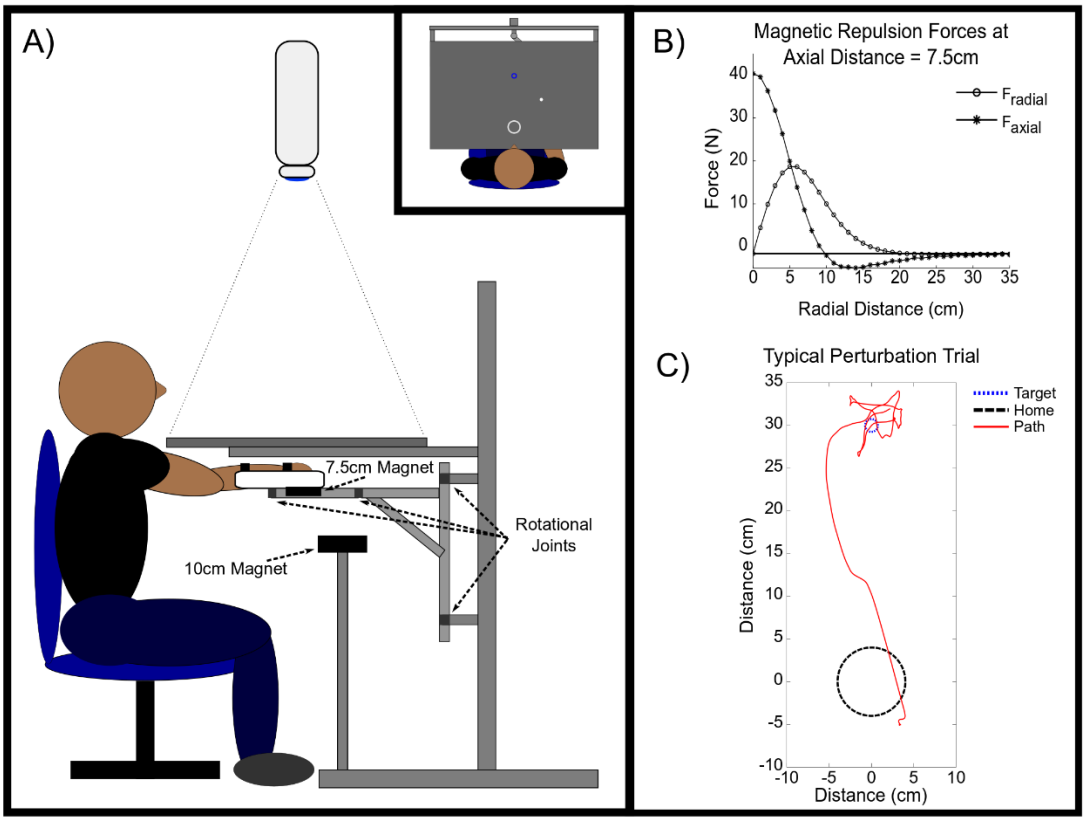

Figure 2-1: Experimental Setup. A) Illustration of the mechanical linkage and experimental setup from the side (inset in top right displays the scene from above). The 10cm diameter magnet was only present during the perturbation trials. The cursor (white circle) projected onto a horizontal screen was linked to hand position. Participants were required to move the cursor from the home location (white annulus) to the target (dark gray annulus). B) Magnetic repulsion forces in the radial and axial directions. The minimum axial distance between the magnets was 7.5cm and occurred when the 2 magnets were directly over one another (radial distance = 0cm). The maximum force in the radial direction of ~20.25N was generated when the center of the 7.5cm magnet was over the edge of the 10cm magnet (~5cm). C) Typical perturbation trial. The time shown in the figure ranges from 0-6s, just after target presentation to the end of the stabilization period. The line represents the cursor's path (linked to hand position) throughout the trial. During the baseline period, the cursor (hand) slowly drifted out of the home location back towards the participant. Supplemental Video S1 (https://doi.org/10.6084/m9.figshare.9199307) displays the typical perturbation trial.

The participant's dominant arm was tested using a period of stabilization following movements of the mechanical linkage. The study consisted of four tasks, each with 40 trials. Each trial consisted of a baseline period (6.5±1.5s before target

presentation), target acquisition/stabilization period (0-6s after target presentation) and return period (~1s between the stabilization and baseline periods). Prior to each trial, participants were required to bring a white cursor (r = 0.5cm), linked to hand position, to the home location (gray annulus, r = 4cm) located ~24cm in front of the participants. The home location then disappeared, and participants relaxed until the target (blue annulus, r = 0.75cm) was presented 30cm away from the home position on an imaginary line orthogonal to the participant's chest. Participants then moved their hand as quickly and accurately as possible to the target, at which point the four tasks began. The following tasks were tested.

Point-to-point Task (PtP): This task was designed to be a control task with minimal arm movements, EMG, co-contraction and stabilization. After the point-to-point movement, participants were instructed to hold their hand at the target. The target and cursor were displayed for the duration of the target acquisition/stabilization period. No visual or physical perturbations were applied at the target.

Co-contraction Task (CoC): This task was designed to isolate the arm's EMG, co-contraction, cortical activity and cortical connectivity associated with a pure co-contraction. After the point-to-point movement, participants were instructed to co-contract (10-20% of MVC) their arm at the target. Feedback regarding the level of co-contraction was given to the participants by way of cursor color (red: <10% deltoid MVC, white: within range, green: >20% deltoid MVC). Visual feedback of the target and cursor (level of co-contraction) was displayed for the first 2s of

the target acquisition/stabilization period after which both were removed. Participants were instructed to hold the level of co-contraction constant after feedback was removed. No visual or physical perturbations were applied at the target.

Voluntary Task (VOL): This task was designed to identify the EMG, co-contraction, cortical activity and cortical connectivity associated with a volitional movement. After the point-to-point movement, participants were instructed to recreate the typical movement profile made when trying to stabilize their arm during the perturbation task (see below). This resulted in participants randomly moving their arm with approximately the same speed and within the same space that they did during the perturbation tasks. Visual feedback of the target was displayed for the first 2s during the target acquisition/stabilization period after which it was removed. Participants continued to recreate movements similar to the perturbation task (see below) after the feedback was removed. No visual or physical perturbations were applied at the target.

Perturbation Task (PER): This task was designed to generate EMG, co-contraction, cortical activity and cortical connectivity associated with arm stabilization in an unstable environment. After the point-to-point movement, participants were instructed to keep the cursor on the target while axial and radial magnetic forces were applied at the target and the visual feedback was simultaneously manipulated to create a hyperbolic distortion of cursor position about the target. The magnetic force perturbation was created using two

Neodymium ring magnets (Applied Magnets, Plano, Texas). The repulsive forces generated between the 2 magnets versus the distance of the hand away from the center of the target can be seen in Figure 2-1B. The first magnet (d = 10cm, thickness = 2.5cm, center hole = 0.8cm) was mounted under the screen target location while the second (d = 7.5cm, thickness = 1.2cm, center hole = 0.8cm) was mounted on the arm support tray under the hand. The minimum distance between the two magnets was 7.5cm, Figure 2-1A. Manipulation of visual feedback of arm position was generated using a hyperbolic function, Equation 2.1, which changed the relationship between hand location and cursor location near the target,

$$\boldsymbol{X}_C(\boldsymbol{X}_H) = \begin{cases} \sqrt{-a^2\left(1-\left(\frac{|\boldsymbol{X}_H-\boldsymbol{X}_T|+a}{a}\right)^2\right)}+\boldsymbol{X}_T; & if\ \boldsymbol{X}_H \geq \boldsymbol{X}_T \\ -\sqrt{-a^2\left(1-\left(\frac{|\boldsymbol{X}_H-\boldsymbol{X}_T|+a}{a}\right)^2\right)}+\boldsymbol{X}_T; & if\ \boldsymbol{X}_H < \boldsymbol{X}_T \end{cases} \quad (2.1)$$

where $\boldsymbol{X}_C$ is the 2-D cursor location, $\boldsymbol{X}_H$ is the 2-D hand location, $\boldsymbol{X}_T$ is the 2-D target location, and a represents the gain, which was randomly selected for each trial and varied between 5±2.5cm. Visual feedback was manipulated in the task to increase the sensitivity of hand movements around the target, effectively making the perturbation task more difficult. The visual gain was randomly selected each trial to prevent the participants from learning the perturbation environment. Figure 2-1C displays a typical perturbation trial time course.

The tasks were designed in order to compare the stabilization mechanisms active in the PER task to those in the CoC task (co-contraction mechanism during stabilization) and the VOL task (cortically-driven voluntary correction mechanism during

stabilization). Trials were blocked by task, with task presentation randomized across participants (the PER task always occurred before the VOL task to allow perturbation movement trajectories to be mimicked). Participants were given breaks between tasks to prevent fatigue.

2.2.4 Physiological Measurements

A 64-channel active electrode actiCAP (Brain Products GmbH, Munich, Germany) system arranged in the conventional 10-20 system with the reference at FCz and the ground at AFz was used to record EEG data. The EEG cap was placed on the participant's head such that the Cz electrode was in line with the prearticular points of the frontal plane and with the nasion and inion points of the sagittal plane. SuperVisc gel (Brain Products GmbH, Munich, Germany) was applied between the scalp and electrodes to lower the electrode impedances below 10kOhms. EEG data were amplified, sampled at 1kHz, filtered from 0.1 to 200Hz and notch filtered at 60Hz using a Synamps^2 amplifier system (Neuroscan, Charlotte, North Carolina), and recorded using the Neuroscan software, Scan 4.5.

A Trigno^{TM} wireless EMG system (Delsys, Inc, Boston, Massachusetts) recorded muscle activation from the anterior deltoid (AD), posterior deltoid (PD), flexor carpi radialis (WF), extensor carpi ulnaris (WE), biceps (BI), and lateral head of the triceps (TRI). The skin was cleaned and lightly abraded before placing electrodes on the muscle. EMG data were amplified by 1000 and sampled at 1kHz.

2.2.5 Data Analysis

EEG data were post processed and analyzed using the EEGLAB toolbox (version v13.4.4b) (Delorme & Makeig, 2004), FieldTrip (version 2016-01-03) (Oostenveld et al., 2011), Brainstorm (version 3.4) (Tadel et al., 2011), and custom MATLAB scripts (version 2014a, MathWorks, Natick, Massachusetts). All EEG data were bandpass filtered (0.1-100Hz) using a fourth order zero-phase Butterworth filter. The data were then epoched (-3 to 6s relative to the movement cue) and baseline corrected (-3s to cue). Bad epochs were removed (average number removed, 4) using EEGLAB's automatic rejection algorithm (200μV threshold, pop_autorej) and manually by using FieldTrip's visual inspection code (epoch removed if its variance/kurtosis was a visual outlier when compared to the other epoch variances/kurtoses for the task, ft_rejectvisual). EEG data were separated into signal and artefactual components using an Adaptive Mixture Independent Component Analysis (AMICA) (APPENDIX C: INDEPENDENT COMPONENT ANALYSIS) (Palmer et al., 2008), with 64 independent temporal components. Signal artifacts, including eye blink, EMG, and movement artifacts, were identified by distinct artefactual characteristics (Delorme et al., 2012; Makeig et al., 2004; Mognon et al., 2011; Puce & Hämäläinen, 2017) and removed from the EEG data (average number of artefact components removed, 14; minimum number: 4; maximum number: 23). The remaining components were then transformed back to the EEG channel space. Finally, EEG data were re-referenced to a common average for all data analyses excluding the connectivity analyses which re-referenced the data to the average of the mastoids (Electrodes TP9 and TP10) (Rappelsberger, 1989). Each re-reference technique reintroduced the FCz electrode to the data set.

EMG data were processed and analyzed using custom MATLAB scripts (version 2014a, MathWorks, Natick, Massachusetts). All EMG data were bandpass filtered (10-350Hz) using a fourth order zero-phase Butterworth filter and then sent through a root-mean square (RMS) calculation using a 100ms sliding window. To normalize the RMS EMG data from the experimental tasks, each muscle's RMS EMG trace was divided by its respective MVC value and multiplied by 100 to obtain the percentage of maximum voluntary EMG activation. Each muscle's MVC was calculated by finding the peak RMS EMG value within the muscle's MVC trial and taking the average of the surrounding 1s window of time. EMG co-contraction was calculated at each sample point in time by taking the minimum normalized EMG activation from each agonist-antagonistic muscle pair (AD/PD, WF/WE, BI/TRI). Normalized EMG and EMG co-contraction data were epoched (-3 to 6s relative to the movement cue) and bad epochs identified from the EEG data were removed. Normalized EMG and EMG co-contraction data were compared across tasks to characterize the contribution of co-contraction mechanisms to stabilize the arm during the PER task.

The speed of the hand was calculated from the x and y hand positions obtained from the optical encoders. Hand displacement was calculated as the Euclidean distance of the hand from the target. Speed and displacement data were both epoched (-3 to 6s relative to the movement cue) and the bad epochs identified in the EEG data were removed. Hand displacement and speed were examined to ensure that the kinematics were matched between the PtP and CoC tasks as well as the VOL and PER tasks.

Distributed source localization was applied to the EEG data to examine the spatiotemporal characteristics of beta band power (cortical activity) of the PER task and

determine the cortical control mechanisms at play. Distributed current dipole maps were computed in Brainstorm using the default MNI/Colin27 anatomical brain template. The standard actiCAP electrode locations were fit to the scalp surface so that the Cz electrode location was at the vertex as described in the physiological measurements section. A boundary element model (BEM) was used to estimate of the forward model (OpenMEEG) (Gramfort et al., 2010; Kybic et al., 2005), and a depth-weighted minimum L2 norm estimator of cortical current density (Hämäläinen & Ilmoniemi, 1994) was used to estimate the inverse model. The source localized data were then bandpass filtered (13-26Hz) using a zero-phase fourth order Butterworth filter, squared to obtain power, averaged across trials, low pass filtered (2Hz) using a zero-phase fourth order Butterworth filter to extract the envelope and normalized. For display purposes, the normalization process for the data shown in Figure 2-3 was the z-score (baseline period: -3s to cue). For statistical analyses, the normalization process was the calculation of the percent change from baseline (baseline period: -3s to cue), equation 2.2,

$$\%\Delta(t) = 100 \times \frac{\boldsymbol{X}(t) - baseline}{baseline} \qquad (2.2)$$

where $\%\Delta(t)$ represents the percent change from baseline, $\boldsymbol{X}(t)$ represents the power time series, t represents time, and $baseline$ represents the average power in the baseline period.

EEG beta band power of the source localization data was segmented into seven regions of interest (ROIs) using the Desikan-Killiany mapping technique (Desikan et al., 2006): left Superior Frontal Gyrus, left Caudal Middle Frontal Gyrus, left Pre-Central Gyrus, left Post-Central Gyrus, left Superior Parietal Gyrus, left Inferior Parietal Gyrus, and left Lateral Occipital Gyrus. The mean beta band power for each of the seven ROIs

were then compared across tasks. To examine hemispheric differences, an identical process was performed by treating the seven ROIs within each hemisphere as one large ROI and comparing the beta band power mean difference between hemispheres.

EEG coherence was used to quantitatively compare cortical network connectivity between the PER task and the VOL (cortically-driven mechanism) and CoC (co-contraction mechanism) tasks. All-to-all (connectivity between all possible pairs of EEG electrodes) temporal connectivity profiles were generated using magnitude squared coherence, (equation 2.3),

$$Coh^2(f) = \frac{|C_{XY}(f)|^2}{C_{XX}(f) \cdot C_{YY}(f)} \qquad (2.3)$$

where Coh^2 represents the magnitude squared coherence between electrodes X and Y, C_{XY} represents the cross spectrum between electrodes X and Y, C_{XX} represents the auto spectrum of electrode X, C_{YY} represents the auto spectrum of electrode Y, and f represents frequency. Every EEG epoch was divided into 9 non-overlapping windows, each containing 1s of data. Coherence was then calculated within each window using the epochs as the measure of consistency. For each participant and task, this resulted in a connectivity matrix that was 4225 (65x65 electrodes) by 9 for every frequency. The resulting connectivity matrices were then averaged across the 13-26Hz range and baseline corrected by removing the mean of the first 3 time points (representing the 3s before the movement cue) to calculate task-based coherence of the beta band. For each participant and task, a threshold was calculated by generating a histogram using the baseline-corrected connectivity values for all electrode-electrode combinations and finding the connectivity value corresponding to the top 5% of all connectivity values across the distribution. Connections that fell above the threshold were considered active.

EEG task-based coherence data were segmented into three ROIs: Frontal cortex (electrodes Fp1, Fp2, AF7, AF3, AF4, and AF8), Sensorimotor cortex (electrodes C3, C1, Cz, C2, C4, CP3, CP1, CPz, CP2, and CP4), and Visual cortex (electrodes PO3, POz, PO4, O1, Oz, and O2). Intra-regional and inter-regional coherence was then examined at each time point by calculating the percentage of active connections (PAC), equation 2.4, within each region (intra-region coherence) and between each region (inter-region coherence), respectively,

$$PAC = 100 \times \frac{\#\ Active}{\#\ Total} \qquad (2.4)$$

where PAC represents the percentage of active connections, $\#\ Active$ represents the number of connections above threshold, and $\#\ Total$ represents the total number of connections.

Hand speed, hand distance, EMG activity, EMG co-contraction, EEG ROI beta band power, EEG hemisphere beta band power, EEG intra-region coherence, and EEG inter-region coherence data were all averaged during the last 2s (4-6s) of the target acquisition/stabilization period (referred to the stabilization period from here on out) and across trials for each participant. While arm postural stabilization began immediately after the reach to the target, we chose to analyze the stabilization period 4-6s after target presentation in order to minimize effects due to reach (about 0.5-1.5s after target presentation) and the removal of visual feedback (2s after target presentation). Gwin and Ferris have shown that beta band desynchronization can persist for around 1s after the initial force generation in a sustained knee and ankle isometric task (Gwin & Ferris, 2012). Pfurtscheller and Lopes da Silva recommend having around 10s between events when studying EEG desynchronization in order to allow the frequency band modulations

to recover (Pfurtscheller & Lopes da Silva, 1999). In our experience, beta band modulations tend to stabilize between 1 and 10s after movement. To prevent fatigue, we chose not to extend the period of stabilization analysis beyond 6s which resulted in our test period being 4-6s after target presentation.

2.2.6 Statistical Analysis

In order to test our hypothesis that cortical error correction networks contribute to visuomotor control of arm posture, changes in EEG ROI beta band power, EEG hemisphere beta band power, EEG intra-region coherence, and EEG inter-region coherence during the stabilization period were characterized across participants using repeated measures two-way ANOVAs with task and space as factors in the analysis. Changes in EMG activity and EMG co-contraction during the stabilization period were characterized across participants using repeated measures one-way MANOVAs (Pillai's Trace) with task as the factor in the analysis; this allowed us to determine if co-contraction mechanisms were being utilized during the PER task. In order to ensure common kinematics between tasks, changes in hand speed and distance during the stabilization period were characterized across participants using repeated measures one-way ANOVAs with task as the factor in the analysis. One-way ANOVAs were used as *post hoc* tests if any effects were found significant in the two-way ANOVAs or one-way MANOVAs. The Holm-Sidak method for correcting for multiple comparisons was used at each level (between multiple ANOVAs) in the analysis except for the pairwise comparisons where the Tukey *post hoc* test was applied. When assumptions of the ANOVA were violated such as normality, a non-parametric bootstrap approach similar to

the Zhou and Wong method (Zhou & Wong, 2011) with 10000 iterations was used to generate the statistical distributions for the two-way ANOVA, one-way ANOVA, and Tukey *post hoc* test. Statistical tests were performed with a Type I error rate of $\alpha = 0.05$. All variables tested had at least one sample population that violated normality.

2.3 Results

2.3.1 Movement Kinematics

Hand kinematics (displacement and speed) during the stabilization period were similar for the PtP and CoC tasks and for the VOL and PER tasks with more movement and displacement occurring in the VOL and PER tasks. The one-way ANOVAs of hand displacement ($F(3,27)=29.93$, $p<0.0001$) and hand speed ($F(3,27)=46.41$, $p<0.0001$) during the stabilization period revealed significant differences among the tasks. The *post hoc* analysis (Tukey test) of task differences for hand displacement and hand speed revealed that hand displacement ($q(27)>8.62$, $p<0.0001$) and hand speed ($q(27)>10.25$, $p<0.0001$) were significantly lower in the PtP and CoC tasks when compared to the VOL and PER tasks. The lack of differences (hand displacement: $q(27)<1.17$, $p>0.848$; hand speed: $q(27)<2.62$, $p>0.27$) between the PtP (hand displacement: 0.24cm (SD 0.06); hand speed: 0.22cm/s (SD 0.08) and CoC (hand displacement: 0.37cm (SD 0.13); hand speed: 0.38cm/s (SD 0.17)) tasks as well as the lack of differences between the VOL (hand displacement: 3.04cm (SD 1.58); hand speed: 11.14cm/s (SD 4.86)) and PER (hand displacement: 2.73cm (SD 0.85); hand speed: 8.96cm/s (SD 2.61)) tasks indicate that hand kinematics were similar within these task pairs during the stabilization period and suggest they did not play a role in the significant differences found in the other variables.

2.3.2 Muscle Activity

In general, the EMG activity during the stabilization period was similar across all muscles in the PtP and VOL tasks and in the CoC and PER tasks with higher activity in the CoC and PER tasks, Figure 2-2A. The one-way MANOVA of EMG activity during the stabilization period revealed a significant difference ($F(18,72)=2.97$, $p=0.001$) between tasks for the muscles. The *post hoc* one-way ANOVAs for tasks showed significant differences between tasks in each muscle ($F(3,27)>2.81$, $p<0.049$). The *post hoc* analysis (Tukey test) of task differences within each muscle revealed that activity in PD and BI muscles was significantly lower in the PtP and VOL tasks when compared to the CoC and PER tasks ($q(27)>3.87$, $p<0.0361$), activity in the TRI and WE muscles was significantly higher in the CoC task when compared to the PtP and VOL tasks ($q(27)>5.15$, $p<0.0041$), activity in the WF was significantly lower in the PtP task when compared to the CoC task ($q(27)=4.73$, $p=0.012$) while the activity in the WF was significantly higher in the PER task when compared to the PtP, CoC, and VOL tasks ($q(27)>4.55$, $p<0.018$), and the activity in the AD did not result in any significant differences across tasks. The similarity in muscle activation between the PER and CoC tasks and the differences between the PER task and the PtP and VOL tasks indicate that more muscle activity was needed to position the arm during a stabilization (PER) task than is normally generated in a volitional arm movement (VOL) task, and that the level of muscle activity in an arm stabilization (PER) task resembles that seen in an arm co-contraction (CoC) task.

2.3.3 Muscle Co-contraction

EMG co-contraction during the stabilization period was similar across all muscle pairs in the PtP and VOL tasks with their EMG co-contraction being lower than the CoC and PER tasks, Figure 2-2B. The CoC and PER tasks had similar EMG co-contraction in the BI/TRI and WE/WF muscle pairs with a trend towards a significant difference in the AD/PD muscle pair. The one-way MANOVA of EMG co-contraction during the stabilization period revealed significant differences ($F(9,81)=6.84$, $p<0.0001$) between tasks for antagonistic muscle pairs. The *post hoc* one-way ANOVAs for tasks showed differences between tasks in each muscle pair ($F(3,27)>6.51$, $p<0.0015$). The *post hoc* analysis (Tukey test) on task differences within each muscle pair indicated that co-contraction in the BI/TRI and WE/WF pairs was significantly lower in the PtP and VOL tasks when compared to the CoC and PER tasks ($q(27)>4.62$, $p<0.0138$) and the co-contraction in the AD/PD pair was significantly higher in the CoC task when compared to the PtP and VOL tasks ($q(27)>5.33$, $p<0.0028$) with evidence for the co-contraction in the AD/PD pair being higher in the CoC task when compared to the PER task ($q(27)=3.58$, $p=0.066$). The similarity in muscle co-contraction between the PER and CoC tasks and the differences between the PER task with the PtP and VOL tasks indicated that more muscle co-contraction was used to position the arm in the stabilization (PER) task while minimal muscle co-contraction was used in the control (PtP) and volitional arm movement (VOL) tasks.

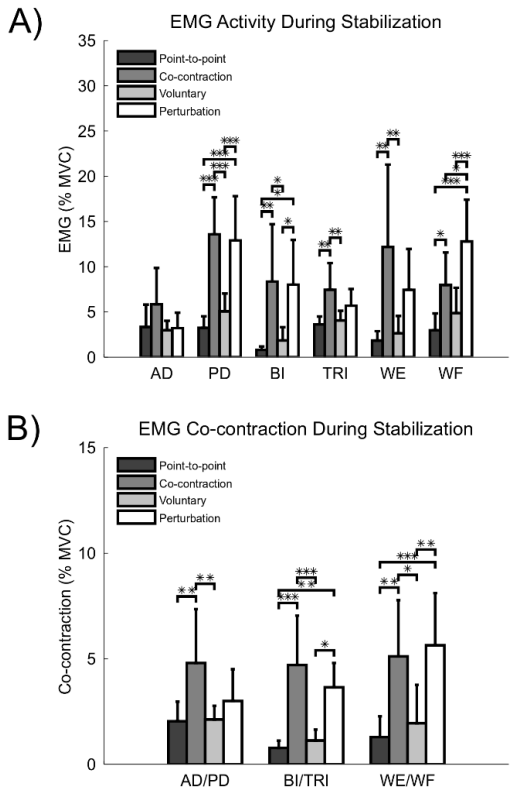

Figure 2-2: Muscle Activity and Co-contraction. A) EMG activity during the stabilization period. B) Co-contraction during the stabilization period. Muscles examined were the anterior deltoid (AD), posterior deltoid (PD), flexor carpi radialis (WF), extensor carpi ulnaris (WE), biceps (BI), and lateral head of the triceps (TRI). Both EMG activity and co-contraction were normalized to the respective muscle's MVC. The figures show the %MVC averaged across all participants (n = 10, 6 male) with the error bars denoting the 95% confidence interval about the mean. Significant differences determined via *post hoc* analysis (Tukey test) are indicated by stars (* indicates $p<0.05$, ** indicates $p<0.01$, and *** indicates $p<0.001$).

2.3.4 Beta Band Spatiotemporal Power

EEG beta band power was examined to identify the time course of task-related activity across the cortex (decrease in beta band power from baseline) and to determine if the cortical activity during a stabilization (PER) task resembled that of volitional control (VOL), co-contraction (CoC) tasks, or neither. A decrease in beta band power relative to baseline was identified in premotor, motor, sensory, and parietal cortices and was located

bilaterally in all tasks as shown in Figure 2-3. Source localization revealed that the spatiotemporal patterns of beta band power decrease were similar between the PtP and CoC tasks and the VOL and PER tasks, respectively. The time course of activity for the PtP and CoC tasks had a transient desynchronization during movement onset followed by a return to baseline power levels during the stabilization period. In contrast, beta band desynchronization was sustained throughout the movement and stabilization periods for the VOL and PER tasks. The spatial extent of decrease in beta band power during the initial reaching movement was slightly more extensive during the reach period for the VOL and PER tasks than the PtP and CoC tasks possibly indicating differences in planned motor commands due to the experimental block design. Similarities in spatiotemporal EEG beta band power between the PER and VOL tasks and the differences between the PER task compared to the PtP and CoC tasks indicate that cortical networks used to control the arm during the stabilization (PER) task share similar areas and levels of activation as those involved in volitional arm movements (VOL), while minimal cortical network activity is associated with stabilization via arm co-contraction (CoC).

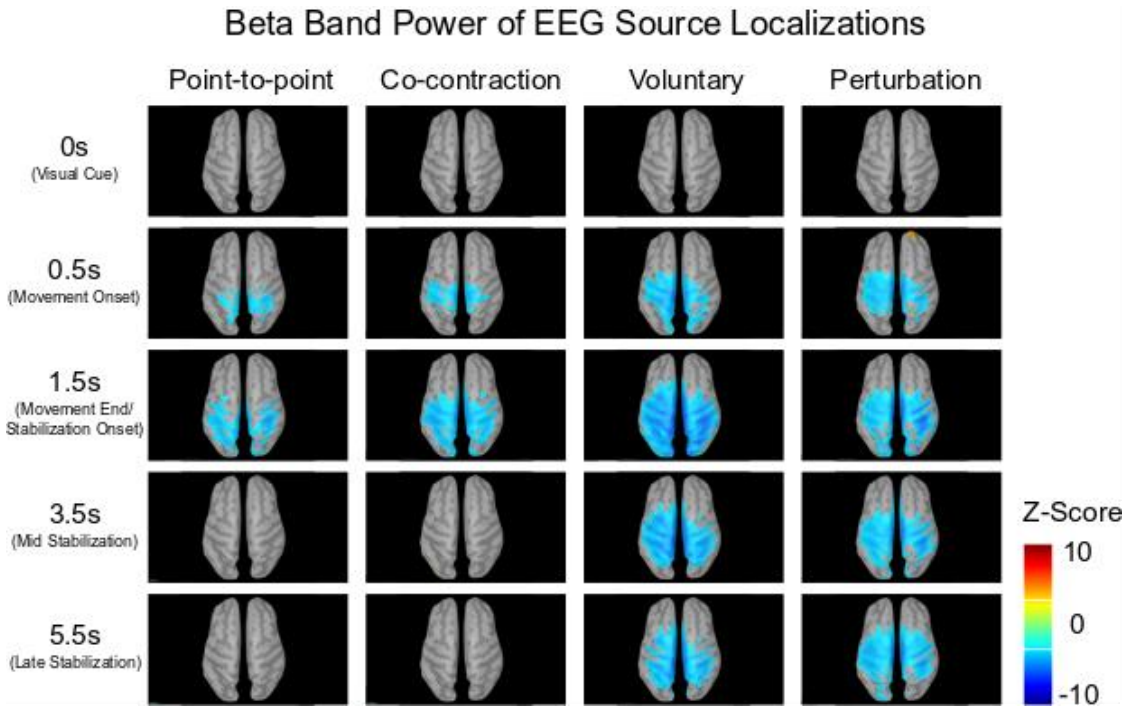

Figure 2-3: EEG Source Localization of Beta Band Power. The z-score averaged across participants (n = 10, 6 male) are shown for each task. Each brain image shows a snapshot of a key time point taken from the continuous activity time course averaged across all participants. Only values above or below a z-score threshold of ±3 are displayed. Negative values indicate beta band desynchronization while positive values indicate a resynchronization. The left hemisphere in each plot represents the hemisphere contralateral to the arm (dominant) tested.

2.3.5 Beta Band Hemisphere Power

The EEG beta band power during the stabilization period was lateralized with the left (contralateral) hemisphere having more beta band desynchronization as shown in Figure 2-4C. The VOL and PER tasks had similar activity as did the PtP and CoC tasks with the VOL and PER tasks' activity being higher, Figure 2-4D. The two-way ANOVA of beta band hemisphere power during the stabilization period showed no interaction effect but revealed a main effect of task ($F(3,27)=14.51$, $p<0.0001$) and hemisphere ($F(1,9)=9.32$, $p=0.012$). The *post hoc* analysis (Tukey test) of task differences indicated

that the decrease in power was significantly lower in the PtP and CoC tasks when compared to the VOL and PER tasks ($q(27)>5.12$, $p<0.008$). The analysis of hemispheric EEG beta band power demonstrated similar patterns of hemispheric activation across all four tasks, although the PtP and CoC tasks activated the pattern to a lower degree than the VOL and PER tasks. This could indicate an increased computational load during volitional movement generation (VOL) and stabilization (PER) of the arm when compared to a control (PtP) and arm co-contraction (CoC) task.

2.3.6 Beta Band ROI Power

In general, beta band power during the stabilization period was similar across all ROIs in the VOL and PER tasks with a larger decrease in beta band power than the PtP and CoC tasks as shown in Figure 2-4B. The PtP and CoC tasks had similar beta band power in all ROIs except for the Lateral Occipital gyrus where the CoC task showed a resynchronization of beta band power. The two-way ANOVA of ROI beta band power during the stabilization period revealed a main effect of task ($F(3,27)=13.2$, $p<0.0001$), a main effect of ROI ($F(6,54)=6.97$, $p<0.0001$) and an interaction effect between task and ROI ($F(18,162)=3.82$, $p<0.0001$). The *post hoc* one-way ANOVAs for task showed differences between tasks in all ROIs ($F(3,27)>5.12$, $p<0.0058$). The *post hoc* analysis (Tukey test) of task differences within each ROI indicated that the decrease in power in the Superior Frontal, Post-Central, and Superior Parietal gyri was significantly lower in the PtP and CoC tasks when compared to the VOL and PER tasks ($q(27)>4.12$, $p<0.038$), the decrease in power in the Caudal Middle Frontal and Pre-Central gyri was significantly higher in the PER task when being compared to the PtP and CoC tasks

($q(27)>4.03$, $p<0.0358$), the decrease in power in the Inferior Parietal gyrus was significantly higher in the PER task when comparing it to the PtP and CoC task ($q(27)>4.26$, $p<0.0293$) while the decrease in power in the Inferior Parietal gyrus was significantly higher in the VOL task when comparing it to the CoC task ($q(27) =6.44$, $p=0.008$), and the decrease in power in the Lateral Occipital gyrus was significantly lower in the CoC task when comparing it to the PtP, VOL, and PER tasks ($q(27)>4.69$, $p<.0123$). Similarities in ROI EEG beta band power between the PER and VOL tasks and the differences between the PER task compared to the PtP and CoC tasks indicated that similar cortical areas with similar levels of activation were used to control the arm in the stabilization (PER) task as those involved in volitional arm movements (VOL). Meanwhile, arm co-contraction (CoC) had minimal activation across ROIs and even inhibited cortical activation (negative beta band power) in the posterior ROIs.

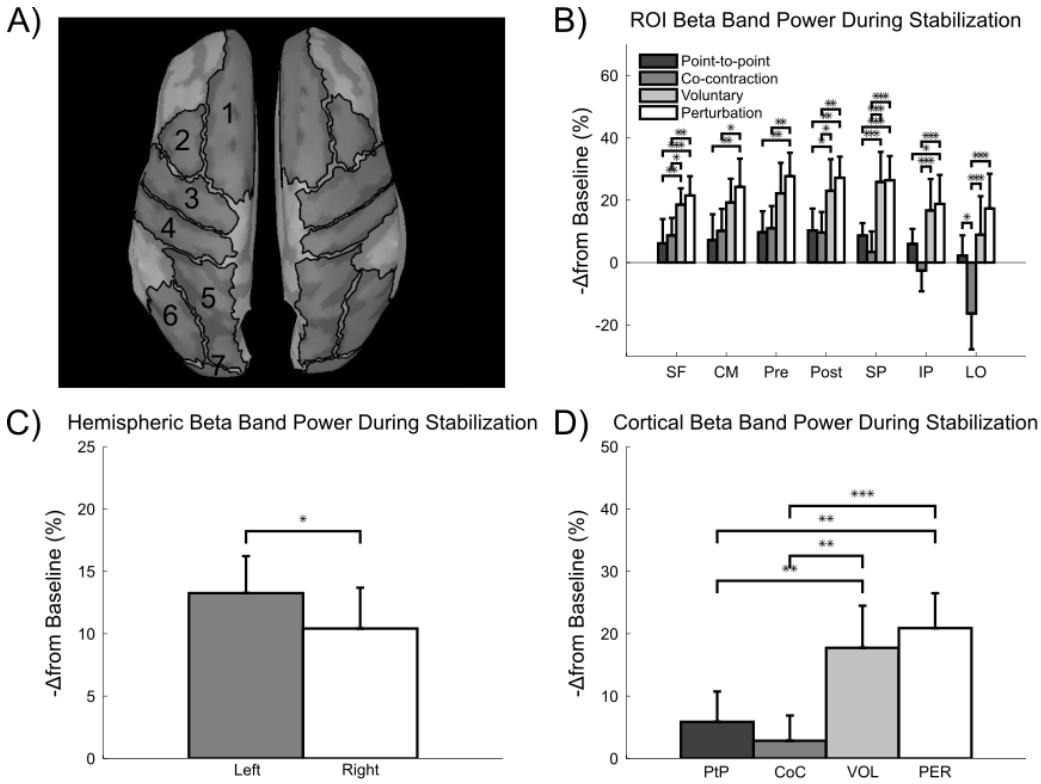

Figure 2-4: ROI Beta Band Power. A) Brain with seven ROIs examined: 1) left Superior Frontal Gyrus (SF), 2) left Caudal Middle Frontal Gyrus (CM), 3) left Pre-Central Gyrus (Pre), 4) left Post-Central Gyrus (Post), 5) left Superior Parietal Gyrus (SP), 6) left Inferior Parietal Gyrus (IP), and 7) left Lateral Occipital Gyrus (LO). B) ROI beta band power during the stabilization period for the left hemisphere (contralateral to tested arm). C) Hemispheric beta band power during the stabilization period. D) Cortical beta band power during the stabilization period, average of 14 ROIs (7 from each hemisphere). The figures show the beta band power percent change from baseline averaged across participants (n = 10, 6 male) with the error bars denoting the 95% confidence interval about the mean. Significant differences determined via *post hoc* analysis (B and D: Tukey test, C: two-way ANOVA main effect) are indicated by stars (* indicates $p<0.05$, ** indicates $p<0.01$, and *** indicates $p<0.001$).

2.3.7 Beta Band Electrode Coherence

EEG beta band coherence was examined to identify the cortical areas that were functionally connected during the tasks, how their interactions evolved over time and to compare the connectivity during stabilization for the task conditions (PER, VOL, CoC, PtP). Task-based coherence maps for electrode C3 (electrode over the sensorimotor

cortex associated with the task) and for all electrode combinations during each task are shown in Figure 2-5 and 2-6, respectively. Every coherence head map for electrode C3 had a similar pattern of coherence with the highest task-based coherence occurring around the mirrored electrode (C4) in the opposite hemisphere and the lowest task-based coherence concentrated in the area around electrode C3. Patterns of task-based coherence were similar between the PtP and CoC tasks and the VOL and PER tasks, respectively. The temporal profile of the PtP and CoC tasks had a transient increase in coherence during movement onset and early stabilization followed by a return to near baseline levels during late stabilization. In contrast, an increase in coherence was sustained throughout the movement and stabilization periods for the VOL and PER tasks. Even though the temporal patterns of task-based coherence were similar between the VOL and PER tasks, the PER task had much higher levels of coherence throughout electrodes that extended into the occipital areas. All-to-All coherence maps (maps of coherence between an electrode and all other electrodes) indicated that the PER task had more active connections at each time point and that the connections had a larger increase in coherence than the other three tasks. Similarities in EEG beta band coherence between the PER and VOL tasks and the differences between the PER task compared with the PtP and CoC tasks indicated that the cortical networks used in an arm stabilization (PER) task share similar task-based functional connectivity patterns as those involved in volitional arm movements (VOL), while minimal task-based functional connectivity seemed to be involved with arm co-contraction (CoC). The fewer functional connections to visual regions during the arm co-contraction (CoC) and volitional arm movement (VOL) tasks

as compared to the arm stabilization (PER) task point to the increased role visual information played in the arm stabilization (PER) task.

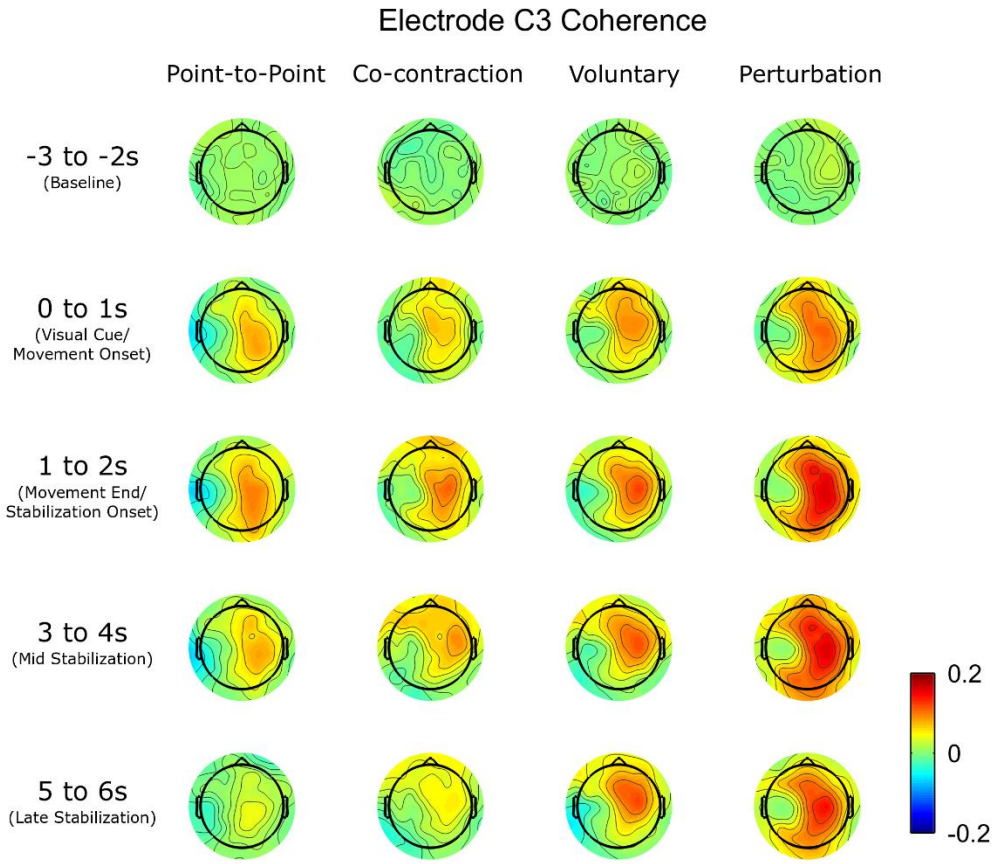

Figure 2-5: Electrode C3 Task-Based Coherence Maps Within the Beta Band. The task-based coherence (coherence change from baseline period) averaged across participants (n = 10, 6 male) is shown for each task. Each head plot corresponds to a one second coherence window displaying key time ranges of the movement that indicate how electrode C3's (left motor cortex) task-based coherence varied spatially with different electrodes. Values of coherence were interpolated between electrodes. Negative values indicate a decrease in coherence while positive values indicate an increase in coherence relative to the baseline period. The left half of each plot represents the hemisphere contralateral to the arm (dominant) tested.

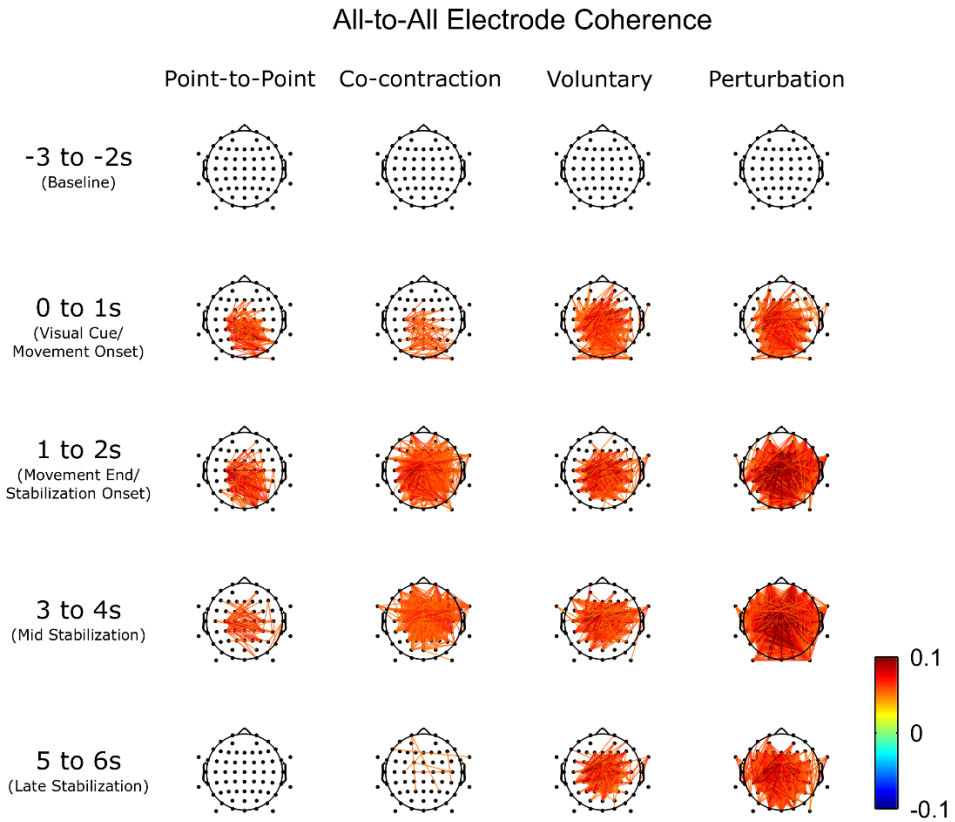

Figure 2-6: All-to-All Coherence Maps of Connectivity Within the Beta Band. Task-based coherence (relative to the baseline period) averaged across participants (n = 10, 6 male) is shown for each task. Each head plot corresponds to a one second coherence window displaying a key time range during the movement period and indicates the degree of functional connectivity between all pairs of electrodes. Only values above or below a task-based coherence threshold of ±0.05 are displayed; corresponding to the top 5% of coherence values observed during the baseline period. For each task, the threshold was calculated by generating a histogram of the baseline period task-based coherence values averaged across participants for all electrode-electrode combinations and finding the coherence value at which only 5% of all coherence values fell above. Negative values indicate a decrease in coherence while positive values indicate an increase in coherence relative to baseline. The left hemisphere in each plot represents the hemisphere contralateral to the arm (dominant) tested.

2.3.8 Beta Band Intra-Region Coherence

The intra-region task-based coherence during the stabilization period was similar in the frontal and visual regions for all tasks (Figure 2-7A). The sensorimotor region

showed differences between the PER task and the PtP and CoC task while the PtP and CoC tasks and VOL and PER tasks had similar task-based coherence during the stabilization period. The two-way ANOVA of intra-region task-based coherence during the stabilization period revealed an interaction effect ($F(6,54)=3.42$, $p=0.0062$) between task and region. The *post hoc* one-way ANOVAs for tasks showed differences between tasks in the sensorimotor region ($F(3,27)=7.04$, $p=0.0018$). The *post hoc* analysis (Tukey test) of task differences within the sensorimotor region indicated that the coherence was significantly higher in the PER task when compared to the PtP and CoC tasks ($q(27)>4.91$, $p<0.0091$). The similarities in intra-region task-based coherence in the frontal and visual regions indicate comparable levels of communication in these regions across tasks. The similar intra-region task-based coherence in the sensorimotor region between the PER and VOL tasks and the higher task-based connectivity in the PER task when compared to the PtP and CoC tasks indicated that the sensorimotor networks used in an arm stabilization (PER) task shared similar task-based functional connectivity patterns as those involved in volitional movements, and they tended to be larger than those found in the co-contraction (CoC) task.

2.3.9 Beta-Band Inter-Region Coherence

The inter-region task-based coherence during the stabilization period was similar for all region pairs for the PtP, CoC and VOL tasks (Figure 2-7B). The sensorimotor/visual region pair showed higher levels of task-based coherence in the PER task compared to all other tasks. The two-way ANOVA of inter-region task-based coherence during the stabilization period revealed an interaction effect ($F(6,54)=4.70$,

$p<0.0001$) between task and region pairs. The *post hoc* one-way ANOVAs for tasks showed differences between tasks in all region pairs ($F(3,27)>3.43$, $p<0.0299$). The *post hoc* analysis (Tukey test) of task differences within region pairs indicated that the coherence in the frontal/visual and the frontal/sensorimotor region pairs was significantly lower in the PtP task when compared to the PER task ($q(27)>5.13$, $p<0.0475$) and the coherence in the sensorimotor/visual region pair was significantly higher in the PER task when compared to the PtP, CoC, and VOL tasks ($q(27)>3.89$, $p<0.048$). The increase in inter-region task-based coherence of the sensorimotor/visual region pair for the PER task, when compared to the PtP, CoC and VOL tasks, suggested an increased reliance of sensorimotor processing on visual information during an arm stabilization (PER) task as compared to an arm co-contraction (CoC) or volitional arm movement (VOL) task.

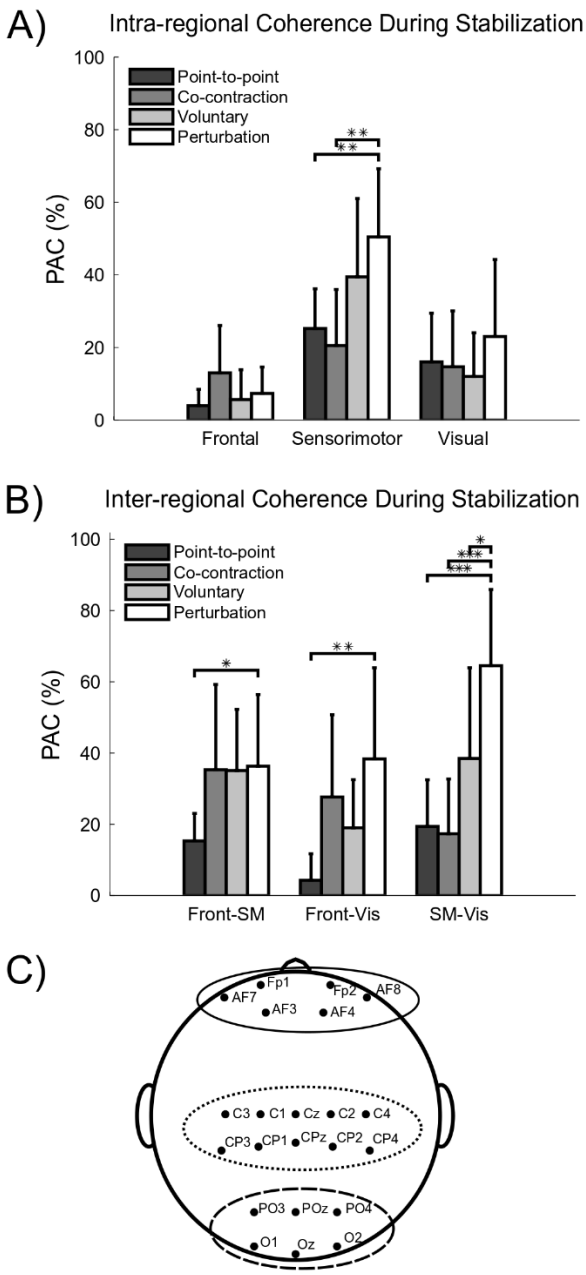

Figure 2-7: Regional Beta Band Coherence. A) Intra-region beta band coherence during the stabilization period. B) Inter-regional beta band coherence during the stabilization period. C) EEG electrode head map with electrode groups identified with circles. Solid circle: Frontal cortex (Front) (electrodes Fp1, Fp2, AF7, AF3, AF4, and AF8), dotted circle: Sensorimotor cortex (SM) (electrodes C3, C1, Cz, C2, C4, CP3, CP1, CPz, CP2, and CP4), dashed circle: Visual cortex (Vis) (electrodes PO3, POz, PO4, O1, Oz, and O2). The figures show the beta band PAC averaged across participants (n = 10, 6 male). Error bars denote the 95% confidence interval about the mean. Significant differences determined via *post hoc* analysis (Tukey test) are indicated by stars (* indicates $p<0.05$, ** indicates $p<0.01$, and *** indicates $p<0.001$).

2.4 Discussion

2.4.1 Main Results

In this study, we set out to identify the cortical mechanisms involved in arm stabilization and to test the hypothesis that cortical error correction networks contribute to visuomotor control of arm posture. This study demonstrated that visuomotor control of arm posture involves co-contraction of antagonistic muscles as well as cortical networks with increased connectivity between pathways associated with error correction. Specifically, during the stabilization period, cortical activity (reduction in EEG beta band power from baseline) during the PER task was comparable to that in the VOL task and did not resemble the activity seen in the PtP or CoC task (Figures 2-3, 2-4B, and 2-4D). The cortical networks identified during arm stabilization resembled those seen in volitional arm movement generation, suggesting volitional corrections may be one of the strategies the brain uses to stabilize the arm. The level of network connectivity (change in EEG beta band coherence from baseline) between the sensorimotor and visual regions was higher in the PER task when compared to the PtP, CoC, and VOL tasks (Figure 2-7B). Increased connectivity between the sensorimotor and visual regions suggests visual feedback of error to the motor cortex for the generation of corrective movements. Stiffening of the arm via co-contraction of antagonistic muscle pairs was higher during the PER task when compared to the PtP and VOL tasks (Figure 2-2), suggesting co-contraction mechanisms were also employed during stabilization of the arm. The presence of high cortical activity that resembled volitional motor generation and high connectivity in error pathways only seen in the stabilization (PER) task indicates the

involvement of cortical mechanisms in postural control of the arm that are distinct from short-latency impedance control of the arm via activation of antagonistic muscles and spinal/supraspinal reflex activity. Cortical networks encompassing sensory, motor and visual areas appear to play an important role in stabilization of arm posture.

2.4.2 Role of the Cortex in Visuomotor Control of Arm Posture

The comparable levels of cortical activation found between the VOL and PER tasks suggests that the brain may be using similar control mechanisms in both tasks. This similarity in cortical activity may arise from mapping the changes in limb position and/or from motor commands generated during the tasks. While passive movements of the upper limb have been found to activate similar cortical areas as active movements, the level of activation tends to be less (Formaggio et al., 2013; Guzzetta et al., 2007; Weiller et al., 1996). Furthermore, isometric force generation (Gwin & Ferris, 2012) and voluntary movements under ischemic nerve block conditions (Christensen et al., 2007) have been shown to involve cortical activation, indicating that motor output as well as sensory feedback/processing is associated with cortical activity. Although it is difficult to distinguish motor output from sensory feedback/processing, the need to identify visual changes in arm position from the target in the PER task, suggests the observed brain activity reflects the processing of sensory feedback in addition to generating volitional commands to stabilize the arm.

Measures of cortical coherence suggest that widespread cortical networks play an important role in arm stabilization. During the PER task, connectivity between the visual and sensorimotor networks was higher than the other tasks, suggesting the transfer of

visual information to sensorimotor cortices (Figure 2-7B). Since the VOL task is also a visuomotor task, we expected a similar network to the PER task, but to a lesser degree due to the lower task relevance of visual information and the lack of an error signal. Although not significantly different, the connectivity between the sensorimotor and visual regions was larger for the VOL task when compared to the PtP and CoC tasks (Figure 2-7B; $p<0.067$). Since the movement kinematics and sensory information were similar between the VOL and PER tasks, the PER task's increase in connectivity between the sensorimotor and visual regions suggests the recruitment a visual error network. Similar sensorimotor/visual networks have been reported in studies involving finger and wrist movements where the frontal lobe, sensory cortex, motor cortex, parietal cortex, and occipital lobe have been shown to function together to control movement (Chen et al., 2003; O'Neill et al., 2017; Sukerkar, 2010). These findings provide support for Hasan's hypothesis that cortically-driven intermittent voluntary corrections provide stability to arm posture (Hasan, 2005).

Although the results support the involvement of a cortical-mediated error network during arm stabilization, it is impossible to rule out the influence of spinal/supraspinal reflex circuitry on the observed cortical activation. Ideally, the study would have included metrics to quantify all three proposed mechanisms of arm stabilization: 1) increased impedance of the arm through the co-contraction of antagonistic muscles (Franklin et al., 2004), 2) spinal or supraspinal reflex circuits to provide corrective muscle activity (Kurtzer et al., 2008), and 3) intermittent voluntary corrections to errors in position (Hasan, 2005). Long latency, supraspinal, reflex activity is cortically modulated, generates cortical activity, and can be task dependent (Abbruzzese et al., 1985; Cheney &

Fetz, 1984; Pruszynski et al., 2011a; Pruszynski et al., 2008; Pruszynski et al., 2011b; Shemmell et al., 2009). Long latency reflexes also have the capacity to incorporate feedback from the task and modulate activity at the cortical level in a fashion similar to volitional movements (Mutha et al., 2008; Pruszynski et al., 2011a; Pruszynski et al., 2011b). However, the cortical activity associated with long latency reflexes is not as extensive as volitional movements (Suminski et al., 2007). Previous EEG research investigating long latency reflexes and volitional responses suggests different cortical mechanisms for each response based on differences in the EEG topographies (Spieser et al., 2010). One study suggests that long latency reflexes are associated with different visual pathways than voluntary corrections (Mutha et al., 2008), while another has even suggested that long latency mechanisms, postural stability and instructed reaction, use different neural pathways (Shemmell et al., 2009). Further, long latency reflex activity is still present in spinalized cats and monkeys (Ghez & Shinoda, 1978; Tracey et al., 1980), raising questions about whether supraspinal structures are directly involved in the reflex response. Spinal turtles can generate a scratch reflex (Stein & Grossman, 1980), and spinal frogs show stability of limb targeted movements (Pfluger, 1853), suggesting, at least in lower vertebrates, that reflexes and stability are still possible without cortical input. Thus, while the cortex may play a role in modulating long latency reflex activity, the associated cortical component/activity may differ from volitional control, and the mechanism of generation may lie within the spinal system.

2.4.3 Stabilization Mechanisms

The use of co-contraction, spinal/supraspinal reflex and cortically-driven voluntary correction mechanisms of postural control are not mutually exclusive and are likely all employed during arm stabilization tasks. We found increased levels of arm co-contraction in our stabilization (PER) task similar to that found in the pure co-contraction (CoC) task, indicating increased impedance of the arm through co-contraction of antagonistic muscles (Franklin et al., 2004). This result is consistent with previous research showing increased co-contraction of the arm provides stability to the limb (Franklin et al., 2003a; Franklin et al., 2003b; Gribble et al., 2003; Scheidt & Ghez, 2007). Although arm co-contraction is utilized, the minimal cortical activity in the CoC task compared to the extensive cortical activity in the PER task suggests that co-contraction is not the only active stabilization mechanism. Though not explicitly tested for in this study, spinal and supraspinal reflex circuits (Kurtzer et al., 2008) are likely also present during the PER task since both short latency (~25ms) and long latency reflexes (40-100ms) are observed in response to muscle stretch (Crago et al., 1976; Marsden et al., 1983). However, the cortical mediated error network identified in the PER task most likely reflects voluntary corrections to errors in position (Hasan, 2005).

Co-contraction, reflex control and voluntary corrections probably work in concert to provide stabilization after a reach. Co-contraction works to stabilize the limb when forces can be subdued with physical properties of the tissues at the joint (Franklin et al., 2003a; Franklin et al., 2003b). If the mechanical properties of the joint cannot provide the required stiffness for stability, reflex activity could increase stability. When reflex activity fails to produce stability or a more dynamic mode of stability is required (Mutha

et al., 2008), cortically driven voluntary corrections may be used (Hasan, 2005). In line with this idea, ankle and wrist stability requires not only intrinsic stiffness and reflex activity but also modulations of joint torque (Loram & Lakie, 2002; Suminski et al., 2007).

While this study focused on increased impedance of the arm through the co-contraction of antagonistic muscles (Franklin et al., 2004), spinal or supraspinal reflex circuits to provide corrective muscle activity (Kurtzer et al., 2008) and intermittent voluntary corrections to errors in position (Hasan, 2005) other potential stabilization mechanisms are possible. For example, fractional power damping, in which ongoing joint movements are braked by stretch reflexes in the antagonistic muscle, could also be used to stabilize the limb (Houk et al., 2000). In fractional power damping, motor commands are used to tune the stretch reflex thresholds, which sets a new equilibrium point of the joint. This model of antagonistic reflex activation around an equilibrium point results in a damped system with no oscillations. The fractional power damping model is limited in that it only describes an open loop process with respect to setting the equilibrium point. A complete model would also need to include visual feedback to generate accurate motor commands in the presence of error.

2.4.4 Bilateral Hemispheric Activation with Lateralization

EEG beta band power revealed extensive bilateral desynchronization during the stabilization phase of movement (Figure 2-3). Active areas of the cortex included but were not limited to the Superior Frontal, Caudal Middle Frontal, Pre-Central, Post-Central, Superior Parietal, Inferior Parietal and Lateral Occipital Gyrus. Previous EEG

studies examining voluntary thumb, finger, hand, and foot movements have reported event related desynchronization that is localized bilaterally near sensorimotor homunculi associated with the active muscle groups (Pfurtscheller et al., 1997, 1999; Pfurtscheller & Lopes da Silva, 1999). During movements of the entire arm, a larger portion of the cortex undergoes event related desynchronization suggesting that the number of muscle groups activated affects event related desynchronization (Pfurtscheller et al., 1999). In addition, Pfurtscheller and colleagues (Pfurtscheller et al., 1994) have shown that visual and parietal areas exhibit event related desynchronization during a visual processing task. In this study, muscle groups of the entire arm were active during a more complicated endpoint visuomotor stabilization task which may have contributed to the extensive cortical activation.

In addition to the extensive bilateral activation during visuomotor control of arm posture, the contralateral hemisphere was significantly more active than the ipsilateral hemisphere (Figure 2-4). This observation supports previous EEG and fMRI studies examining hand movements, which consistently show bilateral cortical activity to be more pronounced on the contralateral hemisphere (Formaggio et al., 2013; McFarland et al., 2000; Yuan et al., 2010). Even though the lateralization of cortical activity to the contralateral hemisphere is expected, there was little interaction between task and hemisphere associated with a “dynamic dominance” mechanism (Sainburg, 2002; Sainburg, 2005), in which the dominant limb/hemisphere is specialized for coordination and the non-dominant limb/hemisphere is specialized for stabilization. The “dynamic dominance” hypothesis would predict that the cortical activity in the PtP, CoC, and PER task (end point stabilization processes) to be lateralized to the ipsilateral (nondominant)

hemisphere while the cortical activity in the VOL task (trajectory control processes) would be lateralized the contralateral (dominant) hemisphere. While cortical activity was lateralized to the contralateral hemisphere, both trajectory control (VOL) and end point stabilization (PtP, CoC and PER) tasks also showed ipsilateral activation.

2.4.5 Decrease of Cortical Activity During Co-contraction

An interesting finding was the lack of a sustained beta band desynchronization during the stabilization period of the CoC task (Figures 2-3 and 2-4B). The lack of cortical activity occurred despite EMG activity at similar levels as the PER task (Figure 2-2A). The only notable differences in the CoC and PER tasks during the stabilization period were that the hand was moving during the PER task (hand speed: 8.96cm/s (SD 2.61)) with the target still visible while the hand was stationary (hand speed: 0.38cm/s (SD 0.17)) with no visual feedback of the target in the CoC task. The lack of cortical activity during the sustained contraction is not unique to this study and has been documented in sustained wrist contractions and isometric contractions of the lower limb (Alegre et al., 2003; Gwin & Ferris, 2012).

One possible explanation for the reduction in cortical activity is that activity associated with sensory feedback is large compared to the actual generation of motor commands (Weiller et al., 1996). Muscle and skin afferents provide feedback of proprioception at the cortical level, evidenced by EEG evoked responses from imposed joint movements (Kornhuber & Deecke, 2016) or nerve stimulation (Dawson, 1947; Giblin, 2006). Although the static proprioceptive feedback was similar across all tasks, movements of the limb during PER and VOL tasks could have triggered sensory EEG

signals that differentiated the EEG patterns from CoC and PtP tasks. EEG and fMRI studies report similar areas of the cortical activation with slightly lower activation in passive versus active movements (Formaggio et al., 2013; Guzzetta et al., 2007; Weiller et al., 1996). Beta desynchronization associated with joint movement is reduced in stroke survivors with pure somatosensory deficits (Platz et al., 2000) or when sensory feedback is muted by prolonged vibration (Lee & Schmit, 2018). While sensory feedback/processing does seem to play a large role in cortical activation associated with the control of movement, imagined hand movements (Formaggio et al., 2013; McFarland et al., 2000), attempted movements in people with spinal cord injury (Gourab & Schmit, 2010), isometric force generation of the lower extremity (Gwin & Ferris, 2012) and voluntary movements under ischemic nerve block conditions (Christensen et al., 2007) produce cortical activation, suggesting that proprioceptive feedback is only one driver of cortical activity in motor tasks.

Another possible explanation for the lack of cortical activity during CoC arises from the concept that beta band activity corresponds to an idling rhythm in the motor system that maintains the current state (Engel & Fries, 2010; Pfurtscheller & Lopes da Silva, 1999). Evidence for the maintenance of the current motor state comes observations of impaired motor performance during naturally or artificially enhanced levels of beta band activity, suggesting that the increased beta band activity prevents the motor system from making dynamic changes (Gilbertson, 2005; Pogosyan et al., 2009). This is supported by Swan and colleagues (Swann et al., 2009), who showed that successful stop trial performance in a Go/NoGo task is associated with enhanced beta band activity.

Lastly, the lack of cortical activity seen during sustained co-contraction may be because co-contraction mechanisms are relegated to the spinal level. After a spinal cord injury, humans have been shown to have altered upper extremity reaching movements (Wierzbicka & Wiegner, 1996; Wierzbicka & Wiegner, 1992). In connection with this, Cremoux and colleagues have shown that co-contraction increases after a spinal cord injury; possibly due to reduced cortical influence on spinal mechanisms that inhibit antagonist muscle activity (Cremoux et al., 2017). These studies suggest that the observed lack of cortical activity witnessed during sustained isometric contraction may be a combination of reduced afferent input, maintenance of the current motor state and co-contraction mechanisms being located at the spinal level.

2.4.6 Study Limitations

The current experimental design controlled for several confounding factors, such as ordering effects and movement kinematics, that may have influenced the results; however, other factors may have impacted the observed changes in beta band desynchronization across tasks including stabilization via trunk muscles, EEG contamination by muscle activity, exclusion of true EEG signals and separation of spinal/supraspinal activity from cortically driven activity. During the study, participants were seated in a chair but were not otherwise restrained. Although participants were monitored throughout the experimental sessions for trunk movements, with none being noted, the setup may have allowed participants to engage stabilizing trunk muscles differently across conditions, eliciting task-specific changes in cortical activity not specifically tied to the arm movement.

Other potential confounding factors arose in the EEG data processing pipeline. During analysis of the EEG data, AMICA was performed to separate the recorded EEG data into signal and artefact components. It is possible that the AMICA algorithm did not fully separate signal and artefacts, resulting in the removal of some cortical signals and/or the inclusion of some artefactual components in the subsequent source imaging and analysis. This could explain the increase in beta band power in the Lateral Occipital region during the CoC task (Figure 2-4B). During the CoC task, participants displayed increased muscle tension in the arm and neck that may have propagated to posterior EEG recording sites and presented as an increase in beta band power that was task-related and not fully separable using AMICA. In an independent component analysis study examining artefact removal, experts label about 17% of independent components as muscle artefact which makes up about 68% of all artefactual components (Winkler et al., 2011). This equates to around 25% of independent components being artefactual. In our case, we removed an average of 14 independent components from each participant which is approximately 22% of all components.

Providing visual feedback of the hand during the PER task may have biased the cortical mediated error networks towards visual display errors and resulted in a cortical network utilizing volitional corrections. Behavioral studies where participants have true or shifted visual feedback of their reaching finger towards visual or proprioceptive targets have shown that the false visual feedback has no effect on movements directed toward proprioceptive targets (Sarlegna & Sainburg, 2007; Sober & Sabes, 2005). This contrasted with the large reaching errors that result from the visual shift when participants reach for visual targets, suggesting that somatosensory input has a greater

influence when planning movements toward proprioceptive targets while visual feedback prevails when reaching for visual targets. (Sarlegna & Sainburg, 2007; Sober & Sabes, 2005). If we had done an arm stabilization task without visual feedback, we believe the patterns of cortical network activity would have differed with respect to the primary sensory areas involved in the corrective movement. Specifically, we would have expected the cortical mediated visual error network to shift to a proprioceptive-based error network located in the somatosensory region (Filimon et al., 2009; Mann et al., 1996), but still including sensory parietal areas (Suminski et al., 2007).

A limitation of this study is the small sample size of only 10 participants. A power analysis conducted prior to running the experiment using pilot data found that a sample size of 10 participants provided experimental power for Type II error greater than 80% for the variables tested. A *post hoc* analysis of experimental power for Type II error was done and confirmed that the assumed level of variability was consistent with that observed.

Another possible limitation to the study centers around the choice of reference electrode and volume conduction effects associated with the coherence analysis used to characterize functional connectivity. Previous studies (Essl & Rappelsberger, 1998; Nunez et al., 1999; Rappelsberger, 1989) examining the effect of reference electrode choice have shown that coherence is dependent on the reference electrode or referencing scheme (common average, linked mastoids, etc.). The use of a single electrode as the reference can inflate or deflate coherence values depending on the level of activity at the reference electrode; with higher values at the reference electrode being detrimental to coherence (Zaveri et al., 2000). Rappelsberger (Rappelsberger, 1989) suggested using a

reference averaging technique, such as linked earlobes, to better approximate a zero-potential reference, which could to help mitigate this issue. While the common average reference provides an alternative averaging technique, the tendency for EEG signals to be synchronized over large areas of the scalp can result in a common average reference remaining high. Coherence is also impacted by volume conduction effects that result in spatial blurring of cortical point sources measured at the scalp due to the spatial filtering properties of the cerebrospinal fluid, skull, and scalp. Volume conduction results in significant coherence between EEG electrodes that can extend over distances larger than 8cm (Nunez et al., 1997) even if the cortical regions immediately below the electrodes are not functionally connected. Imaginary coherence (Nolte et al., 2004) and orthogonalization techniques (Brookes et al., 2012; Hipp et al., 2012) can be used to mitigate this issue. In the current study, we chose to examine task-based coherence (Rappelsberger et al., 1994) which effectively subtracts out the baseline level of coherence, along with the volume conduction effect, from the task period coherence (Chen et al., 2003). While the subtraction approach significantly reduced the impact of the volume conduction artefact on the coherence measure, it rendered near zero task-based coherence values for adjacent electrodes due to the dominant effect volume conduction has on nearby electrodes (Figure 2-5). The impact was minimized, however, by comparing the same connections across tasks rather than different connections within tasks.

During the CoC task, co-contraction during the stabilization period was not sustained at the targeted 10-20% but was instead found to hover around 5%. Throughout the feedback period of the CoC task (0-2s), it was noted that participants tended to

fluctuate their level of co-contraction around the lower threshold of 10%. Once feedback was removed, participants maintained high levels of co-contraction that slowly reduced in magnitude over time. This slow drift continued through the stabilization period (4-6s). The reduction is consistent with participants' self-reports following testing that sustaining a 10-20% co-contraction was difficult. This indicates a higher than expected effort during the CoC task, which may result from the fact that the levels of co-contraction were normalized by MVC and that people asked to maximally co-contract only produce about 50% of the EMG produced during muscle maximal contraction (Milner et al., 1995; Tyler & Hutton, 1986). Another possible explanation may be that the arm was in a different orientation when the co-contraction was being produced during the tasks than when the MVCs were collected. Collecting MVCs in different limb positions has been shown to alter the amount of EMG being produced in the muscle (Boettcher et al., 2008; Buchanan et al., 1989; Singh & Karpovich, 1966). Although the level of co-contraction was not sustained at the requested level during the CoC task, the increased levels of co-contraction in the CoC task compared to the PtP task in Figure 2-2B, together with the participant feedback indicate that they were actively co-contracting at higher levels than normal throughout the task.

2.5 Conclusion

Cortical activity during stabilization of the arm was similar to that during volitional movement of the arm suggesting the brain might generate volitional movement commands to stabilize the arm. Cortical connectivity during stabilization of the arm was increased between sensorimotor and visual regions which might be attributed to a

visuomotor error network that utilizes visual error information to update the motor commands of the arm. Cortical activity and connectivity during stabilization of the arm indicate the involvement of cortical networks that contribute to visuomotor control of arm posture. This chapter has been published previously in the Journal of Neurophysiology (Snyder et al., 2019).

CHAPTER 3: ELECTROENCEPHALOGRAPHY RESTING STATE NETWORKS IN PEOPLE WITH STROKE

3.1 Introduction

The purpose of this study was to characterize reorganization of resting state cortical networks after stroke using electroencephalography (EEG). Functional magnetic resonance imaging (fMRI), magnetoencephalography (MEG) and EEG all reveal regions of the brain that have common activation patterns, which are thought to be representative of functionally connected networks (Aoki et al., 2015; Biswal et al., 1995; Brookes et al., 2011; Rosazza & Minati, 2011). Some of the more common cortical networks obtained during resting state include the default mode, sensorimotor, executive control, visual, lateralized fronto-parietal, auditory and temporo-parietal networks (Aoki et al., 2015; Biswal et al., 1995; Brookes et al., 2011; Rosazza & Minati, 2011). The brain utilizes these cortical networks in different ways including memory consolidation, cognition, vision, and movement (Bressler, 1995; Corbetta, 1998; Mazoyer et al., 2001; Sukerkar, 2010). An improved understanding of the changes in cortical networks after stroke would provide insight into the mechanisms underlying functional loss and recovery.

Based on fMRI, there is generally an increased activity in both hemispheres (excluding the lesioned region) and decreased connectivity within and between hemispheres during motor tasks (Carey et al., 2002; Grefkes et al., 2008; Mintzopoulos et al., 2009; Rossini et al., 1998; Ward et al., 2003). While fMRI offers excellent spatial resolution (~1mm) of the cortex, it lacks temporal resolution (~1s) which prevents the study of underlying brain processes that act at the millisecond time scale (Koenig et al., 2005; Lopes da Silva, 2013). EEG and MEG imaging modalities, with better temporal

resolution (~1ms) (although poorer spatial resolution (~5cm)), have been employed to overcome this issue. EEG and MEG sensorimotor task-based studies in people with stroke show impairment-specific changes in activity, with a decrease in activity near the lesion, increased asymmetries, and connectivity increases within the lesioned motor networks (Bönstrup et al., 2018; Platz et al., 2000; Rossiter et al., 2014; Stępień et al., 2011; Strens et al., 2004). Although fMRI and EEG/MEG measurements yield differing results after stroke (likely due to the differing spatial/temporal scales, metrics examined and/or the stroke group's impairment level), both imaging modalities have identified similar networks, demonstrate that activity/connectivity relates to functional/behavioral outcomes and indicate that patterns normalize with recovery (Bönstrup et al., 2018; Grefkes et al., 2008; Grefkes & Fink, 2014; Strens et al., 2004; Ward et al., 2003). Despite task-based studies being useful, they tend to be limited to stroke participants who can perform the tasks and can result in mirror movements that confound interpretation of the results (Calautti et al., 2007; Dong et al., 2006; Ward et al., 2007; Weiller et al., 1993; Wittenberg et al., 2000).

Resting state paradigms, where participants remain still and relaxed, have the advantage of including participants of all functional abilities and are easier and quicker to administer. After stroke, resting state EEG demonstrates increased bilateral power in the delta and theta bands, increased power asymmetries and decreased connectivity in the alpha and beta bands within the lesioned area (Assenza et al., 2013; Dubovik et al., 2012, 2013; Köpruner & Pfurtscheller, 1984; Wang et al., 2012; Wu et al., 2015). While resting state networks in people with stroke indicate changes in cortical activity and connectivity,

there are elements of the analysis that confound the identification of the networks and hamper interpretation of the resulting data.

The analysis of resting state EEG is influenced by electrode impedance, neuronal density under each electrode and volume conduction. The power of resting state EEG is affected by electrode impedance such that electrodes with lower impedance display higher signal power. In addition, larger synchronous neuronal populations beneath an electrode produce greater signal power, which may influence interpretation of the signal size, especially in people with loss of brain tissue after stroke. EEG estimates of functional connectivity are also affected by volume conduction. Volume conduction results in significant connectivity between EEG electrodes that can extend over distances as large or larger than 8cm (Nunez et al., 1997) even if the cortical regions immediately below the electrodes are not functionally connected. Imaginary coherence (Nolte et al., 2004), orthogonalization techniques (Brookes et al., 2012; Hipp et al., 2012) and other phase metrics that exclude zero lag connectivity (Nolte et al., 2008) can be used to mitigate this issue.

The frequency characteristics of resting state EEG can provide valuable insight into the functional networks of the brain after stroke. Brain networks with a large neuronal population or spatial extent oscillate at lower frequencies (Bullock et al., 1995; Eckhorn, 1994; Kopell et al., 2000; von Stein & Sarnthein, 2000). This observation led Nunez to develop a theoretical framework for the inverse relationship between frequency of activity and spatial scale of a network (Nunez, 2000). Further, local sensory integration invokes gamma band activity, multisensory integration produces upper alpha and lower beta band activity, while long range interactions invoke theta and alpha band activity

(von Stein & Sarnthein, 2000). Gamma band synchronization decreases with distance, with lower frequency oscillations associated with longer range interactions (Bullock et al., 1995; Eckhorn, 1994; Kopell et al., 2000). These cortical network frequency dependencies arise from the physical architecture of the networks, speed of communication due to axon conduction/synaptic delays and the number of synapses involved in the network path (Nunez, 1995; von Stein et al., 2000). Thus, it is important to consider spectral information in the interpretation of EEG activity and connectivity data.

In this study, we set out to quantify the changes in resting state cortical network power and connectivity in people with chronic stroke. We collected EEG data while participants were in a relaxed, resting state. EEG power was normalized to reduce bias and used as an indicator of network activity. Correlations of orthogonalized EEG activity were used to measure of functional connectivity between cortical areas. We hypothesized that cortical networks are more asymmetric after stroke and that there is a shift in the frequency due to changes in cortical communication after stroke. Specifically, we expected cortical networks to have a higher reliance on local network activity with less efficient pathways connecting distant regions, resulting in a shift to higher frequency.

3.2 Methods

3.2.1 Participants

A sample of 14 chronic stroke participants and 11 age-matched neurologically-intact controls participated in this study. Stroke participants (8 male, aged 36-79yr) were required to be at least 1-year poststroke. Exclusion criteria included the diagnosis of any

other neurological disorder or recent treatment that interfered with neuromuscular function, such as botulinum toxin injection. The impairment level of stroke participants was assessed using the upper extremity Fugl-Meyer Assessment (FMA), which consists of a motor portion (maximum score 66) and a sensory/proprioception portion (maximum score 12) (Fugl-Meyer et al., 1975), and the Semmes-Weinstein monofilament test (Semmes et al., 1960). The monofilament test was performed at seven locations on the palmar surface of the paretic hand and averaged (distal phalanx of the small finger, index finger and thumb; proximal phalanx of the small and index finger; thenar and hypothenar). Control participants (7 male, aged 34-77yr) reported no history of stroke or any other neuromuscular pathology. Detailed demographic data for all participants is shown in Table 3-1. All participants gave written informed consent, and all procedures were approved by the Marquette University Institutional Review Board in accordance with the Declaration of Helsinki.

Table 3-1: Participant Information. Demographic and clinical data for stroke (S) and control (C) participants. “Fugl-Meyer” indicates the Fugl-Meyer upper extremity score (Motor: maximum of 66; Sensory: maximum of 12). Monofilament values indicate the average force in grams (g) across the seven hand locations tested with the degree of sensation (N: normal (g<=0.07), ‘-’: diminished light tough (0.07>g<=0.4), ‘--’: diminished protective sensation (0.4>g<=2.0), ‘---’: loss of protective sensation (2.0>g<=180.0), ‘----’: deep pressure sensation only (g>180)). (F: female; M: male; ND: non-dominant).

Participant Identifier	Sex	Age (yr)	Time after Stroke (yr)	Fugl-Meyer (Motor:66)	Fugl-Meyer (Sensory:12)	Monofilament (g,sensation)
S1	F	60	23	63	12	0.08 (-)
S2	F	79	7	62	11	0.15 (-)
S3	F	67	30	29	12	0.05 (N)
S4	M	57	2	28	6	134.29 (---)
S5	M	64	16	61	8	0.19 (-)
S6	F	66	26	51	4	60.00 (---)
S7	M	61	11	31	12	0.35 (-)
S8	F	65	13	38	8	94.29 (---)
S9	M	64	14	34	12	50.28 (---)
S10	M	59	14	23	8	60.00 (---)
S11	M	73	7	21	8	100.00 (---)
S12	M	36	8	21	8	71.43 (---)
S13	F	71	4	30	12	0.01 (N)
S14	M	55	15	27	12	37.43 (---)
C1	F	68	-	-	-	-
C2	M	64	-	-	-	-
C3	M	61	-	-	-	-
C4	M	51	-	-	-	-
C5	F	77	-	-	-	-
C6	F	57	-	-	-	-
C7	M	67	-	-	-	-
C8	M	65	-	-	-	-
C9	F	63	-	-	-	-
C10	M	34	-	-	-	-
C11	M	64	-	-	-	-

3.2.2 Experimental Protocol

During the study, participants were seated in a chair and asked to remain as still as possible, keep their eyes closed, refrain from making any eye movements and clear their mind. EEG data were collected for approximately 3 minutes in this relaxed, resting state.

3.2.3 Physiological Measurements

A 64-channel active electrode actiCAP (Brain Products GmbH, Munich, Germany) system was used to record EEG data. EEG electrodes were arranged in the conventional 10-20 system with the reference at FCz and the ground at AFz. The EEG cap was placed on the participant's head such that the Cz electrode was in line with the prearticular points in the frontal plane and with the nasion and inion points in the sagittal plane. SuperVisc gel (Brain Products GmbH, Munich, Germany) was applied between the scalp and electrodes to lower the electrode impedances below 10kOhms prior to data collection. EEG data were amplified, sampled at 1kHz, filtered from 0.1 to 200Hz and notch filtered at 60Hz using a Synamps^2 amplifier system (Neuroscan, Charlotte, North Carolina), and recorded using Neuroscan software, Scan 4.5.

3.2.4 Data Analysis

EEG data were post processed and analyzed using the EEGLAB toolbox (version v13.4.4b) (Delorme & Makeig, 2004) for storing and configuring the data, FieldTrip (version 2016-01-03) (Oostenveld et al., 2011) for removing bad epochs and electrodes, Brainstorm (version 3.4) (Tadel et al., 2011) for source localization, Network Based Statistic Toolbox (version 1.2) (Zalesky et al., 2010) for statistically comparing network connectivity, BrainNet Viewer (version 1.62) (Xia et al., 2013) for visualizing network

connectivity and custom MATLAB scripts (version 2014a, MathWorks, Natick, Massachusetts). All EEG data were bandpass filtered (1-50Hz) using a fourth order zero-phase Butterworth filter. Trial epochs of the EEG data were then extracted by creating 2s, consecutive, non-overlapping windows starting at the beginning of the file and continuing until a complete 2s window could not be formed. This process resulted in approximately 90 epochs per participant. EEG epochs were then zero-meaned and bad channels and epochs removed manually using FieldTrip's visual inspection code (channel/epoch removed if variance/kurtosis >2 standard deviations from the mean, 'ft_rejectvisual', average number channels/epochs removed, 0.8/10.4). If a channel was rejected from the EEG data, its value was replaced with interpolated data from the surrounding electrode channels. Stroke participant EEG data were flipped so that the hemisphere associated with the lesion was always represented on the left. EEG data were then separated into signal and artefactual components using an Adaptive Mixture Independent Component Analysis (AMICA) (APPENDIX C: INDEPENDENT COMPONENT ANALYSIS) (Palmer et al., 2008), with 64 independent temporal components. Signal artifacts, including electromyography and movement artifacts, were identified by distinct artefactual characteristics (Delorme et al., 2012; Makeig et al., 2004; Mognon et al., 2011; Puce & Hämäläinen, 2017) and removed from the EEG data (average number of artefact components removed, 6.6; minimum number: 3; maximum number: 15). The remaining components were then transformed back to the EEG channel space. Finally, EEG data were re-referenced to a common average reference for all data analyses. The re-reference technique reintroduced the FCz electrode to the data set. For the following analyses, EEG data were separated into ten non-overlapping 5Hz frequency bands

ranging from 1 to 50Hz (first band only ranged from 1-5Hz due to the 1Hz high pass filter applied during preprocessing) to determine if frequency shifts occurred in the stroke group relative to the controls.

A power spectrum analysis was performed at the electrode level to examine the spatial characteristics of resting state EEG power across frequency bands. The power spectrum at every electrode was calculated using Welch's method with epochs as the measure of consistency (Welch, 1967). The frequency bands were then extracted from the power spectrum and normalized at each electrode using equation 3.1,

$$NP = 100 \times \frac{\sum F}{\sum Total} \qquad (3.1)$$

where NP represents the normalized power, $\sum F$ represents the sum of power within a frequency band, and $\sum Total$ represents the sum of power across the frequency spectrum (1-50Hz). By normalizing power in this fashion, we can determine if the cortical area's function (distribution of power across the spectrum) is changing while removing any dependence on electrode impedance or neuronal population size. To characterize any effects that stroke lesions may have on spatial distribution of frequency, the control and stroke groups were compared at every electrode within each frequency band using a two-sample t-test with a false discovery rate (FDR) of $\alpha = 0.05$ for multiple comparisons correction. To facilitate interpretation of normalized power, average absolute power within frequency bands was computed and plotted for each electrode to determine if normalized power differences between controls and stroke survivors were due to true absolute power changes within frequency bands or if a normalization bias was driving the normalized power differences. For instance, a loss of absolute power in one frequency band could result in normalized power increases in other frequency bands, even though

they are not changed on an absolute level. Similar to normalized power, absolute power for control and stroke groups were compared at every electrode within each frequency band using a two-sample t-test with a false discovery rate (FDR) of $\alpha = 0.05$ for multiple comparisons correction.

To determine if frequency bands displayed power differences between hemispheres, an electrode directional asymmetry (*EDA*) metric was computed between analogous electrodes in the two hemispheres using equation 3.2,

$$EDA = 100 \times \frac{1}{n} \sum \frac{NP_L - NP_R}{|NP_L| + |NP_R|} \qquad (3.2)$$

where EDA is the whole head electrode directional asymmetry, NP_L is the normalized power of the homologous electrode in the left hemisphere, NP_R is the normalized power of the homologous electrode in the right hemisphere and n is the total number of electrode pairs. Electrodes along the midline were ignored for calculation of the EDA.

Volume source localization of EEG data was performed to enable volumetric connectivity analyses. Distributed current dipole volumes were computed in Brainstorm using the default MNI/ICBM152 anatomical brain template with the cerebellum included (Tadel et al., 2011). The standard actiCAP electrode locations were fit to the scalp surface so that the Cz electrode location was at the vertex as described in the physiological measurements section. A boundary element model (BEM) was used to estimate the forward model (OpenMEEG) (Gramfort et al., 2010; Kybic et al., 2005) with volumetric vertices (5x5x5 mm) placed on a regular grid spanning the entire brain. A depth-weighted minimum L2 norm estimator of current density (Hämäläinen & Ilmoniemi, 1994) was used to estimate the inverse model where each vertex consisted of three orthogonal dipoles (representing the x, y and z directions). The three-dimensional

dipole activity for every vertex was subsequently processed using a principle component analysis (PCA) to obtain a single activity time course that best represented the volumetric source.

Following the projection of EEG data into volumetric source space, the functional connectivity between all brain regions was calculated within the defined frequency bands, Figure 3-1. First, the source localized data were bandpass filtered using a zero-phase fourth order Butterworth filter to extract the different frequency bands; the resulting data were then concatenated across epochs within frequency bands. A reduced version (described below) of the Automated Anatomical Labeling (AAL) atlas (Tzourio-Mazoyer et al., 2002) from the MRIcron software package (https://people.cas.sc.edu/rorden/mricron/index.html) was used to define volumes of interest (VOI) for input into the connectivity analysis. Reductions to the original AAL atlas VOIs were necessary because we intended to orthogonalize the VOI time courses to reduce the effect of volume conduction on connectivity analyses. Orthogonalization by way of a symmetric multivariate correction (Colclough et al., 2015) is dependent on the rank of the data (which was limited to 61 due to one participant only having a maximum of 61 valid electrodes after preprocessing). Therefore, we reduced the original 116 AAL atlas VOIs to 61 VOIs, Figure 3-1. The 12 subcortical structures (left and right) were left unaltered, while the 9 cerebellar VOIs within each hemisphere and 8 vermis VOIs were merged, respectively. The 34 cortical VOIs in the left hemisphere were reduced to 23 iteratively by finding the smallest VOI and merging it with the nearest VOI based on VOI centroid locations. The homologous VOIs merged in the left hemisphere were then merged in the right hemisphere in order to maintain a symmetrical VOI distribution.

Once the reduced AAL atlas was defined, PCA was performed across the voxel time courses within each VOI with the largest component of the PCA retained, resulting in a single activity time course that best represented each VOI. All VOI time courses were then orthogonalized using a symmetric multivariate correction with twenty iterations (Colclough et al., 2015) to reduce the EEG volume conduction artefact and spatial leakage that results from source localization estimates. Power envelopes of the orthogonalized VOI time courses were then calculated by taking the absolute value of their Hilbert transform; a similar approach for calculating activity envelopes has been done in previous studies (Brookes et al., 2011; Hipp et al., 2012). VOI power envelopes were then correlated within frequency bands resulting in a connectivity matrix of correlation coefficients that was 61 (number of VOIs) by 61 (number of VOIs) by 10 (number of frequency bands) for each participant. Connectivity correlation coefficients were Fisher z-transformed to normalize the sample distribution for statistical analysis. An additional normalization was performed across frequency bands to account for the inverse relationship between correlation and frequency band for a fixed time window. For the bias normalization, we performed a Monte Carlo simulation using 1000 iterations on the pipeline described above by randomizing the VOI time series phase information while retaining the magnitude information. This resulted in a random ‘noise’ correlation distribution for each participant, frequency band and VOI-to-VOI interaction. The true Fisher z-transformed connectivity data was then bias corrected by subtracting the mean and dividing by the standard deviation of the random ‘noise’ distributions converting the true connectivity data to a z-score relative to the null distribution.

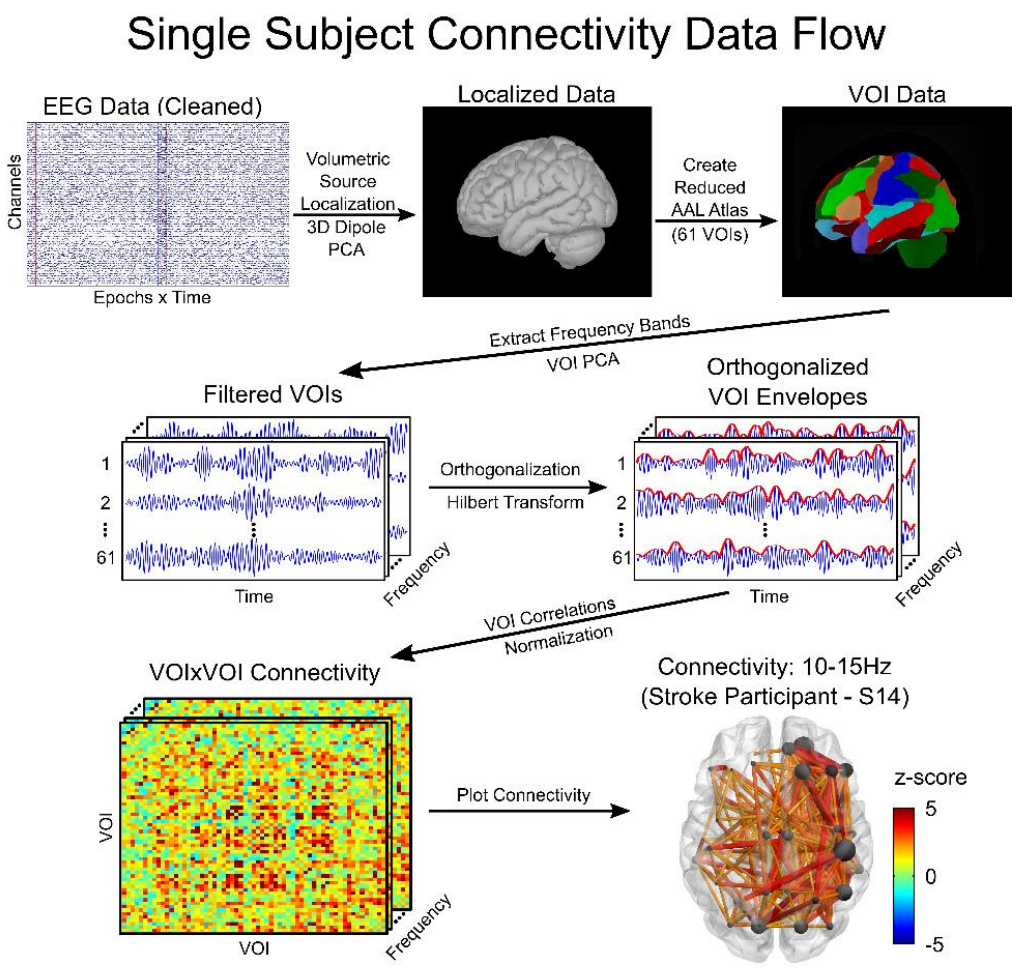

Figure 3-1: Diagram of Connectivity Work-Flow. Diagram of connectivity work-flow and the 10-15Hz frequency band connectivity for a single stroke participant (S14) thresholded at a z-score of ±2. After preprocessing, EEG data were projected into a volumetric source space where a PCA was applied to each three-dimensional dipole to extract the time course that best represented the dipole's activity. The brain was then segmented into 61 VOIs based on a reduced AAL atlas. All VOIs were filtered voxel-wise to extract the frequency bands of interest and PCA was applied to reduce the dipole activity within the VOIs to a single time course. For each frequency band, VOI time series were orthogonalized after which the envelope of the VOI activity was obtained via the Hilbert transform. Correlations between the envelopes of VOI activity were performed within frequency bands to characterize connectivity between VOI's. For the representative stroke participant shown (S14), the hemisphere associated with the stroke lesion is displayed on the left. Stronger connections between nodes are represented by larger z-scores and line widths. Node size indicates the number of connections a node makes with other nodes.

To determine if frequency bands displayed connectivity differences between hemispheres, a connectivity directional asymmetry (*CDA*) metric was computed between analogous connections in the two hemispheres using equation 3.3,

$$CDA = 100 \times \frac{1}{n} \sum \frac{C_L - C_R}{|C_L| + |C_R|} \qquad (3.3)$$

where CDA represents the whole brain connectivity directional asymmetry metric, C_L represents the connectivity of the homologous connections in the left hemisphere, C_R represents the connectivity of the homologous connections in the right hemisphere and n represents the total number of homologous connection pairs. Connectivity between homologous regions was ignored.

To visualize frequency dependent shifts in the stroke group relative to the control group, connectivity spectra (connectivity versus frequency) were plotted for connections within the left (lesioned) and right (non-lesioned) hemispheres. To quantify deviations in the shape of the connectivity spectrum from the control group, the connectivity spectrum of each participant (control and stroke) was correlated with the average connectivity spectrum from the control group. Finally, connectivity spectrum correlation values were Fisher z-transformed to normalize the sample distribution for statistical testing.

The Network Based Statistic Toolbox (Zalesky et al., 2010) was used at the group level to identify significantly connected networks in the control and stroke groups and networks that were significantly different between groups. The Network Based Statistic, a graph analogue of cluster-based statistical methods, used permutation testing to control the family-wise error rate ($p<0.05$) associated with multiple comparisons tests based on the extent (number of connections in a network) of the network above a predefined (defined by the user) threshold. For our analysis, we tested networks that were either

positively or negatively correlated between VOI's. We modified the Network Based Statistic code (added the capability to perform one-sample t-tests) to compute the network statistics within the control (threshold: t-value = 3.169) and stroke (threshold: t-value = 3.012) groups using a one-sample t-test (thresholds for both groups were equivalent to a two-tailed one-sample t-test p-value of 0.01). Significant differences between the networks of control and stroke groups (threshold: t-value = 2.5) were identified using a two-sample t-test applied to the Network Based Statistic (the threshold for differences between groups was equivalent to a two-tailed two-sample t-test p-value of 0.02).

3.2.5 Statistical Analysis

Changes in electrode and connectivity directional asymmetry were characterized across participants using a two-way mixed ANOVA with frequency as the within-participant factor and group as the between-participant factor in the analysis. One-way ANOVAs and t-tests were applied *post hoc* to characterize specific interaction effects identified in the two-way ANOVAs. Changes in the connectivity spectra correlation between groups were characterized by using a two-sample t-test. If Mauchly's Test of Sphericity indicated that the assumption of sphericity was violated, a Greenhouse-Geisser correction was used for the ANOVA results. The Holm-Sidak method for correcting for multiple comparisons was used at each level (between multiple ANOVAs and t-tests) of the analysis except for the pairwise comparisons where the Tukey *post hoc* test was applied. Raw p-values were reported and stated as significant if they survived the correction for multiple comparisons. A non-parametric bootstrap approach similar to the

Zhou and Wong method (Zhou & Wong, 2011) with 10000 iterations was used to generate the statistical distributions for the Tukey *post hoc* test. Statistical tests were performed with a Type I error rate of $\alpha = 0.05$. If significant differences were identified between the control and stroke groups for the electrode normalized power distributions, electrode directional asymmetry, connectivity directional asymmetry, connectivity spectra or connectivity networks analysis, the variable was plotted against the upper extremity motor FMA for the stroke participants. Plots were displayed if the correlation was significant (t-test of correlation coefficient different than 0, $p <= 0.05$).

3.3 Results

3.3.1 Normalized Power: Control Group

Electrode level normalized power was examined to identify the spatial distribution of power across electrodes for each frequency band of interest and to determine if the power distribution was different between control and stroke groups (Figure 3-2A). In the controls, the lower half of the frequencies examined (1-25Hz) accounted for ~85% of the total power while the upper half of the frequencies (25-50Hz) contributed ~15%. The regions that contributed the most power in the 1-5Hz frequency band were located above the bilateral frontal cortices while for the 5-10Hz band, the power was largest above the medial frontal cortices and the medial/lateral parietal cortices. There was a posterior to anterior shift in the regions that contributed the most power for the frequency bands ranging from 10-50Hz, with regions located above the bilateral visual cortices for the 10-15Hz band, consisting of two nodes located above the bilateral parietal/sensory/motor cortices for the 15-20Hz band, located above the bilateral

motor/premotor cortices for the 20-25Hz band, located above the bilateral premotor/frontal cortices for the 25-30Hz band, and regions located over the bilateral frontal cortices for the remaining frequency bands (30-50Hz).

3.3.2 Normalized Power Differences

The normalized power of the stroke group was similar to the controls, particularly for the distribution of power across frequency bands. However, within frequency bands the normalized power from 1-10Hz and 30-50Hz was larger in the stroke group while the normalized power from 10-25Hz was smaller in the stroke group when compared to the control group (Figure 3-2A). In general, absolute power within frequency bands displayed differences between the stroke and control groups similar to the normalized power. Absolute power from 1-10Hz and 30-50Hz was larger in the stroke group while the absolute power from 10-25Hz was smaller in the stroke group when compared to the control group (Figure 3-3).

To assess significant changes in spatial power distribution, normalized power was compared between the control and stroke groups at every electrode within each frequency band. Even though there were changes in power across all frequency bands examined, only the 10-15Hz and 15-20Hz frequency bands resulted in significant differences ($p<0.05$) following FDR correction. In the stroke group, the 10-15Hz band contained significantly less power across the entire brain except above the right (non-lesioned) visual cortex while the 15-20Hz band contained significantly less power across electrodes located over the left (lesioned) sensory/parietal cortices (Figure 3-2A) compared to controls. Across significantly different electrodes, average normalized power was

correlated with motor function (upper extremity motor FMA) in both the 10-15Hz and 15-20Hz bands (R^2 = 0.47, p=0.006 and R^2 = 0.48, p=0.006, respectively), (Figures 3-2B,C). When assessing significant changes in spatial power distribution of absolute power between the control and stroke groups at every electrode within each frequency band, no frequency bands revealed electrodes with significant differences following FDR correction.

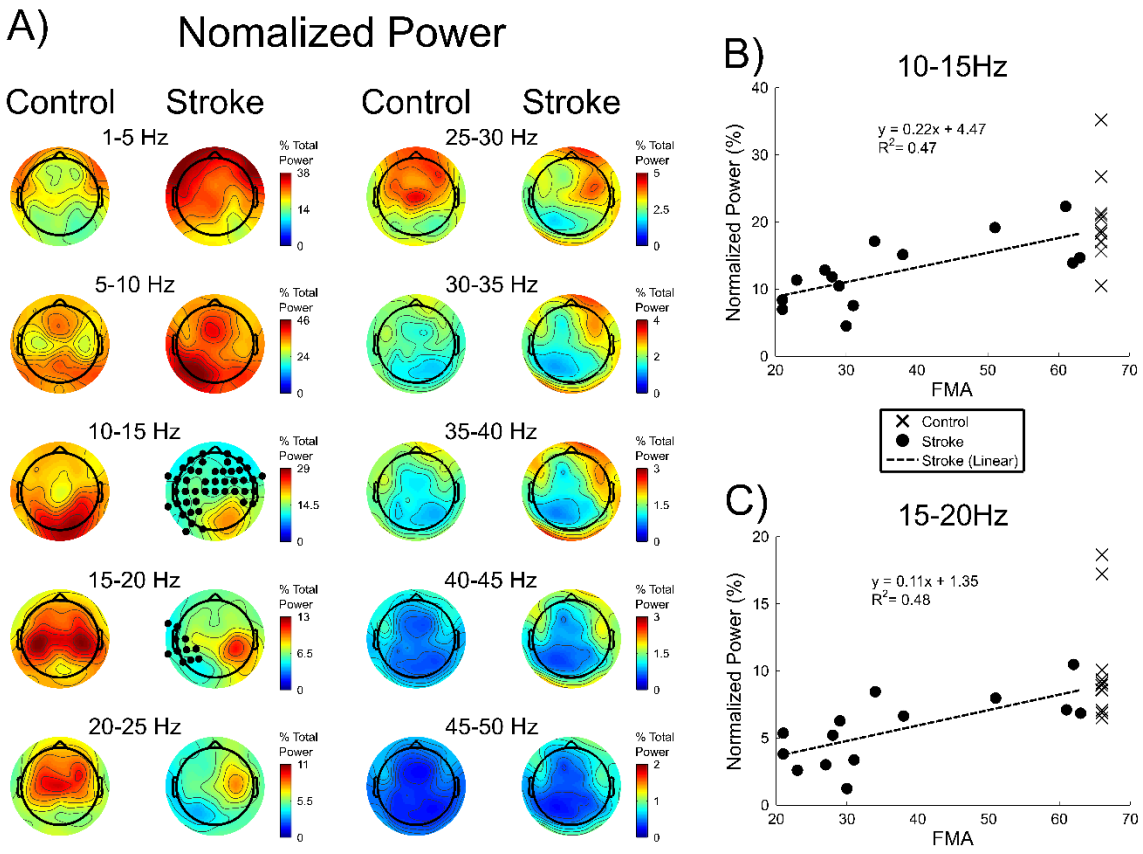

Figure 3-2: Electrode Normalized Power and Correlations During Resting State. The hemisphere associated with the stroke lesion is displayed on the left. A) Topographic maps of the normalized electrode power averaged across participants are shown for each group and frequency band of interest. Black dots indicate electrodes whose power was significantly different between the control and stroke groups, using an FDR correction of $\alpha = 0.05$. Values are interpolated between electrodes for visualization purposes. B&C) Correlation of the stroke group normalized power averaged across significantly different electrodes with upper extremity motor FMA scores for the 10-15Hz and 15-20Hz

frequency bands respectively. Normalized power for each frequency band was plotted against a perfect upper extremity motor FMA of 66 for controls.

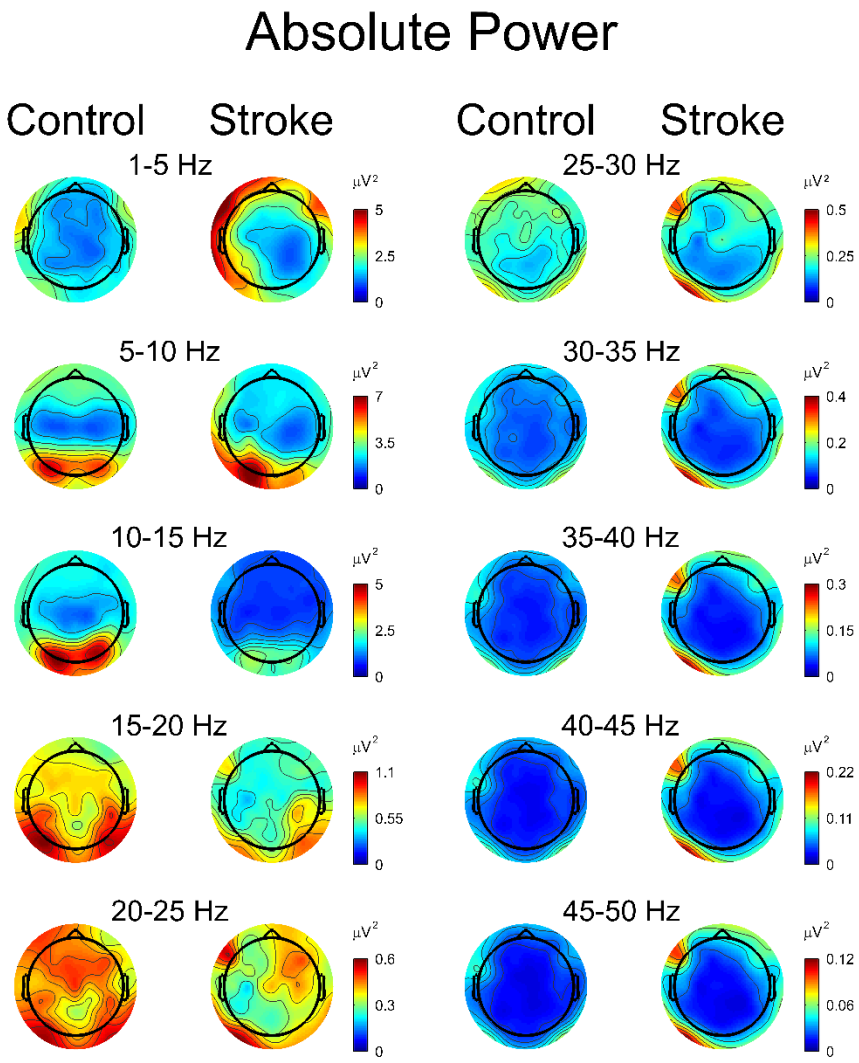

Figure 3-3: Electrode Absolute Power During Resting State. The hemisphere associated with the stroke lesion is displayed on the left. Topographic maps of the absolute electrode power averaged across participants are shown for each group and frequency band of interest. Values are interpolated between electrodes for visualization purposes.

3.3.3 Normalized Power Asymmetry

In addition to the differences in normalized power, the power topographies for the stroke group were more asymmetric when compared to those of the control group (Figure 3-2A). In the stroke group, power in the 1-10Hz frequency bands showed larger power in the left (lesioned) hemisphere while the 10-50Hz frequency bands exhibited larger power in the right (non-lesioned) hemisphere. The two-way ANOVA for differences in electrode directional asymmetry indicated that there was a main effect of frequency ($F(2.697,62.038)=6.466$, $p=0.001$) and group ($F(1,23)=16.207$, $p=0.001$) with an interaction effect between frequency and group ($F(2.697,62.038)=6.884$, $p=0.001$). The *post hoc* two-sample t-tests for group differences within frequencies indicated that the frequency bands ranging from 15-50Hz ($t(23)>=2.99$, $p<=0.01$) were significantly more asymmetric in the stroke group with the power being larger in the right (non-lesioned) hemisphere, (Figure 3-4). The 5-10Hz ($t(23)=2.02$, $p=0.055$) frequency band approached significance with more power being found in the left (lesioned) hemisphere while the frequency bands 1-5Hz and 10-15Hz ($t(23)<=1.47$, $p>=0.15$) were not significantly different between the control and stroke groups. The *post hoc* one-way ANOVAs for frequency showed significant differences between frequencies for the stroke group ($F(2.397,31.156)=9.827$, $p=0.0003$) but not the control group ($F(2.321,23.209)=0.759$, $p=0.498$). The *post hoc* analysis (Tukey test) of frequency within the stroke group indicated that the electrode directional asymmetry was significantly different between the frequency bands in the 1-10Hz range and all other frequency bands ($q(117)>=4.91$, $p<=0.0249$) while no other frequency bands showed significant differences ($q(117)<=3.56, p>=0.27$). Correlations of directional asymmetry (for significantly

different frequency bands) with function (upper extremity motor FMA) indicated that directional asymmetry was not a good predictor of motor function ($R^2 < 0.2$, $p>=0.11$).

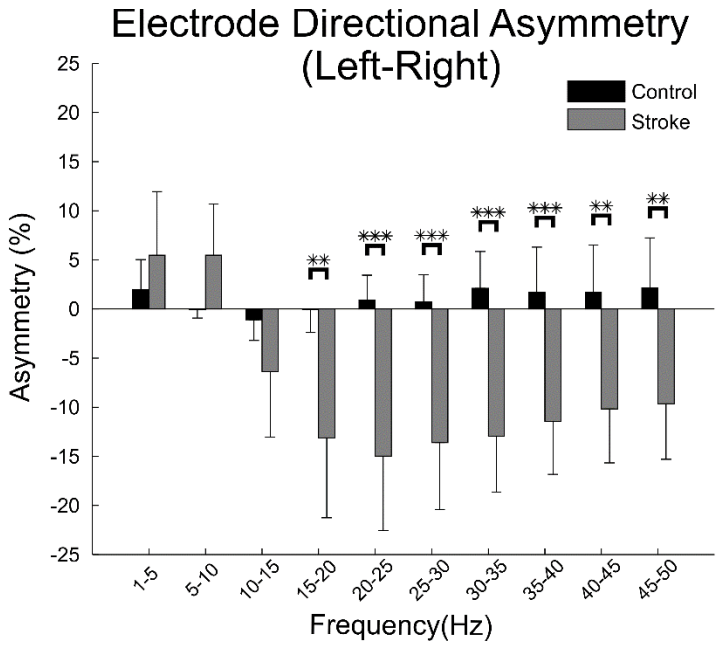

Figure 3-4: Directional Asymmetry in Electrode Power During Resting State. The directional asymmetry in electrode power averaged across participants is shown for each group and frequency band of interest. Positive asymmetry values indicate that the frequency band had larger normalized power in the left (lesioned) hemisphere while negative asymmetry values indicate the right (non-lesioned) hemisphere had larger normalized power. Error bars denote the 95% confidence interval about the mean. Significant differences determined via *post hoc* analysis (Tukey test) are indicated by stars (* indicates $p<0.05$, ** indicates $p<0.01$, and *** indicates $p<0.001$).

3.3.4 Functional Connectivity: Networks

Networks identified via functional connectivity analysis were examined to identify the spatial extent of connectivity for each frequency band of interest and to determine whether the connectivity spectra were different between stroke and control groups. No networks defined by negative correlations were found in the control ($p>=0.9568$) or stroke groups ($p>=0.9999$). All networks described below resulted from

positive correlations between VOIs in the control ($p<=0.0008$) and stroke ($p<=0.0002$) groups. In the control group, connectivity was stronger (i.e. higher correlations) and more extensive at lower frequencies (1-20Hz), which peaked in the 5-15Hz frequency range. In contrast, higher frequencies (25-50Hz), exhibited fewer connections that tended to be located in the anterior half of the brain (Figure 3-5A). Connectivity spectra for the control group in the left and right hemispheres (Figures 3-5B,C), mirrored the frequency dependences shown in the network plots (Figure 3-5A). The high connectivity in the lower frequencies (1-20Hz) sloped downwards until it reached a plateau in the higher frequencies (25-50Hz).

The stroke group showed similarities to the control network patterns, however, there were also notable differences. Lower frequencies (1-20Hz) had more extensive functional connectivity throughout the brain while higher frequencies (25-50Hz) had fewer connections that tended to be located in the anterior half of the brain (Figure 3-5A). However, for the stroke group, connectivity in the 5-20Hz frequency bands tended to be more asymmetric with lower connection strength occurring in the left (lesioned) hemisphere. Conversely, stroke networks in the 25-50Hz frequency bands contained more (and larger) connections. The two-way ANOVA for differences in connectivity directional asymmetry indicated that there was a main effect of frequency ($F(4.576,105.243)=2.889$, $p=0.003$), no effect of group ($F(1,23)=0.745$, $p=0.109$), and a trend towards significance in the interaction effect between frequency and group ($F(2.261,105.243)=4.576$, $p=0.06$). The *post hoc* analysis (Tukey test) of frequency indicated that the connectivity directional asymmetry was significantly different between the 10-15Hz band and the 1-5Hz/40-45Hz bands ($q(216)>=4.73$, $p<=.03$), trended

towards a significant difference between the 1-5Hz and 15-20Hz bands ($q(216)=4.27$, $p=0.08$) and showed no differences for the remaining frequencies ($q(216)<=4.07$, $p>=0.119$). While there was no significant interaction effect between frequency and group for the connectivity asymmetry analysis ($p=0.06$), the stroke group data did seem to drive the results found in the main effect of frequency. In general, the stroke group had larger connectivity directional asymmetry in all bands with the 5-25Hz bands displaying larger connectivity in the right (non-lesioned) hemisphere and 1-5Hz/25-50Hz bands displaying larger connectivity in the left (lesioned) hemisphere.

When comparing the connectivity spectra between groups, the left (lesioned) hemisphere was significantly different ($t(23)=2.55$, $p=0.018$) while the right (non-lesioned) hemisphere showed no differences ($t(23)=1.08$, $p=0.29$) between stroke and controls. The only noticeable differences in the right (non-lesioned) hemisphere connectivity spectrum of the stroke group was that the it peaked in the 1-10Hz range instead of the 5-15Hz range while the connectivity in the 10-20Hz frequency was slightly lower. On the contrary, the left (lesioned) hemisphere of the stroke group displayed a different spectrum entirely, peaking in the 1-5Hz frequency band, sloping downwards until the 15-20Hz frequency band and gradually increasing throughout the 15-50Hz frequencies. The stroke group's left (lesioned) hemisphere connectivity spectrum also showed a decrease in connectivity for the 5-25Hz frequency bands and an increase in connectivity for the 25-50Hz bands when compared to the control group. Correlations of the left connectivity spectrum with function (upper extremity motor FMA) showed a limited correspondence between measures ($R^2=0.18$, $p=0.13$).

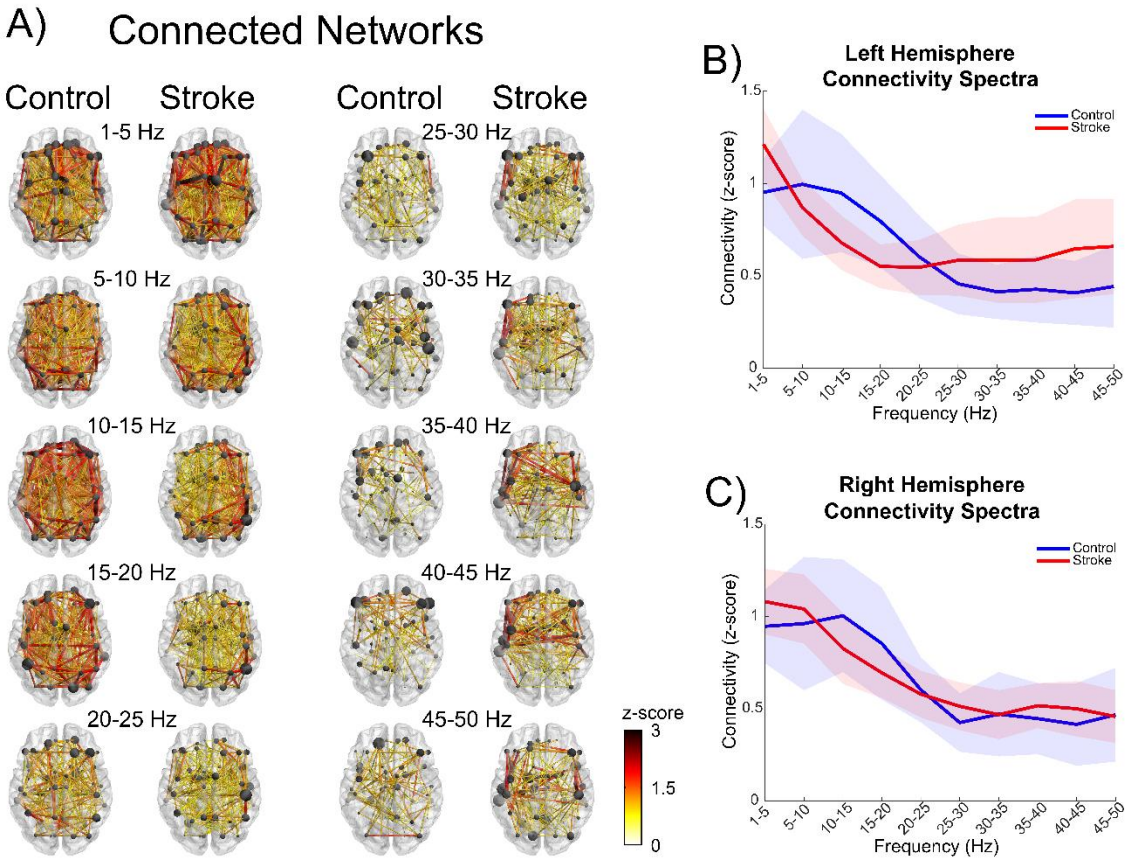

Figure 3-5: Functional Connectivity Networks and Connectivity Spectra During Resting State. The hemisphere associated with the stroke lesion is displayed on the left. A) Networks deemed significantly connected within control ($p<=0.0008$) and stroke ($p<=0.0002$) groups are shown for each frequency band of interest. Stronger connections between nodes are represented by larger z-scores (color) and line widths. Node size indicates the degree of connectivity (number of connections a node makes with other nodes) and is normalized by the maximum degree within each frequency band of interest for each group. B&C) Left (lesioned) and right (non-lesioned) hemisphere connectivity spectra, respectively. Average connectivity of all connections (not just the significantly connected networks) within the frequency band of interest. Shaded areas indicate the 95% confidence interval about the mean.

3.3.5 Functional Connectivity: Different Networks

To better visualize and quantify the changes between resting state connectivity in the control and stroke groups, we identified networks that were significantly different between groups within each frequency band of interest (Figure 3-6A). Note that here we

define ‘network’ as a group of connections within a frequency band. Networks with significantly larger connectivity in the control group occurred in the 10-15Hz (p=0.0492) and 15-20Hz (p =0.03) frequency bands. In the stroke group, one network showed significantly larger connectivity in the 35-40Hz (p=.031) frequency band while another network in the 30-35Hz frequency band approached significance (p=0.0662). No other frequency bands contained significantly different networks (p>=0.176). The 10-15Hz and 15-20Hz networks with significantly larger connectivity in the control group included connections throughout the brain, however, there were more connections in the left (lesioned) hemisphere compared to the right (non-lesioned) hemisphere (Figures 3-6A,B). The 10-15Hz network included nodes with high degree (degree>=4) located in the left inferior frontal, middle frontal, middle/inferior occipital, middle/superior temporal pole and right middle/superior temporal pole, and heschl/rolandic operculum/superior temporal regions with the highest degree occurring in the left cerebellum (degree=8). The 15-20Hz network included nodes with high degree (degree>=4) located in the left inferior frontal, superior frontal, heschl/rolandic operculum/superior temporal, cerebellum and right lingual, middle temporal, inferior/middle occipital, cuneus/superior occipital regions with the highest degree occurring in the left angular/inferior parietal and left postcentral/supramarginal regions (degree=6). The 35-40Hz network present in the stroke group was localized toward the anterior portion of the brain with an equal number of connections in the left (lesioned) and right (non-lesioned) hemispheres (Figures 3-6A,B) The 35-40Hz network included nodes with high degree in the right superior frontal gyrus (degree=4) and right amygdala (degree=5). In all three networks with between-group differences, approximately 50% of the connections occurred between hemispheres

(Figures 3-6A,B). For the networks that were different between groups, no correlation was found between average connectivity and motor function (upper extremity motor FMA), (R^2 <= 0.05, p>=0.43).

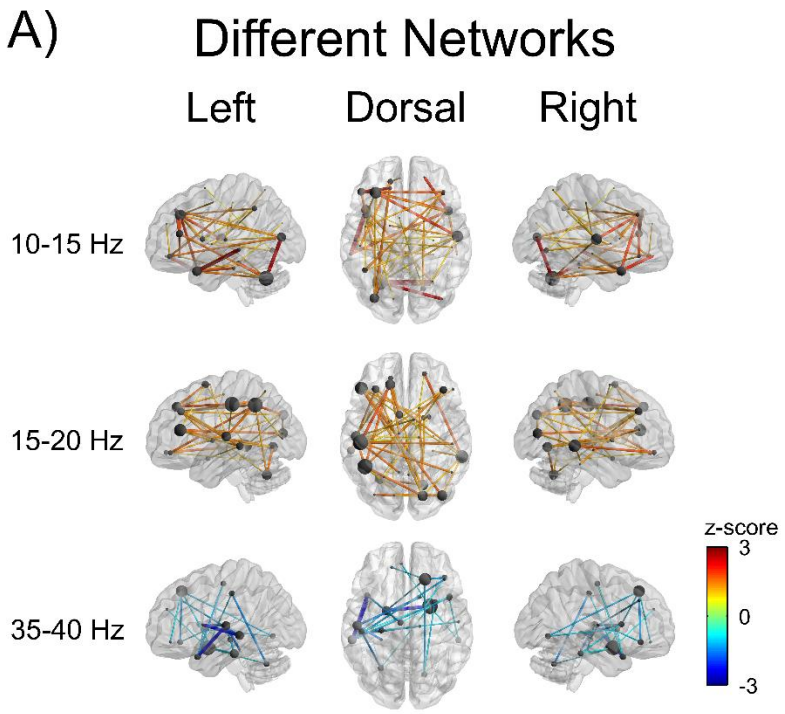

B)

Number of Different Connections				
Frequency (Hz)	Whole Brain	Inter-Hemispheric	Left Hemisphere	Right Hemisphere
10-15	42	21	17	4
15-20	43	23	14	6
35-40	26	12	7	7

Figure 3-6: Resting State Functional Connections. Resting state functional connections with statistically significant differences (p<=0.0492) between control and stroke groups. The hemisphere associated with the stroke lesion is displayed on the left. A) Networks with statistically significant differences across frequency bands. Z-values correspond to the differences between the control and stroke groups with a positive or negative z-value indicating stronger connections in the control or stroke group respectively. Larger differences in connectivity are also denoted by larger line widths between nodes. Node size indicates the degree (number of connections a node makes with other nodes) and is normalized by the maximum degree within each frequency band of interest. B) Comparison of the numbers of inter and intra-hemispheric connections within networks that were significantly different between groups.

3.4 Discussion

3.4.1 Main Results

In this study, we set out to identify the changes in resting state cortical signal power and connectivity in people with chronic stroke. We hypothesized that cortical activity and connectivity are more asymmetric after stroke and that there is a shift in the frequency of cortical communication. The results demonstrated that cortical activity patterns after stroke display asymmetric patterns and that shifts in the frequency of communication occur. Specifically, during resting state, stroke cortical network activity (EEG normalized power) in the upper frequency ranges (15-50Hz) becomes more asymmetric with less activity occurring in the lesioned hemisphere (Figures 3-2 and 3-4). The cortical network activity identified in stroke was lower in the alpha and lower beta bands (10-20Hz), suggesting a disruption of normal cortical activity (Figure 3-2). The level of connectivity in the stroke group (correlation of orthogonalized EEG band envelope activity) was reduced in the alpha and beta bands (10-20Hz) and increased in the gamma band (35-40Hz) when compared to controls (Figures 3-5 and 3-6). Differences in connectivity were driven by changes occurring within the lesioned hemisphere (Figures 3-5 and 3-6). The shift from typical alpha/beta band communication to increased gamma band communication suggests a reorganization to more local cortical networks after stroke. The presence of decreased cortical activity, increased cortical activity asymmetries and shifts in cortical communication indicate the disruption of typical cortical networks and a reorganization to more local networks after stroke.

3.4.2 Patterns of Resting State Power

In controls, lower frequencies contributed the most to the total power and different frequencies exhibited different spatial topographies (Figures 3-2). Areas with larger normalized power were located above the bilateral frontal cortices for the 1-5Hz band, above the medial frontal cortices and the medial/lateral parietal cortices for the 5-10Hz band while there was a bilateral posterior to anterior shift for the frequency bands ranging from 10-50Hz. Previous EEG studies examining resting state have shown similar topography patterns for the delta (1-4Hz), theta (4-8Hz), alpha (8-12Hz), and gamma (>30Hz) bands with lower frequencies containing higher power; however, spatial topographies for the beta (13-30Hz) band in previous studies were found to be focused above the bilateral occipital regions (Barry et al., 2007; Chen et al., 2008; Qin et al., 2010). The differences in beta band spatial topography between our results and previous literature was due to normalization of power in the current study. When examining the nonnormalized power of our data, all frequency bands resembled results seen in published literature, Figure 3-3.

The different spatial patterns of EEG power suggest that certain cortical regions are associated with specific frequency bands. Theta/alpha (5-10Hz) band power had larger normalized power above the medial frontal cortices and the medial/lateral parietal cortices suggesting a relationship to the default mode network, Figure 3-2. Specifically, the regions with the highest power in the theta/alpha frequency band resided over the medial prefrontal gyrus, anterior cingulate, posterior cingulate, and the angular gyri, which are all nodes associated with the default mode network (Damoiseaux et al., 2006; Muldoon et al., 2016; Raichle et al., 2001). EEG theta power negatively correlates with

the fMRI blood oxygen level dependent (BOLD) signal within the default mode network (Scheeringa et al., 2008). The alpha/beta (10-15Hz) band displayed the largest normalized power above the bilateral visual cortices hinting at an association with the visual network, Figure 3-2. Alpha band activity is known to relate to visual stimulation/processing and shows decreased power during increased levels of visual stimuli (Barry et al., 2007; Chen et al., 2008; Gale et al., 1969, 1971). Further, the EEG alpha band power is correlated with the fMRI BOLD signal in the visual areas during resting state (Goldman et al., 2002; Scheeringa et al., 2012). The largest amount of beta (15-30Hz) band power was found to be localized over the bilateral parietal, sensory, motor and premotor cortices, which links the beta band to the sensorimotor network. These regions have all been shown to modulate beta band activity during the control of movement in EEG event related desynchronization studies (Pfurtscheller et al., 1997, 1999; Pfurtscheller & Lopes da Silva, 1999). Although the current results support previous literature linking EEG resting state power to well defined cortical networks, EEG theta, alpha and beta frequency bands should not be interpreted as being associated with only one cortical network or process. When examining resting state under either eyes-open or eyes-closed conditions, all frequencies ranging from delta to gamma show decreased power during the eyes open condition possibly linking these bands to the arousal state of the cortex (Barry et al., 2007; Chen et al., 2008). In addition, resting state research involving fMRI, EEG and MEG have indicated that multiple frequency bands are associated with the default mode, sensorimotor, executive control, visual, lateralized fronto-parietal, auditory and temporo-parietal networks (Aoki et al., 2015; Brookes et al., 2011; Mantini et al., 2007).

3.4.3 Power Changes After Stroke

The spatial topographies observed in the stroke group differed substantially from controls. The stroke group had significantly lower power in the alpha/beta (10-15Hz) band across the entire brain except for the right non-lesioned visual cortex. Interestingly, the changes in alpha/beta band power after stroke were not localized to areas above the visual cortices but were found globally across the scalp. While the alpha band has been related to the visual network (Barry et al., 2007; Chen et al., 2008; Gale et al., 1969, 1971; Goldman et al., 2002; Scheeringa et al., 2012), stroke participants in our study did not report any stroke related visual deficits such as loss of visual field or visual neglect. However, the reported widespread decreases in the alpha/beta band could be related to changes in visual processing. Visual processing changes after stroke have been identified in studies examining visual memory performance and visual attention (Lange et al., 2000; Mazer et al., 2001). Alternatively, the widespread decreases in stroke alpha/beta (10-15Hz) band power could be representative of an altered baseline arousal or activity state of the cortex after stroke. Alpha band activity has been shown to reduce power when the brain is more aroused in an eyes open versus eyes closed state (Barry et al., 2007; Chen et al., 2008). Further, alpha band resting state power shares an inverse relationship to cortical activity (Goldman et al., 2002; Scheeringa et al., 2012), suggesting the resting brain might be in a state of higher arousal or activity after stroke.

Analysis of the stroke group's spatial power distribution within the beta (15-20Hz) band revealed significantly lower power localized to areas over the lesioned hemisphere's sensory/parietal cortex indicative of dysfunction in the sensorimotor network. This result supports previous literature showing altered beta band activity above

the lesioned motor cortex after stroke (Platz et al., 2000; Rossiter et al., 2014). Both the 10-15Hz and 15-20Hz levels of power in the stroke group correlated with impairment, supporting past research indicating that functional ability can be predicted from resting state information (Assenza et al., 2013; Kawano et al., 2017; J. Wu et al., 2015). While no electrodes showed significant differences within the delta (1-5Hz) and theta (5-10Hz) frequency bands in our study, both frequency bands did show increases in normalized power relative to the controls supporting previous findings from Assenza indicating that delta and theta band powers are increased after stroke (Assenza et al., 2013).

When examining absolute power, it was found that absolute power differences between the stroke and control groups mimicked the differences seen in normalized power. This indicates that the observed differences in normalized power between the control and stroke groups were likely due to true absolute power changes within frequency bands as opposed to a bias arising from normalization. One may wonder why normalizing power is useful if normalized power reflects the same trends seen in absolute power. The main benefit of normalizing power is that it removes the influence of electrode impedance and underlying population size on absolute power measures and allows insight into the how cortical areas are functioning (relative weighting of frequency band powers). While we focused our analysis on normalized power in the present study, analyzing absolute power should not be neglected because it offers valuable insight into the interpretation of normalized power results.

The stroke group had greater asymmetry in the upper (15-50Hz) frequency bands with less power in the lesioned hemisphere. Previous studies have shown that people with stroke tend to have more asymmetric EEG power distributions and can be classified into

either a stroke or control group based on their level of asymmetry (Köpruner & Pfurtscheller, 1984). Underlying networks, including the default mode network, are also more asymmetric after stroke (Tuladhar et al., 2013). The increased asymmetry is likely due to both a loss of neural substrate in the lesioned cortex as well as a shift in functional activity to the contralesional cortex due to cortical plasticity associated with recovery (James et al., 2009; Johansen-Berg et al., 2002; Liepert et al., 2000).

3.4.4 Patterns of Resting State Connectivity

In controls, theta/alpha/beta (5-15Hz) frequency band connections were the most numerous, had the largest values of connectivity and were symmetrically distributed throughout the cortex, suggesting they may be the dominant frequencies for cortical communication during resting state (Figure 3-5). Similar connectivity profiles with peaks in connectivity in the alpha and beta bands have been observed in resting state MEG (Brookes et al., 2011; Hipp et al., 2012). The widespread distribution of connections found in the theta/alpha/beta frequency bands may be attributed to the fact that these frequencies are associated with multiple resting state cortical networks distributed throughout the brain (Aoki et al., 2015; Brookes et al., 2011; Mantini et al., 2007). Interestingly, networks were only revealed when examining positive connectivity correlations as opposed to negative connectivity correlations. This indicates, at least under the constraints of our connectivity pipeline, that the brain's resting state connectivity between regions may be dominated by excitatory versus inhibitory interactions.

3.4.5 Connectivity Changes After Stroke

In comparison to the connectivity patterns seen in controls, the stroke group's connectivity displayed lower, more asymmetric connectivity values in the theta/alpha/beta (5-15Hz) frequency bands with larger connectivity values in the upper (25-50Hz) frequencies (Figure 3-5). When testing for significant differences in connectivity between the control and stroke groups, we found networks with decreased connectivity in the alpha/beta (10-20Hz) bands and increased connectivity in the gamma (35-40Hz) band for the stroke group (Figure 3-6). Around half the connections of the significantly different networks in the alpha, beta and gamma bands were identified to be interhemispheric connections, adding further evidence to the notion that stroke disrupts inter-hemispheric communication (Carter et al., 2009; Pellegrino et al., 2012). The decrease in connectivity observed in the alpha/beta band networks after stroke consisted of connections in both hemispheres, with most of the connections lateralized to the lesioned hemisphere, consistent with research showing deficits in functional connectivity throughout the brain but mainly in the lesioned hemisphere (Crofts et al., 2011; Crofts & Higham, 2009; De Vico Fallani et al., 2009; Tuladhar et al., 2013). Decreased connectivity of the alpha and beta bands in resting state paradigms has been reported using other EEG approaches (Dubovik et al., 2012, 2013; Wu et al., 2015). Decreased alpha (10-15Hz) connectivity within a prefrontal-cerebellar network in the stroke group is consistent with previous findings from our laboratory indicating decreased fMRI functional connectivity in a similar network after stroke (Kalinosky et al., 2017). The beta (15-20Hz) band network consisted of prominent nodes in the lesioned hemisphere's sensory/parietal regions, indicating it may be a marker of sensorimotor disfunction after

stroke (Inman et al., 2012; Platz et al., 2000; Rossiter et al., 2014; Sharma et al., 2009; Wu et al., 2015). Although most connectivity research shows a reduction in functional connectivity after stroke, our finding of increased connectivity in the gamma (35-40Hz) band supports EEG and modeling results showing stroke lesions can increase connectivity and may do so as a compensatory mechanism (Alstott et al., 2009; Bönstrup et al., 2018).

Interestingly, we found that connectivity patterns were not correlated with motor impairment when analyzed using our approach. This finding is at odds with observations that EEG resting state connectivity predicts functional and behavioral outcomes after stroke (Dubovik et al., 2012, 2013; Wu et al., 2015). This suggests that connectivity patterns are complex, with likely increases and decreases in different frequencies and regions of the brain that challenge functional interpretation.

3.4.6 Functional Reorganization after Stroke

The stroke group's loss of cortical activity and connectivity in the alpha/beta bands along with their increase of cortical activity and connectivity in the gamma band suggests a disruption of typical widespread cortical networks with a reorganization to more local cortical networks after stroke (Figures 3-2, 3-5, and 3-6). The shift to more local (higher frequency) networks is most prevalent within the lesioned hemisphere with the largest changes observed in the connectivity spectrum (Figures 3-5B,C). Cortical networks with smaller neuronal populations/spatial extent oscillate at higher frequencies than networks with larger neuronal populations/spatial extent (Bullock et al., 1995; Eckhorn, 1994; Kopell et al., 2000; von Stein & Sarnthein, 2000). The frequency of

network oscillations may not only depend on the distance or size of the two connected sites but also the number of synapses involved in an interaction (von Stein et al., 2000). Our interpretation of high frequency activity representing local network activity and low frequency activity representing large scale network activity is supported by Zhu and colleagues who examined different frequency bands of resting state fMRI in the stroke population (Zhu et al., 2015). Zhu and colleagues discovered that differences in neural activity between the stroke and control groups were frequency dependent with slower oscillations identifying widespread cortical areas and faster oscillations identifying local areas (Zhu et al., 2015).

After stroke, lesions to the cortex disconnect pathways linking disparate cortical regions resulting in smaller, isolated, more local (high frequency) networks. Although not significantly different, the lower (delta/theta) frequency bands showed a trend towards higher network activity and connectivity in the stroke group (Figures 3-2 and 3-5). This phenomenon could be the result of the brain being forced to rewire and use longer path lengths (more synaptic connections) between local regional nodes after stroke. In agreement with our results, Wang and colleagues showed that stroke causes a reorganization of cortical networks from a small world topology to more random, less optimized network architectures (Wang et al., 2010). In other words, less clustering within regions and/or longer path lengths connecting regions. It has been theorized that the random growth of new axonal connections after stroke may contribute to new randomized networks (Carmichael, 2006, 2008; Wang et al., 2010).

3.4.7 Study Limitations

The current experimental design controlled for several confounding factors, such as the raw power bias in resting state EEG and volume conduction in EEG connectivity. However, other factors may have impacted the EEG power and connectivity, including brain signals associated with trunk stabilization, EEG contamination by muscle activity and removal of EEG signal in the signal processing pipeline. During the study, participants were seated in a chair but were not otherwise restrained. Although participants were monitored throughout the experimental sessions for trunk movement, with no movement noted, the control and stroke groups might have engaged stabilizing trunk muscles differently, eliciting group-specific changes in cortical activity not specifically related to EEG resting state. Other potential confounding factors arose in the EEG data processing pipeline. It is possible that the AMICA algorithm did not fully separate signals and artefacts, resulting in the removal of some cortical signals and/or the inclusion of some artefactual components in the subsequent source imaging and analysis.

Another possible limitation centers around performing the connectivity analysis at the source level as opposed to the sensor level. When performing connectivity analysis at the source level, results depend on the choice of anatomical template, electrical model, inverse method and connectivity metric (Mahjoory et al., 2017). When estimating the forward model, we chose to use a MNI/ICBM152 anatomical brain template with the BEM, which has advantages over spherical-shell models (Vatta et al., 2010). We estimated cortical sources using the weighted minimum norm estimate as opposed to beamforming methods, which has been shown to be more accurate for cortical patch sources (Hincapié et al., 2017). Lastly, source level connectivity was performed using

orthogonalized amplitude correlations that show better test-retest reliability than other volume conduction independent connectivity measures such as imaginary coherence (Colclough et al., 2016). While performing connectivity analyses at the sensor level avoids these issues, sensor connectivity estimates have other complications. Coherence (connectivity) is dependent on the reference electrode or referencing scheme (common average, linked mastoids, etc.) (Essl & Rappelsberger, 1998; Nunez et al., 1999; Rappelsberger, 1989). The use of a single electrode as the reference can inflate or deflate coherence values depending on the level of activity at the reference electrode; with higher values at the reference electrode being detrimental to coherence (Zaveri et al., 2000). Rappelsberger (Rappelsberger, 1989) suggested using a reference averaging technique, such as linked earlobes, to better approximate a zero-potential reference and mitigate this issue. While the common average reference provides an alternative averaging technique, the tendency for EEG signals to be synchronized over large areas of the scalp can result in a common average reference remaining high. While both sensor level and source level connectivity analyses have their idiosyncrasies, we opted to use the source level approach to obtain a better approximation of how cortical regions of the brain are connected.

3.5 Conclusion

After stroke, cortical activity and connectivity indicate a shift from dominant alpha/beta band (widespread) networks typically seen in controls towards higher frequency gamma (local) networks. Stroke related changes in cortical activity and connectivity showed the largest effect in the lesioned hemisphere resulting in

asymmetrical cortical networks. These findings suggest that stroke lesions cut pathways within the brain and cause network reorganization into more local, asymmetric networks.

CHAPTER 4: CORTICAL EFFECTS OF WRIST TENDON VIBRATION DURING ARM TRACKING IN CHRONIC STROKE SURVIVORS

4.1 Introduction

The purpose of this study was to determine the cortical mechanisms associated with improved tracking performance of the paretic arm when wrist tendon vibration is applied. Previously, Conrad and colleagues demonstrated that applying vibration to the forearm tendons of stroke survivors improves performance during a figure-8 tracking task (Conrad et al., 2011b). Tendon vibration has also been shown to improve hand end-point stability after targeted arm movements and within unstable workspaces (Conrad et al., 2011a, 2015). While tendon vibration improves tracking performance and end-point stabilization in stroke survivors, the cortical mechanism/s underlying the improvements are unclear. A study examining the effect of wrist flexor tendon vibration on spinal cord stretch reflex activity following stroke found no modulation of the biceps or triceps stretch reflexes during vibration, suggesting that vibration-induced improvements in tracking performance and end-point stabilization may arise from nervous system changes at the supraspinal level (Gadhoke, 2011). A transcranial magnetic stimulation study found that vibration at the muscle can modulate the excitability of the motor cortical circuits and increase motor evoked potentials (Rosenkranz & Rothwell, 2003), furthering the idea that vibration induces supraspinal changes during motor control. Understanding the mechanism(s) behind these improvements might facilitate and enhance current stroke rehabilitation therapies.

Supplemental sensory feedback can alter the control of movement of the limb in many ways. The application of extraneous vibration improves motor learning and motor

control (Conrad et al., 2011a, 2011b, 2015; Priplata et al., 2003; Rosenkranz & Rothwell, 2012). In people with stroke, the application of extraneous vibration or somatosensory electrical stimulation to the limb improves spasticity, balance control, arm tracking, arm stabilization and hand function (Celnik et al., 2007; Conrad et al., 2011a, 2011b, 2015; Dewald et al., 1995; Levin & Hui-Chan, 1992; Priplata et al., 2006; Wu et al., 2006). The mechanisms underlying these changes in sensorimotor control are unclear. When vibration is applied to wrist flexor tendons during a motor task, improvements in motor function are not isolated to the wrist, but are seen throughout the arm (Conrad et al., 2011a, 2011b, 2015). This observation suggests that vibration enhances not only neural structures linked to the stimulated area, but also areas not directly associated with stimulation, possibly by way of altered cortical networks. This concept is further supported by transcranial magnetic stimulation and transcranial electric stimulation studies that show increased excitability of the cortex in regions distant from stimulation (Grefkes et al., 2010; Grefkes & Fink, 2011; Polanía et al., 2011). The possibility that an enhanced sensory signal may excite widespread cortical networks raises prospects for using these modalities for rehabilitation in people with stroke.

In this study, we set out to identify cortical mechanisms of improved tracking performance of the paretic arm with the application of wrist tendon vibration. We collected electroencephalography (EEG) and arm kinematic data while chronic stroke and neurologically-intact participants tracked a target moving in a figure-8 pattern in the horizontal plane. Vibration was applied to the wrist forearm flexor tendons during a portion of the trials. EEG beta band (13-26Hz) power fluctuations were used as indicators of brain activity associated with motor function (Pfurtscheller & Lopes da Silva, 1999;

Pfurtscheller & Lopes da Silva, 1999; Steriade et al., 1990). Spatially correlated coherence (SCORCH) of EEG electrodes was introduced and used as a measure of functional connectivity between cortical areas. We hypothesized that application of tendon vibration to the wrist forearm flexor tendons causes tracking improvements in the paretic arm by increasing the cortical activity and connectivity in the regions displaying cortical deficits after stroke.

4.2 Methods

4.2.1 Participants

A sample of 10 chronic stroke participants and 10 age-matched neurologically-intact controls participated in this study. Stroke participants (5 female, aged 36-79yr) were required to be at least 1-year post stroke and experience upper extremity hemiparesis. Exclusion criteria included the diagnoses of any other neurological disorder or recent treatment that interfered with neuromuscular function, such as botulinum toxin injection. Stroke participants completed the experiment using their paretic arm, whereas controls used their non-dominant arm. The impairment level of stroke participants was assessed using the upper extremity Fugl-Meyer Assessment (FMA) which consists of a motor portion (maximum score 66) and sensory/proprioception portion (maximum score 12) (Fugl-Meyer et al., 1975) and the Semmes-Weinstein monofilament test (Semmes et al., 1960). The monofilament test was performed at seven locations on the palmar surface of the paretic hand and averaged (distal phalanx of the small finger, index finger and thumb; proximal phalanx of the small and index finger; thenar and hypothenar). Control participants (4 female, aged 34-77yr) reported no history of stroke or any other upper

extremity pathology. Detailed demographic data for all participants is shown in Table 4-1. All participants gave written informed consent, and all procedures were approved by the Marquette University Institutional Review Board in accordance with the Declaration of Helsinki.

Table 4-1: Participant Information. Demographic and clinical data for stroke and control participants. Stroke (S) and control (C) participants. The "Arm Tested" corresponded to the paretic side for stroke participants and the non-dominant hand for control participants. "Fugl-Meyer" indicates the Fugl-Meyer upper extremity score (Motor: maximum of 66; Sensory: maximum of 12). Monofilament values indicate the average force in grams (g) across seven hand locations tested with the degree of sensation (N: normal (g<=0.07), '-': diminished light tough (0.07>g<=0.4), '—': diminished protective sensation (0.4>g<=2.0), '---': loss of protective sensation (2.0>g<=180.0), '----': deep pressure sensation only (g>180)). (F: female; M: male; R: right; L: left).

Participant Identifier	Sex	Age (yr)	Time after Stroke (yr)	Arm Tested	Fugl-Meyer (Motor:66)	Fugl-Meyer (Sensory:12)	Monofilament (g,sensation)
S1	F	60	23	R	63	12	0.08 (-)
S2	F	79	7	R	62	11	0.15 (-)
S3	F	67	30	L	29	12	0.05 (N)
S4	M	64	16	L	61	8	0.19 (-)
S5	F	66	26	R	51	4	60.00 (---)
S6	M	61	11	R	31	12	0.35 (-)
S7	F	65	13	L	38	8	94.29 (---)
S8	M	59	14	L	23	8	60.00 (---)
S9	M	36	8	L	21	8	71.43 (---)
S10	M	55	15	R	27	12	37.43 (---)
C1	F	68	-	L	-	-	-
C2	M	61	-	L	-	-	-
C3	M	51	-	L	-	-	-
C4	F	77	-	L	-	-	-
C5	F	57	-	L	-	-	-
C6	M	67	-	L	-	-	-
C7	M	65	-	L	-	-	-
C8	F	63	-	L	-	-	-
C9	M	34	-	R	-	-	-
C10	M	64	-	L	-	-	-

4.2.2 Test Apparatus

The study was conducted using a custom-built mechanical linkage (APPENDIX A: MANIPULANDUM) (Figure 4-1A). The linkage constrained movement to the horizontal plane and provided measurements of end-point trajectory using optical encoders (Celesco Transducer Products, Inc., Chatsworth, California; BEI Sensors, Goleta, California) located at each joint. The device frame was constructed using 2.5x2.5cm extruded aluminum (80/20 Inc., Columbia City, Indiana) and contained three rotational joints to allow unrestricted movement in the horizontal plane. While seated at the device, the participant's forearm was secured to an Ultra High Molecular Weight Polyethylene tray located at the end of the manipulandum. An overhead projector displayed hand position and target location on an opaque screen (80x60cm) directly above the plane of hand motion. The device was interfaced with LabVIEW (National Instruments Corporation, Austin, Texas) in order to control the projector display, record (1kHz sampling rate) kinematic data, and generate digital pulses used to synchronize the timing of movement and EEG data collection.

A custom-made tendon vibrator was affixed to the skin adjacent to the forearm flexor tendons on the arm (APPENDIX B: TENDON VIBRATOR). The vibrator consisted of an offset mass that rotated about the shaft of a motor (Faulhaber Group, Clearwater, FL) and was enclosed in a Teflon casing. The vibrator was then encased by a thin aluminum foil sheet that was electrically grounded to minimize the effect of electromagnetic noise from the vibrator on the EEG recordings. Vibration was applied at 70Hz to the wrist forearm flexor tendons of the arm being tested. The 70Hz vibration

frequency was selected because it lies within the range of frequencies shown to activate the most muscle spindles at the highest response rate (Roll et al., 1989).

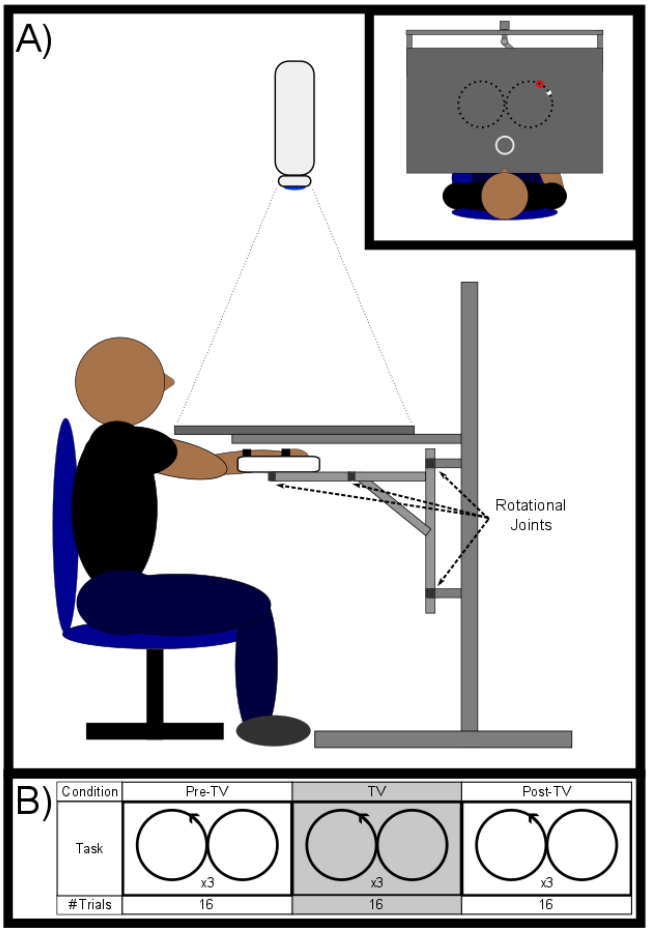

Figure 4-1: Experimental Setup. A) Illustration of the mechanical linkage and experimental setup from the side (inset in top right displays the scene from above). The white cursor projected onto a horizontal screen was linked to hand position. Participants were required to move the cursor from the home location (light gray annulus) to the target (dark gray annulus) and track the target while it moved in a figure-8 pattern. B) Experimental protocol: a single trial consisted of 3 repetitions of the figure-8 pattern. Participants performed three blocks of 16 trials each, where the middle block included tendon vibration applied to the wrist flexor tendons.

4.2.3 Experimental Protocol

During the study, the mechanical linkage was used to characterize the participant's performance on 16 trials of the target tracking task. Each trial consisted of a baseline period (11.5±1.5s before target presentation), reach period (0-1.75s after target presentation), figure-8 tracking period (1.75-43.75s after target presentation), and return period (~2s between the tracking and baseline periods). Prior to each trial, participants were required to bring a white cursor (r = 0.5cm), linked to horizontal hand position, to the home location (gray annulus, r = 4cm) located ~20cm in front of the participant. The home location then disappeared, and participants relaxed until the target (red annulus, r = 0.75cm) was presented ~24cm away from the participant on an imaginary line orthogonal to the participant's chest. Participants then moved their hand as quickly and accurately as possible to the target, at which point the figure-8 tracking period began. During the figure-8 tracking period, the target moved in a figure-8 pattern formed by 2 virtual side-by-side circles (radius = 7cm) centered at the original point of target presentation. As the target moved (0.91rad/s), participants were instructed to follow the target, attempting to keep the cursor in the center of the target. The target moved through the figure-8 pattern three times in a row with the start direction of the figure-8 moving to the left (clockwise or counterclockwise) randomly chosen for each trial.

Before testing, participants completed 8 trials of the tracking task in order to practice and minimize learning effects. During testing, the tracking task was completed 3 times per trial with 16 trials in each block. Tendon vibration (TV) was applied to the middle block of trials allowing for comparisons before (Pre-TV), during (TV), and after (Post-TV) vibration. During the TV block, the vibrator was turned on at the presentation

of the target and turned off after the tracking period ended. The vibrator was not attached to the participants during the Pre-TV and Post-TV blocks. Participants were given breaks halfway through each block and between each block to minimize fatigue.

All participants returned for a control (Sham) session on a separate day with at least 5 days between sessions. During the control session, the tracking experiment was repeated using the previously described protocol. However, during the session a "sham" vibration was applied in place of the true vibration during the TV block of trials. During the sham vibration trials, the vibrator was placed on the wrist tendon flexors, but the vibrator was not turned on. Vibrator placement was noted and controlled between sessions. The purpose of the control session was to assess whether changes in tracking performance and cortical activity were in fact due to wrist TV or other confounding factors such as motor learning or a placebo effect. The order of the sessions (Vibe vs. Sham) was counterbalanced across participants to prevent ordering effects.

4.2.4 Physiological Measurements

A 64-channel active electrode actiCAP (Brain Products GmbH, Munich, Germany) system was used to record EEG data. EEG electrodes were arranged in the conventional 10-20 system with the reference at FCz and the ground at AFz. The EEG cap was placed on the participant's head such that the Cz electrode was in line with the prearticular points in the frontal plane and with the nasion and inion points in the sagittal plane. SuperVisc gel (Brain Products GmbH, Munich, Germany) was applied between the scalp and electrodes to lower the electrode impedances below 10kOhms prior to data collection. EEG data were amplified, sampled at 1kHz, filtered from 0.1 to 200Hz and

notch filtered at 60Hz using a Synamps^2 amplifier system (Neuroscan, Charlotte, North Carolina), and recorded using the Neuroscan software, Scan 4.5.

4.2.5 Data Analysis

Trial epochs of the kinematic variables (defined below) and EEG data were extracted from the data (-5 to 42s relative to the movement cue, 16 trial epochs per block of trials). From these trial epochs, circle epochs (-0.5 to 6.905s), defined relative to target location, were extracted for each of the 6 circles (half of a figure-8) in the trial. Unique, non-overlapping baseline segments extracted from the -5 to -2s time period at the beginning of the trial epoch were inserted into the -0.5 to 0s time range of the circle epochs while the remaining 6.905s contained individual circle data. This process resulted in 96 circle epochs per block of trials used in the subsequent analysis.

Hand path kinematic data were processed and analyzed using custom MATLAB scripts (version 2014a, MathWorks, Natick, Massachusetts). Absolute error was calculated as the Euclidean distance of the cursor (hand) from the target. Speed was calculated from the x and y cursor (hand) positions obtained from the optical encoders. Absolute error and speed were then epoched, resulting in 96 epochs per block. Bad epochs were removed manually by using FieldTrip's visual inspection code (epochs were removed if the speed variance/kurtosis >2 standard deviations from the mean, ft_rejectvisual, average number removed, 22.2). Standard deviation (SD) of hand speed was calculated for each epoch's tracking period (0–6.905s). The MATLAB 'trapz' function was used to find the area under the speed curve indicating the total path length of the hand during the tracking period of the epochs. To evaluate motor planning time,

the number of sub-movements made by the hand during the epoch tracking period were counted. Sub-movements were identified by local minima in the speed traces with a single sub-movement being considered the activity occurring between consecutive local minima. Hand absolute error and speed were each averaged during the tracking period. All kinematic variables (Hand absolute error, speed, SD of speed, total path length and number of sub-movements) were averaged across epochs for each participant and compared across conditions to determine if vibration improved behavioral performance.

EEG data were post processed and analyzed using the EEGLAB toolbox (version v13.4.4b) (Delorme & Makeig, 2004) for storing and manipulating the data, FieldTrip (version 2016-01-03) (Oostenveld et al., 2011) for removing bad trials and electrodes, Brainstorm (version 3.4) (Tadel et al., 2011) for source localizing the data, and custom MATLAB scripts (version 2014a, MathWorks, Natick, Massachusetts). All EEG data were bandpass filtered (1-50Hz) using a fourth order zero-phase Butterworth filter. All EEG data were then epoched resulting in 96 epochs per block. EEG epochs were then baseline corrected (-0.5 to 0s) and bad channels and epochs were removed manually using FieldTrip's visual inspection code (channel/epoch removed if variance/kurtosis >2 standard deviations from the mean, ft_rejectvisual, average number channels/epochs removed, 1.9/22.2). If a channel was rejected from the EEG data, its value was replaced with interpolated data from the surrounding electrodes. EEG data were flipped so that the hemisphere contralateral to the arm being tested (paretic/non-dominant) was always represented on the left hemisphere. EEG data were separated into signal and artifactual components using an Adaptive Mixture Independent Component Analysis (AMICA) (APPENDIX C: INDEPENDENT COMPONENT ANALYSIS) (Palmer et al., 2008). To

ensure consistent artifact removal across blocks, sessions, participants and groups, EEG data were standardized (z-scored across electrode, time and epoch relative to baseline), temporally concatenated across independent variables (block, session, participant and group) for each electrode channel and used as input to the AMICA algorithm, Figure 4-2. This process resulted in 64 independent temporal components. Signal artifacts, including eye blink, EMG, and movement artifacts, were identified by distinct artifactual characteristics (Delorme et al., 2012; Makeig et al., 2004; Mognon et al., 2011; Puce & Hämäläinen, 2017) and removed from the EEG data (on average, 25 components were removed). The remaining components were then transformed back to the EEG channel space where the individual block, session, participant and group data were extracted. Finally, EEG data were re-referenced to a common average reference for all data analyses excluding the functional connectivity analyses (below), which re-referenced the data to the average of the mastoids (Electrodes TP9 and TP10) (Rappelsberger, 1989). Each re-reference technique reintroduced the FCz electrode to the data set.

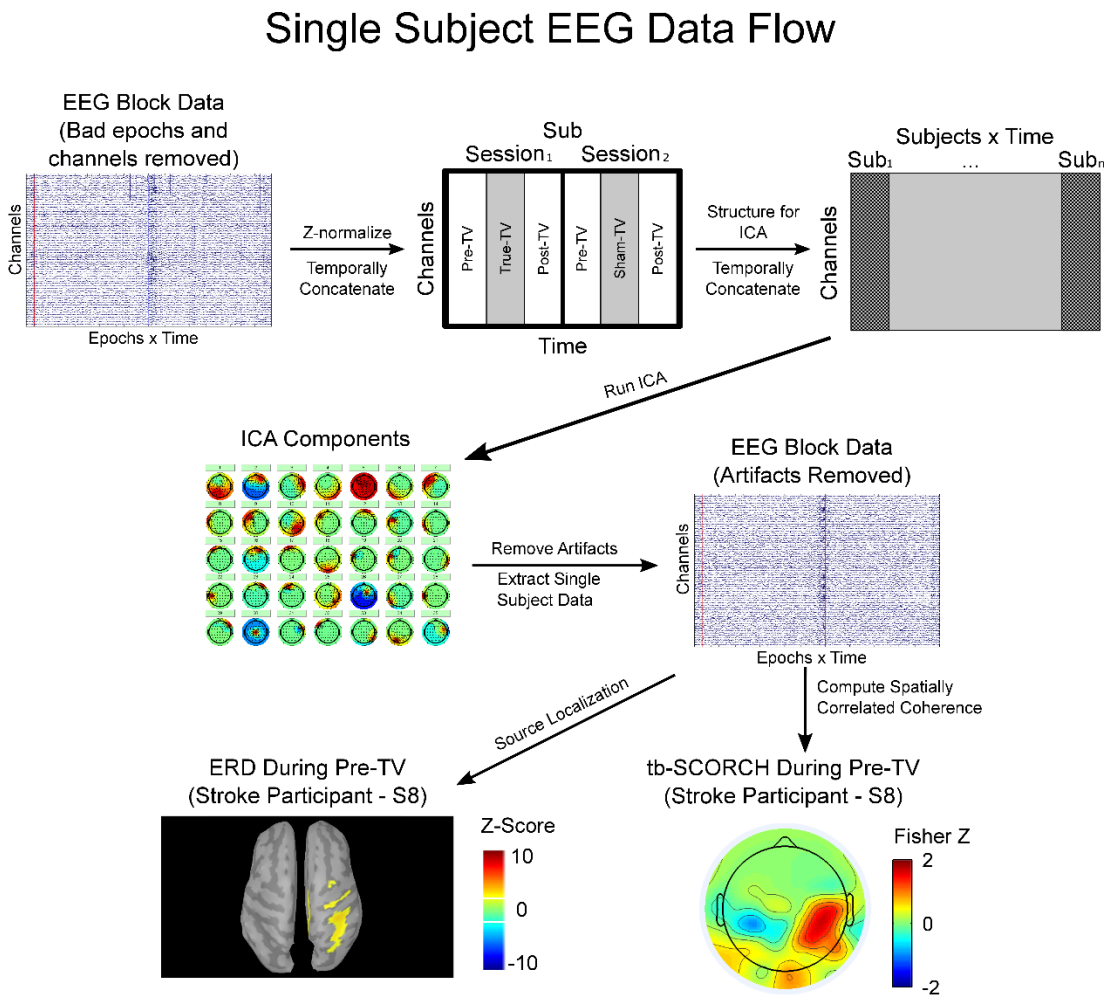

Figure 4-2: Diagram of EEG Data Flow. Diagram of EEG data flow for artifact removal via ICA and the tracking period beta band ERD and tb-SCORCH analyses for a single stroke participant (S8). After preprocessing, EEG data were standardized (z-score) and temporally concatenated across block, session, participant and group. The resulting matrix was then input into an ICA, which output 64 independent temporal components. ICA components containing artifacts (eye blink, EMG and movement) were removed and the remaining components were transformed back to the EEG channel space where individual data were extracted. The tracking period beta band ERD averaged across epochs was thresholded at a z-score of two and tb-SCORCH topographic maps were displayed using the corresponding Fisher z-values. The hemisphere contralateral to the tested arm (paretic) was displayed on the left.

Source localization of EEG data was performed to examine the spatial characteristics of cortical activity. Distributed current dipole maps were computed in Brainstorm using the default MNI/Colin27 anatomical brain template (Tadel et al., 2011).

The standard actiCAP electrode locations were fit to the scalp surface so that the Cz electrode location was at the vertex as described in the physiological measurements section. A boundary element model (BEM) was used to estimate of the forward model (OpenMEEG) (Gramfort et al., 2010; Kybic et al., 2005), and a depth-weighted minimum L2 norm estimator of cortical current density (Hämäläinen & Ilmoniemi, 1994) was used to estimate the inverse model. The source localized data were then bandpass filtered (beta band: 13-26Hz) using a zero-phase fourth order Butterworth filter, squared to obtain power, averaged across epochs, normalized (see below), and averaged across the tracking period (0 – 6.905s). For cortical activation, a z-score normalization process was used to display the data shown in Figure 4-2 (baseline period: -0.5 to 0s). For statistical analyses and difference calculations, the power was normalized using percent change from baseline (baseline period: -0.5 to 0s),

$$\%\Delta(t) = 100 \times \frac{\boldsymbol{X}(t) - baseline}{baseline} \qquad (4.1)$$

where $\%\Delta(t)$ represents the percent change from baseline, $\boldsymbol{X}(t)$ represents the power time series, t represents time, and $baseline$ represents the average power in the baseline period. Beta band z-score and percent change from baseline values were characterized in terms of the associated event related desynchronization (ERD). ERD is a decrease in power relative to baseline, is thought to represent active cortical areas (Pfurtscheller & Lopes da Silva, 1999) and is defined here in terms of the average beta band event-related desynchronization during the tracking period.

ERD from the EEG source localization data was obtained from a region of interest (ROI) corresponding to the region of deficit activity in the stroke group. The deficit ROI was identified by comparing ERD within the Pre-TV blocks of the stroke-

Vibe and stroke-Sham sessions with the control-Vibe and control-Sham sessions using a two-sample t-test, resulting in four unique maps of t-values that were subsequently thresholded (t >= 2.262). Vertices on the cortical surface that survived the threshold in all four maps were identified as the deficit ROI. The mean ERD for the deficit ROI was then compared across blocks, sessions and groups. Correlations between the cortical activity (average of stroke-Vibe and stroke-Sham ERD in the Pre-TV block) of stroke participants and their functional ability (upper extremity motor FMA) were evaluated by calculating the correlation coefficient at each vertex on the cortical surface. Vertices on the cortical surface that resulted in significant correlations (t-test of correlation coefficient different than 0, p <= 0.05) were defined as the functional ROI. The mean ERD in the deficit ROI and functional ROI for the Pre-TV block (averaged across stroke-Vibe and stroke-Sham) were also plotted against the upper extremity motor FMA for stroke participants.

To examine EEG connectivity, all-to-all (connectivity between all possible pairs of EEG electrodes) temporal connectivity profiles were generated using magnitude squared coherence (Coh^2) between electrodes X and Y,

$$Coh^2(f) = \frac{|C_{XY}(f)|^2}{C_{XX}(f) \cdot C_{YY}(f)} \qquad (4.2)$$

where C_{XY} is the cross spectrum between electrodes X and Y, C_{XX} is the auto spectrum of electrode X, C_{YY} is the auto spectrum of electrode Y, and f denotes frequency. Every EEG epoch was divided into 29 nonoverlapping windows, each containing 0.25s of data (the last 0.155s of each epoch was ignored, epochs were divided up in this fashion to remove a comparable baseline coherence from tracking period coherence). Coherence was then calculated within each window using the epochs as the measure of consistency. For each participant, block, session and group, this resulted in a connectivity matrix that

was 4225 (65x65 electrodes) by 29 elements for each frequency. The resulting connectivity matrices were then averaged across the beta band (13-26Hz range), the connectivity during baseline was removed by masking first 2 time points (representing the 0.5s of baseline data before the tracking period) and the remaining connectivity measures averaged across the last 27 time points (tracking period) to calculate the tracking period beta band task-based coherence (tb-Coh, matrix size: 65x65) (Rappelsberger et al., 1993). To examine differences between control and stroke groups, we extracted hemispheric and single electrode connectivity information from the connectivity matrix. Hemispheric tb-Coh was defined as tb-Coh between analogous electrodes in the two hemispheres. Hemispheric coherence values for electrodes along the midline were calculated as the average tb-Coh between the midline electrode and the electrodes to the immediate left and right. Finally, single-electrode tb-Coh was also extracted from the connectivity matrix and represented the tb-Coh of a single electrode with every other electrode.

To quantify spatial patterns of tb-Coh, we developed a spatially correlated coherence (SCORCH) metric (APPENDIX D: SPATIALLY CORRELATED COHERENCE). SCORCH quantifies how well a participant's single-electrode connectivity map matches the ground truth connectivity map (see following). The first step in calculating SCORCH is to generate a ground truth data set. Our ground truth data set was calculated by averaging the control-Vibe and control-Sham Pre-TV block tb-Coh matrices (matrix size: 65x65). We then spatially correlated each single-electrode tb-Coh map (65x1 array for each electrode) from every participant, block, group and session with the respective single-electrode tb-Coh map from the ground truth coherence matrix

defined across controls. Correlation values for tb-SCORCH were Fisher z-transformed to normalize the population distribution for statistical testing. This resulted in a task-based SCORCH array (tb-SCORCH, 65x1) with a single correlation coefficient value for each single-electrode tb-Coh map in every participant, block, group and session. An electrode displaying a high value of tb-SCORCH indicates that its global coherence topography (i.e. network functional connectivity pattern) resembles that seen in the ground truth data set whereas a low value of tb-SCORCH would imply the opposite.

Tb-SCORCH data were obtained from an electrode exemplifying the connectivity deficit in the stroke group. The deficit electrode was selected by comparing tb-SCORCH of the stroke-Vibe and stroke-Sham sessions with the control-Vibe and control-Sham sessions within the Pre-TV block using a two-sample t-test, resulting in four unique maps of t-values that were subsequently thresholded ($t >= 2.262$). If more than one electrode survived the threshold in all four maps, the electrode showing the largest reduction in tb-SCORCH in the stroke group was deemed the deficit electrode. The tb-SCORCH for the deficit electrode was compared across blocks, sessions and groups. To visualize any effects of TV, the tb-SCORCH in TV and Post-TV blocks from the control and stroke groups were compared to control Pre-TV block using a paired-sample t-test (control group) and two-sample t-test (stroke group) with a false discovery rate (FDR) of $\alpha = 0.05$ for multiple comparisons correction. Correlations between cortical connectivity (average of stroke-Vibe and stroke-Sham tb-SCORCH in the Pre-TV block) for the stroke participants and motor impairment (upper extremity motor FMA) were evaluated by calculating the correlation coefficient at every electrode. The electrode that resulted in a significant correlation (t-test of correlation coefficient different than 0, $p <= 0.05$) and had

the highest functional correlation was identified as the functional electrode. The tb-SCORCH in the deficit and functional electrodes for the Pre-TV block (averaged across stroke-Vibe and stroke-Sham) were plotted against the upper extremity motor FMA for the stroke participants.

4.2.6 Statistical Analysis

Changes in hand absolute error, speed, SD of speed, total path length, number of sub-movements, deficit ROI ERD and deficit electrode tb-SCORCH data were characterized across participants using three-way mixed ANOVAs with block and session as within-participant factors and group as the between-participant factor in the analysis. Two-way ANOVAs, one-way ANOVAs and t-tests were applied *post hoc* to characterize specific interaction effects identified in the 3-way ANOVAs. If Mauchly's Test of Sphericity indicated that the assumption of sphericity was violated, a Greenhouse-Geisser correction was used for the ANOVA tests. The Holm-Sidak method for correcting for multiple comparisons was used at each level (between multiple ANOVAs and t-tests) in the analysis except for multiple pairwise comparisons, where the Tukey *post hoc* test was applied. Raw p-values were reported and stated as significant if they survived the correction for multiple comparisons. A non-parametric bootstrap approach similar to the Zhou and Wong method (Zhou & Wong, 2011) with 10000 iterations was used to generate the statistical distributions for the Tukey *post hoc* test. Statistical tests were performed with a Type I error rate of $\alpha = 0.05$. Hand absolute error data was found to be positively skewed and was transformed to a normal distribution using a base 10 logarithmic function.

4.3 Results

4.3.1 Movement Kinematics

Analysis of the movement kinematics during the tracking period revealed differences between the control and stroke groups (for hand absolute error, SD of hand speed and number of sub-movements) and improvements over time or blocks (for hand speed, SD of hand speed and total path length) but did not indicate any improvements in movement kinematics due to the tendon vibration, Table 4-2. Hand absolute error and SD of hand speed were significantly higher in the stroke group (absolute error: 2.43±1.36cm; SD of hand speed: 3.48±1.05cm/s) when compared to the control group (absolute error: 0.81±0.17cm; SD of hand speed: 2.06±0.44cm/s) (absolute error: $F(1,18)=30.752$, $p<0.001$; SD of hand speed: $F(1,18)=15.46$, $p=0.001$; 3-Way ANOVA), while the number of sub-movements during the tracking period was significantly lower in the stroke group (10.26±0.59) when compared to the control group (11.37±0.61) ($F(1,18)=17.056$, $p=0.001$, 3-Way ANOVA). Hand speed, SD of hand speed and total path length during the tracking period were significantly different between blocks (hand speed: $F(1.153,20.754)=6.748$, $p=0.014$; SD of hand speed: $F(1.521,27.37)=22.172$, $p<0.001$; total path length: $F(1.153,20.754)=6.748$, $p=0.014$, 3-Way ANOVAs). *Post hoc analyses* (Tukey test) of block differences for hand speed, SD of hand speed and total path length revealed that hand speed (Pre-TV: 6.95±0.55cm/s; TV: 6.77±0.47cm/s; Post-TV: 6.80±0.48cm/s), SD of hand speed (Pre-TV: 2.94±1.13cm/s; TV: 2.71±1.04cm/s; Post-TV: 2.66±1.06cm/s) and total path length (Pre-TV: 48.66±3.83cm; TV: 47.41±3.27cm; Post-TV: 47.60±3.37cm) were significantly lower in the TV ($q(38)>=4.69$, $p<=0.005$)

and Post-TV ($q(38)>=3.97$, $p<=0.021$) block when compared to the Pre-TV block while the TV and Post-TV blocks showed similar activity ($q(38)<=1.68$, $p>=0.467$). No other factors or interactions reached significance in the three-way ANOVA of the movement kinematic variables (absolute error: $p>=0.118$; hand speed: $p>=0.16$; SD of hand speed: $p>=0.461$; total path length: $p>=0.16$; number of sub-movements: $p>=0.125$).

Table 4-2: Behavioral Performance Data. Tracking period behavioral performance data (hand absolute error, hand speed, SD of hand speed, total path length of the hand and number of hand sub-movements) during the vibration (Vibe) and sham (Sham) session. Data was averaged across participants with the standard deviation given in parentheses.

	Vibe Session			**Sham Session**		
	Pre-TV	TV	Post-TV	Pre-TV	TV	Post-TV
Absolute Error (cm)						
Control	**0.84** (0.25)	**0.80** (0.22)	**0.79** (0.20)	**0.84** (0.15)	**0.80** (0.17)	**0.77** (0.17)
Stroke	**2.39** (1.34)	**2.30** (1.42)	**2.49** (1.78)	**2.34** (1.13)	**2.56** (1.49)	**2.51** (1.34)
Speed (cm/s)						
Control	**6.84** (0.26)	**6.70** (0.17)	**6.75** (0.15)	**6.72** (0.13)	**6.67** (0.14)	**6.71** (0.13)
Stroke	**7.14** (0.98)	**6.88** (0.62)	**6.93** (0.68)	**7.11** (0.98)	**6.84** (0.62)	**6.82** (0.68)
SD of Speed (cm/s)						
Control	**2.27** (0.70)	**2.11** (0.58)	**1.99** (0.54)	**2.18** (0.34)	**1.94** (0.37)	**1.88** (0.38)
Stroke	**3.67** (1.22)	**3.39** (0.99)	**3.38** (0.98)	**3.65** (1.13)	**3.41** (1.07)	**3.39** (1.06)
Total Path Length (cm)						
Control	**47.86** (1.80)	**46.92** (1.18)	**47.26** (1.06)	**47.05** (0.88)	**46.65** (0.95)	**46.95** (0.89)
Stroke	**49.96** (6.89)	**48.16** (4.31)	**48.47** (4.76)	**49.76** (4.94)	**47.90** (5.63)	**47.71** (5.57)
Sub-movements (#)						
Control	**11.14** (0.72)	**11.42** (0.69)	**11.29** (0.68)	**11.40** (0.57)	**11.50** (0.72)	**11.46** (0.67)
Stroke	**10.24** (0.60)	**10.27** (0.68)	**10.22** (0.68)	**10.32** (0.69)	**10.30** (0.58)	**10.23** (0.62)

4.3.2 Initial Tracking ERD

ERD was examined during the Pre-TV block to identify any initial differences in the movement related activity across the cortex between the control and stroke groups, Figure 4-3A. In the control group, ERD was identified in premotor, motor, sensory and

parietal cortices and was located bilaterally. The stroke group showed ERD in the premotor, motor, sensory and parietal cortices that was lateralized to the hemisphere ipsilateral to the paretic limb, with some ERD in the parietal cortex of the contralateral hemisphere. Along with the drastic decrease in spatial extent of cortical activation in the stroke group, the areas that did display ERD were lower in magnitude when compared to the controls.

4.3.3 Deficit ROI ERD

The deficit ROI was located above the lateral pre-motor, motor and sensory cortices in the hemisphere associated with arm (paretic/non-dominant) movement, Figures 4-3A,C. Stroke participant S9's deficit ROI ERD data was excluded from the analysis because their data was found to be an extreme outlier (exceeded 3 standard deviations of the group mean). ERD in the deficit ROI was similar across blocks and sessions but different between groups, Figure 4-3B. ERD in the deficit ROI was significantly lower in the stroke group (13.71±23.66 %Δ when compared to the control group (35.08±14.93 %Δ) ($F(1,17)=5.674$, $p=0.029$, 3-Way ANOVA). No other factors or interactions reached significance ($p>=0.061$) although the two-way interaction of block and session ($F(1.333,22.664)=3.06$, $p=0.084$) and three-way interaction of block, session and group fell just below the threshold for significance ($F(1.333,22.664)=3.573$, $p=0.061$). Figure 4-3B shows the ERD in the deficit ROI; during the sham session, both the control (Pre-TV: 31.62±14.61 %Δ; TV: 37.88±16.37 %Δ; Post-TV: 39.86±18.04 %Δ) and stroke (Pre-TV: 9.03±29.37 %Δ; TV: 13.36±25.54 %Δ; Post-TV: 20.19±21.61 %Δ) groups' deficit ROI ERD increased over time (blocks). The application of tendon

vibration increased the ERD in the deficit ROI for the stroke group (Pre-TV: 8.73±27.88 %Δ; TV: 27.29±22.40 %Δ) to levels near those of the control group (C Pre-TV: 33.08±16.22 %Δ), but the increase in ERD did not persist in the Post-TV block (3.66±47.24 %Δ). Tendon vibration did not alter the ERD in the control group (TV: 32.27±14.49 %Δ), however, it did disrupt the increase in ERD over time (blocks) seen in the control and stroke sham sessions.

4.3.4 Differences in Spatial ERD

Spatial maps of the differences between TV/Post-TV and Pre-TV ERD were examined to investigate whether the trends found in the deficit ROI were present more generally in the movement related activity across the cortex (Figure 4-3C). An increase in ERD over time (blocks) in the control-Sham session was present bilaterally in the premotor, motor, sensory and parietal cortices and grew in magnitude over time (see Figure 4-3C). Application of tendon vibration in the control group caused minimal changes in ERD across the cortex but disrupted the increases in ERD over time that were observed in the sham session. The increase in ERD over time in the stroke-Sham session was less pervasive than in the control-Sham session and was focused in the lateral premotor and frontal cortices contralateral to paretic arm movement (Figure 4-3C). Contrary to controls, when tendon vibration was applied to stroke participants, the ERD increased in the lateral frontal, premotor, motor and sensory cortices contralateral to paretic arm movement. The increase in ERD with tendon vibration in the stroke group did not persist into the Post-TV block and disrupted the lateralized increases in ERD seen over time in the sham session.

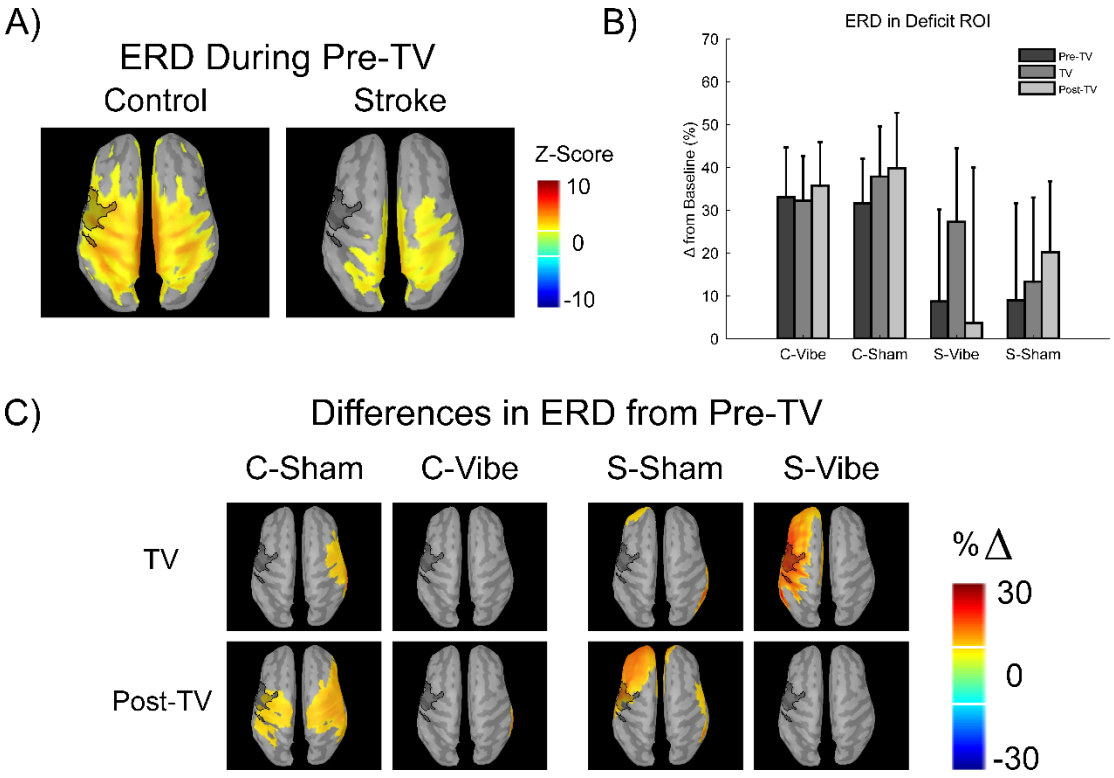

Figure 4-3: EEG Source Localization. EEG source localization of beta band ERD during the tracking period. The hemisphere contralateral to the tested arm (paretic/non-dominant) is displayed on the left. A) Average ERD during the Pre-TV block. Z-scores averaged across participants and sessions are shown for each group. Only values above or below a z-score threshold of ±2 are displayed. Positive values indicate ERD while negative values indicate a resynchronization, relative to baseline. The dark translucent overlay denotes the deficit ROI. B) Average ERD in the deficit ROI expressed as the percent change from baseline averaged across participants (error bars denote the 95% confidence interval about the mean). C) Difference ERDs from Pre-TV (Control: C-Vibe and C-Sham, Stroke: S-Vibe and S-Sham). The percent change (%Δ) values denotes the difference between the respective block and the Pre-TV block for each session with a positive/negative %Δ indicating a larger/smaller ERD within the respective block. Only values above or below a %Δ difference of ± 9 are displayed for clarity. The dark translucent overlay denotes the deficit ROI.

4.3.5 Initial Tracking tb-Coh

Electrode level tb-Coh was examined during the Pre-TV block to identify differences in functional connectivity of the cortex between the control and stroke groups. Maps for hemispheric, electrode C3 (electrode over the sensorimotor cortex

contralateral to the movement arm) and electrode C4 (electrode over the sensorimotor ipsilateral to the movement arm) tb-Coh are shown in Figure 4-4. In general, the control and stroke groups had similar patterns of tb-Coh for each metric with consistently higher levels of tb-Coh in the control group compared to the stroke group. Hemispheric tb-Coh indicated strong levels of connectivity between the homologous electrodes located above the premotor, motor, sensory and partial areas in controls while the stroke participants showed lower levels of connectivity between the homologous electrodes above the same areas. The tb-Coh for electrode C3 also showed greater connectivity in controls compared to the stroke group. Control participants had high values of tb-Coh occurring above the ipsilateral motor and sensory cortices extending up into the frontal areas of both hemispheres with low values of tb-Coh located around electrode C3 suggesting the importance of frontal/sensorimotor communication during a figure-8 tracking task. In stroke participants, the tb-Coh for electrode C3 showed minimal changes from baseline with small increases occurring above the ipsilateral parietal cortex and contralateral motor and sensory cortices. The tb-Coh for electrode C4 was comparable between control and stroke groups and was a mirror image of electrode C3's tb-Coh map in controls, although with slightly smaller connectivity.

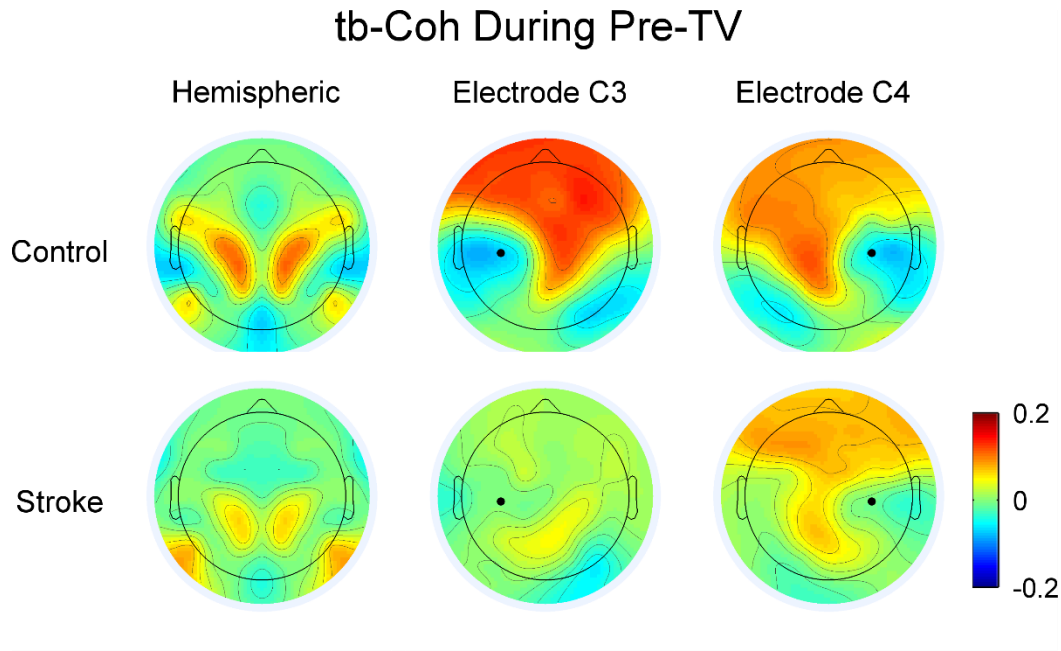

Figure 4-4: Electrode Coherence. Tracking period task-based coherence (tb-Coh) in the beta band during Pre-TV. The hemisphere contralateral to the tested arm (paretic/non-dominant) is displayed on the left. The spatial variation in tb-Coh (coherence change from baseline period) averaged across participants and sessions is shown for each coherence measure. Values of tb-Coh were interpolated between electrodes. Negative values indicate a decrease in tb-Coh while positive values indicate an increase in tb-Coh relative to the baseline period. The black dot on the single electrode coherence maps indicates the location of the electrode.

4.3.6 Initial Tracking tb-SCORCH

The tb-SCORCH was examined during the Pre-TV block to identify differences in the global functional connectivity patterns between control and stroke groups (Figure 4-5A). Two nodes with high levels of tb-SCORCH in the control group were identified bilaterally above motor, sensory and parietal areas. The node above the contralateral hemisphere (associated with arm movement) was spatially larger and contained higher tb-SCORCH values than the node in the ipsilateral hemisphere. The tb-SCORCH pattern was similar in the stroke group but contained considerably lower tb-SCORCH values across the brain. The stroke group had the highest values of tb-SCORCH in the node

above the ipsilateral hemisphere while the node in the contralateral hemisphere was almost nonexistent.

4.3.7 Deficit Electrode tb-SCORCH

The deficit electrode, identified as C3, was located above the sensorimotor cortices located in the hemisphere associated with arm (paretic/non-dominant) movement (Figure 4-5A). The tb-SCORCH of the deficit electrode was significantly lower in the stroke group (0.37±0.54) compared to controls (1.18±0.50) ($F(1,18)=11.739$, $p=0.003$, 3-Way ANOVA). The three-way mixed ANOVA of the deficit electrode's tb-SCORCH also revealed a significant interaction between block and group ($F(2,36)=3.416$, $p=0.044$) and between block and session ($F(2,36)=5.571$, $p=0.008$). No other factors or interactions in the three-way ANOVA reached significance ($p>=0.246$).

When examining the block by group interaction, the *post-hoc analysis* (1-Way ANOVA) for blocks revealed no significant results for the control (Pre-TV: 1.16±0.59; TV: 1.13±0.53; Post-TV: 1.24±0.44) ($F(1.278,11.504)=0.992$, $p=0.362$) or stroke groups (Pre-TV: 0.27±0.55; TV: 0.53±0.50; Post-TV: 0.32±0.67) ($F(2,18)=3.259$, $p=0.062$) although there was a trend towards the TV block having a significantly higher value in the stroke participants. The *post-hoc analysis* (two-sample t-test) for groups indicated a significantly larger tb-SCORCH in the controls compared to the stroke group for each block ($t(18)>=2.591$, $p<=0.019$).

When examining the block by session interaction, the *post-hoc* analysis (1-Way ANOVA) of blocks revealed significant results for the vibration session ($F(1.505,28.595)=4.913$, $p=0.022$) with a significantly lower tb-SCORCH in the Pre-TV

(0.69±0.83) and Post-TV (0.69±0.85) blocks compared to the TV (1.02±0.65) block ($q(38)>=3.843$, $p<= 0.029$) but no difference between the Pre-TV and Post-TV blocks ($q(38)=0.009$, $p \sim 1$). No significant results for the sham session were found (Pre-TV: 0.74±0.71; TV: 0.64±0.69; Post-TV: 0.87±0.66) ($F(2,38)=2.353$, $p=0.109$; 1-Way ANOVA). The *post-hoc analysis* (paired-sample t-test) for sessions indicated a significantly higher tb-SCORCH in the vibration session when compared to the sham session for the TV block ($t(19)=2.647$, $p<=0.016$) and no differences between sessions for the Pre-TV or Post-TV blocks ($t(19)<=1.708$, $p>=0.104$).

Figure 4-5B displays the tb-SCORCH in the deficit electrode and shows that the significant interactions of block/group and block/session found in the three-way ANOVA were most likely driven by the stroke group's response to tendon vibration. The application of tendon vibration increased the amount of deficit electrode tb-SCORCH in the stroke group (Pre-TV: 0.22±0.74; TV: 0.80±0.59) closer to the level of tb-SCORCH in the controls (Pre-TV: 1.17±0.65), but this increase in tb-SCORCH did not persist in the stroke Post-TV block (0.16±0.82). The tendon vibration only slightly increased the tb-SCORCH in the control group (TV: 1.25±0.65). It was noted that there was not an increase in tb-SCORCH over time (blocks) during the control-Sham session (Pre-TV: 1.16±0.63; TV: 1.01±0.52; Post-TV: 1.27±0.44) or stroke-Sham session (Pre-TV: 0.32±0.52; TV: 0.27±0.67; Post-TV: 0.48±0.62) as was seen in the ERD of the sham session.

4.3.8 Differences in Spatial tb-SCORCH

The differences in tb-SCORCH between TV/Post-TV and Pre-TV were examined at every electrode to see if the results found in the deficit electrode were present in the global functional connectivity patterns across the cortex (Figure 4-5C). Application of the tendon vibration in the controls caused minimal changes in tb-SCORCH across the cortex. Contrary to the controls, when the tendon vibration was applied in the stroke participants, an increase in tb-SCORCH was found throughout the brain nearly eradicating the large deficit in tb-SCORCH located above the sensorimotor areas in the hemisphere associated with arm movement. The increase in tb-SCORCH with application of tendon vibration in the stroke participants did not persist in the Post-TV block (see Figure 4-5C).

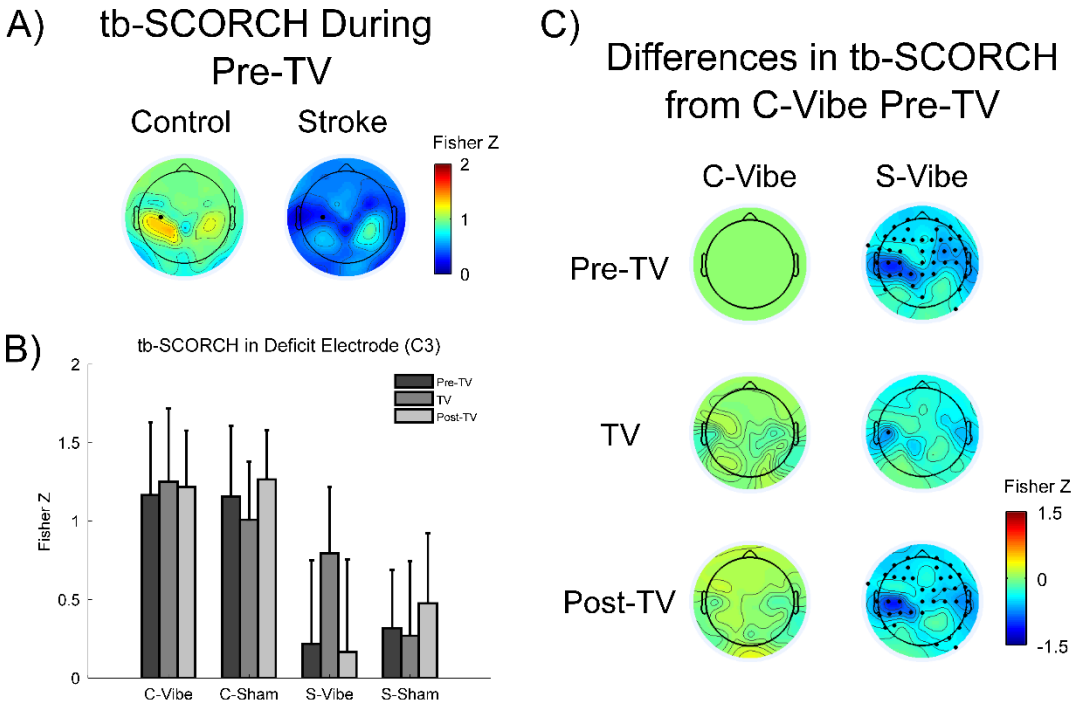

Figure 4-5: Spatially Correlated Coherence. Beta band tb-SCORCH during the tracking period. The hemisphere contralateral to the tested arm (paretic/non-dominant) is

displayed on the left. A) tb-SCORCH in the Pre-TV block (Control: C-Vibe and C-Sham, Stroke: S-Vibe and S-Sham). The tb-SCORCH Fisher z-values averaged across participants and sessions are shown for each group. Larger Fisher z-values indicate a stronger correlation of connectivity patterns between the group and the ground truth connectivity pattern (average of control-Vibe and control-Sham Pre-TV) during tracking. The black dot indicates the deficit electrode (C3). Values of tb-SCORCH were interpolated between electrodes B) tb-SCORCH in the deficit electrode. The bar chart shows tb-SCORCH Fisher z-values averaged across participants. Error bars denote the 95% confidence interval about the mean. C) Differences in beta band tb-SCORCH from Pre-TV for control participants. Black dots indicate the electrodes that were significantly different, using an FDR correction at $\alpha = 0.05$. The Fisher z-values correspond to the differences between the respective block and the control Pre-TV block with a positive/negative Fisher z-value indicating an increase/decrease in the correlation of the connectivity maps within the respective block. Values of tb-SCORCH were interpolated between electrodes.

4.3.9 Deficit Electrode tb-Coh

To characterize the effect of tendon vibration on the connectivity maps of the stroke participants, the deficit electrode (C3) tb-Coh was examined during the Pre-TV, TV and Post-TV blocks for the stroke-Vibe and stroke-Sham sessions and compared to the control Pre-TV block (Figure 4-6). As noted previously, the deficit electrode's tb-Coh for the stroke group displayed minimal changes from baseline connectivity with small increases occurring above the ipsilateral parietal cortex and contralateral motor and sensory cortices for all blocks except TV. During the TV block, the deficit electrode's tb-Coh resembled the control group (see inset of Figure 4-6); both displayed high values of tb-Coh above the ipsilateral motor and sensory cortices extending up into the frontal areas of both hemispheres with low values of tb-Coh located around the deficit electrode.

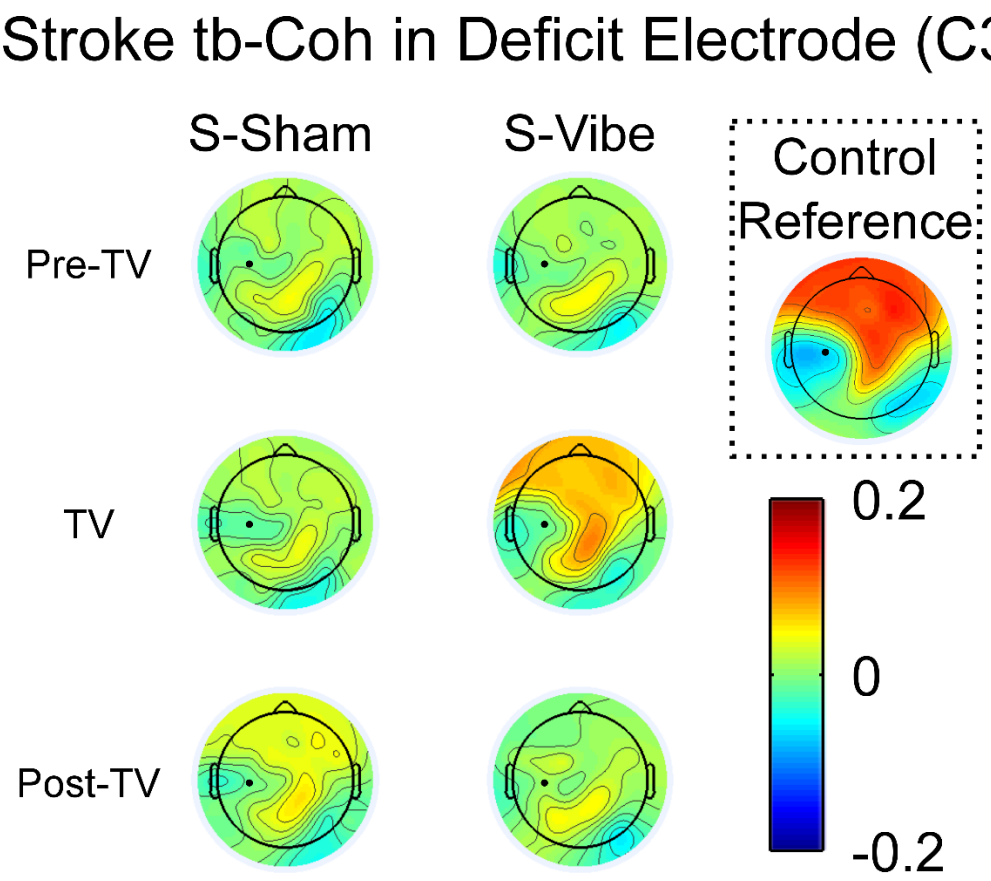

Figure 4-6: Deficit Electrode Coherence. Stroke beta band tb-Coh in the deficit electrode (C3) during the tracking period. The hemisphere contralateral to the tested arm (paretic/non-dominant) is displayed on the left. The tb-Coh (coherence change from baseline period) averaged across participants is shown for the deficit electrode (C3). The control reference inset shows electrode C3's tb-Coh averaged across participants and sessions (control-Vibe and control-Sham) for the Pre-TV block. Values of tb-Coh were interpolated between electrodes for mapping. Positive/negative values indicate an increase/decrease in tb-Coh relative to the baseline period. The black dots indicate the location of the deficit electrode (C3).

4.3.10 ERD and tb-SCORCH Correlations

Deficit ROI ERD (cortical activity) and deficit electrode (C3) tb-SCORCH (cortical connectivity) were correlated with upper extremity motor FMA (function ability) to determine whether the level of cortical deficit predicted functional outcome in the stroke participants. Figures 4-7A,B show the whole brain correlations of ERD and tb-

SCORCH with upper extremity motor FMA. Both images display similar patterns of correlation with the largest positive values of correlation occurring over the sensorimotor and parietal areas associated with paretic arm movement and the largest negative correlation values occurring over the sensorimotor areas associated the non-paretic limb movement. The correlation of function with activity and connectivity of the deficit ROI/electrode was poor, with values of $R^2 = 0.07$ ($p=0.45$) and $R^2 = 0.09$ ($p=0.40$), respectively (Figures 4-7C,D). However, the functional ROI for ERD was correlated with functional outcome in parts of the paracentral, precuneus and superior parietal gyri in the hemisphere associated with arm (paretic/non-dominant) movement ($R^2 = 0.46$, $p=0.03$), while for tb-SCORCH the functional electrode (Cz), which is centrally located between motor cortices, was best correlated with functional outcome ($R^2 = 0.52$, $p=0.02$), (Figures 4-7C,D).

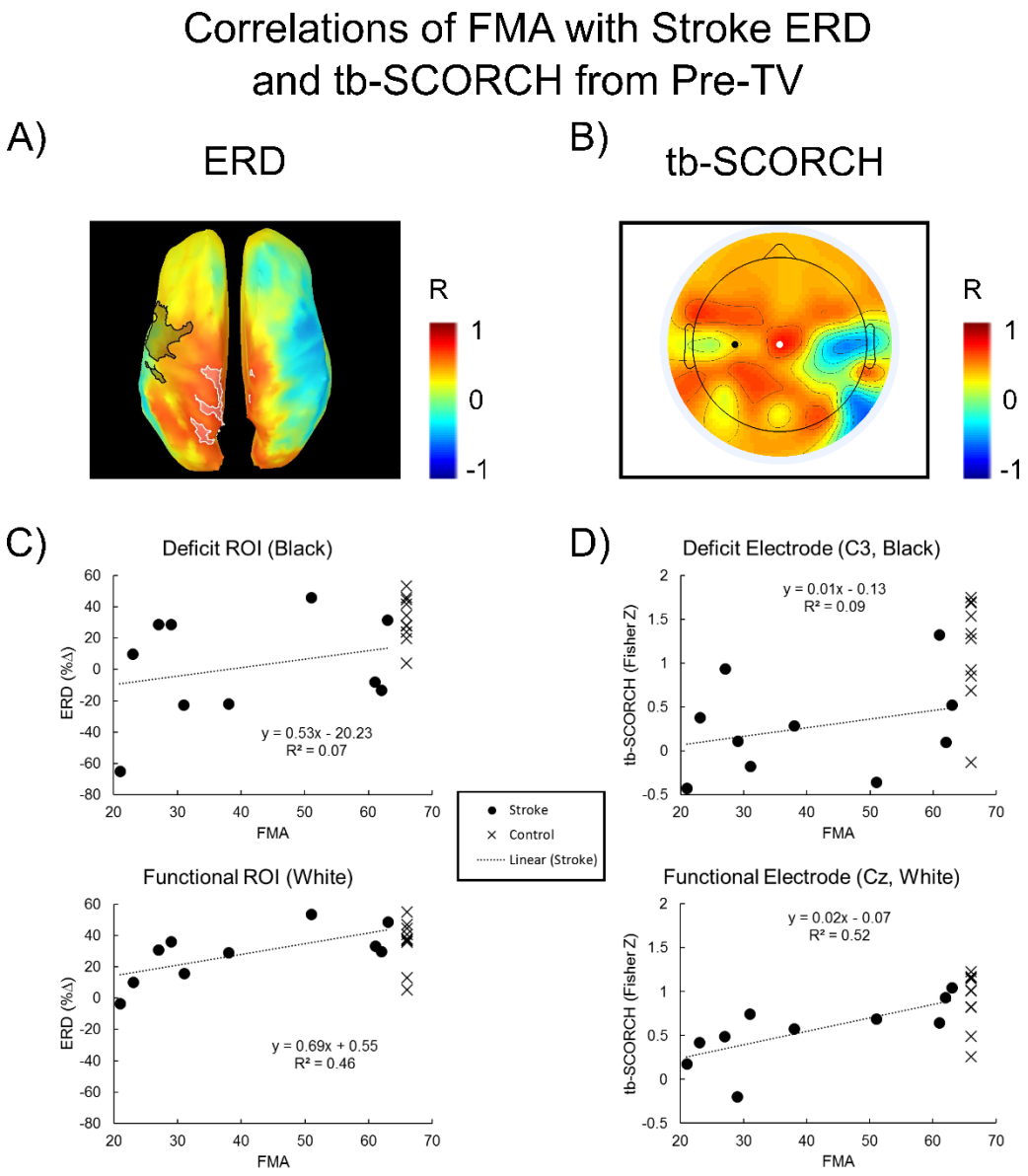

Figure 4-7: Correlations with Functional Ability. Correlations of upper extremity motor FMA scores with tracking period beta band ERD and tb-SCORCH during the Pre-TV block for stroke participants. The hemisphere contralateral to the tested arm (paretic/non-dominant) is displayed on the left. A) Correlations of vertex-wise ERD within the Pre-TV block (averaged across sessions: stroke-Vibe and stroke-Sham) with upper extremity motor FMA scores. Black and white shaded overlays indicate the deficit and functional ROIs, respectively. B) Correlations of tb-SCORCH for each electrode, within the Pre-TV block (averaged across sessions: stroke-Vibe and stroke-Sham), with upper extremity motor FMA scores. Correlation values are interpolated between electrodes for display purposes. The black and white dots indicate the deficit (C3) and functional (Cz) electrodes, respectively. C) Correlation of the ERD within the Pre-TV block for the deficit and functional ROIs with upper extremity motor FMA scores. ERD was averaged across sessions (stroke-Vibe and stroke-Sham) before correlation with the motor FMA.

Control ERD during the Pre-TV block for the same ROIs was averaged across sessions (control-Vibe and control-Sham) and plotted against a perfect upper extremity motor FMA of 66. D) Correlation of stroke electrode tb-SCORCH within the Pre-TV block with upper extremity motor FMA scores. Tb-SCORCH was averaged across sessions (stroke-Vibe and stroke-Sham) before correlation with the motor FMA. Control tb-SCORCH during the Pre-TV block for the same electrodes were averaged across sessions (control-Vibe and control-Sham) and plotted against a perfect upper extremity motor FMA of 66.

4.4 Discussion

4.4.1 Main Results

In this study, we set out to identify changes in cortical activity and connectivity associated with tendon vibration during visuomotor tracking in people with stroke. We tested the hypothesis that forearm tendon vibration increases cortical activity (ERD) and connectivity (tb-Coh and tb-SCORCH). The results demonstrated stroke-related deficits in cortical activity during a figure-8 tracking task when compared to controls. The level of functional connectivity in stroke participants was also decreased across the brain when compared to controls, with the largest deficits localized to the sensorimotor cortices associated with the paretic arm. When tendon vibration was applied to the stroke participants during the tracking task, sensorimotor cortical activity and connectivity contralateral to the paretic arm increased to levels near those of control participants. The increased cortical activity and functional connectivity in people with stroke suggests that tendon vibration during arm movement might improve cortical function.

4.4.2 Kinematic Results

The greater error in hand position and variability of hand speed in stroke participants indicated a reduction in tracking performance that is consistent with other

studies reporting reduced motor performance in people with stroke (Beer et al., 2000; Conrad et al., 2011a, 2011b, 2015; Dewald et al., 1995; Hyngstrom et al., 2010; Kamper et al., 2002; Trombly, 1992). The stroke participants also had fewer sub-movements during the tracking period, suggesting a prolonged motor planning period. Similar effects have been reported in a circle drawing task, in which a longer processing time in stroke survivors was related to an increase in perceived task difficulty (Fang et al., 2007).

The kinematic improvements seen in this study were not statistically different across the vibration and sham experiments, suggesting that vibration did not significantly improve tracking performance. This contrasts previous results showing significant improvements in tracking performance with the application of tendon vibration (Conrad et al., 2011b). One explanation might lie in the differences between experimental protocols. In this study, the protocol consisted of practice trials (8 trials, ~8 min), Pre-TV block (16 trials, ~16 min), TV block (16 trials, ~16 min) and a Post-TV block (16 trials, ~16 min) with a total of 56 trials taking about 56 minutes. The Conrad and colleagues study consisted of practice trials (~8 trials, ~8 min), Pre-TV block (4 trials, ~4 min), TV block (4 trials, ~4 min) and a Post-TV block (4 trials, ~4 min) with a total of about 20 trials taking about 20 minutes, (Conrad et al., 2011b). The extended protocol in the current study was done to increase the number of trials for EEG data processing. The extended duration of our study might have allowed early consolidation of the task motor plan, making it less susceptible to the influence of tendon vibration. Motor plan consolidation can begin within 15 minutes after a task (Denny et al., 1955; Rachman & Grassi, 1965) and consolidation of a motor plan has been shown to provide resistance to interference (Krakauer & Shadmehr, 2006; Muellbacher et al., 2002). It also is possible

that participants in our study might have learned the task before the vibration was applied, leaving no room for further statistically detectable improvement. Considering the differing lengths between the two studies and the fact that motor learning rate follows a power law, a floor effect may be the cause of the varying levels of improvements in tracking performance due to tendon vibration, Figure 4-8A (Newell & Rosenbloom, 1981; Snoddy, 1926; Stratton et al., 2007).

To better understand the time course of motor learning and the effect of tendon vibration on tracking performance (SD of hand speed), control and stroke participants were separated into two groups, depending on which session they received tendon vibration, Figures 4-8B,C. For stroke participants, when tendon vibration is applied early in the motor learning process as in the Conrad and colleagues study (Conrad et al., 2011b), tendon vibration produces a large, statistically detectable improvement in tracking performance, Figure 4-8A. While an improvement in tracking performance is observable in the stroke group who received tendon vibration during the first session, tendon vibration was applied much later in the motor learning process than the Conrad and colleagues study (Conrad et al., 2011b) resulting in a smaller improvement in tracking performance and a lack of statistical detection, Figures 4-8A,B. When the stroke group who received tendon vibration during session 2 was introduced to tendon vibration, the participants' tracking performance was very close to the performance floor leaving little room for detectable tendon vibration influence, Figure 4-8B.

Interestingly, for control participants, tendon vibration seemed to disrupt the typical power law curve associated with motor learning and reduce tracking performance improvements, Figure 4-8C (Newell & Rosenbloom, 1981; Snoddy, 1926; Stratton et al.,

2007). Similar to stroke participants, the time at which tendon vibration is applied during the motor learning process is critical to the effect's magnitude in control participants. While tracking performance improvements followed the traditional power law curve in the control group who received tendon vibration late in the motor learning process (TV during second session), tracking performance improvements decreased and displayed a linear relationship over time in the control group who received tendon vibration early in the motor learning process (TV during first session), Figure 4-8C.

The opposite effect of tendon vibration on kinematic performance for the control and stroke groups may be due to the two groups interpreting and/or utilizing tendon vibration differently. In the control group, tendon vibration may be interpreted as noise causing a disruption of the motor learning process. This is supported by studies that show sensory signals are weighted proportionally to their reliability with larger sensory noise in any one modality resulting in poorer task performance (Burns & Blohm, 2010; Ernst & Banks, 2002; Faisal et al., 2008; van Beers et al., 1996, 1999). Alternatively, the stroke group may be utilizing the tendon vibration (noise) in a stochastic resonance fashion (Cordo et al., 1996) which may boost the poor somatosensory signals typically present in stroke participants and improve motor learning (Connell et al., 2008).

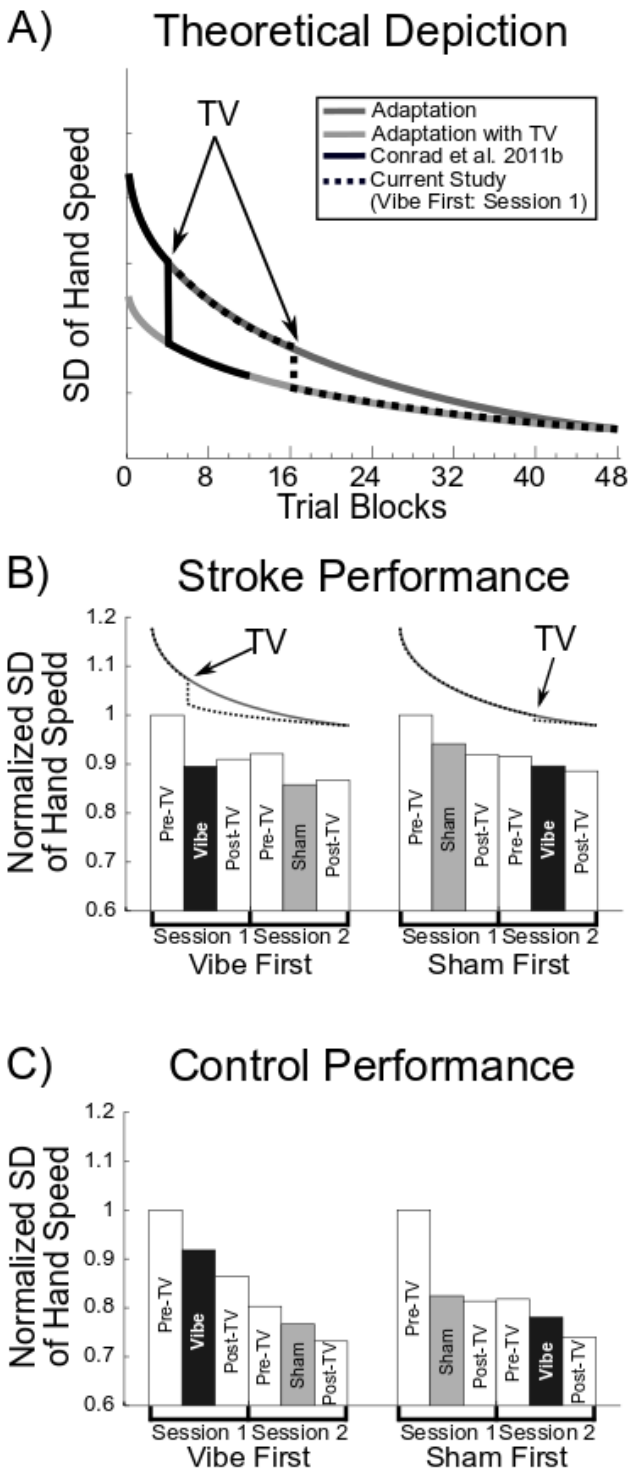

Figure 4-8: Tracking Performance. Tracking period standard deviation of hand speed adaptation over time with probable step increase in adaptation due to application of tendon vibration. A) Theoretical depiction of typical tracking period standard deviation of hand speed adaptation curve and hypothesized TV adaptation curve. When TV is applied near the beginning of the adaptation process (Conrad et al., 2011b) there is a larger

decrease in standard deviation of hand speed than when TV is applied later (current study). B) Stroke standard deviation of hand speed during tracking period. Data was averaged across the 5 stroke participants that received TV during session 1 (Vibe First) and the across the 5 stroke participants that received the sham TV during session 1 (Sham First). The curves above the bar plots display the theoretical tracking period standard deviation of hand speed adaptation curve with the point at which TV was applied. C) Control standard deviation of hand speed during tracking period. Data was averaged across the 5 control participants that received TV during session 1 (Vibe First) and the across the 5 control participants that received the sham TV during session 1 (Sham First). Data for B and C was normalized (for each participant) by calculating the ratio of each condition relative to session 1's Pre-TV condition. Error bars were withheld for display purposes.

4.4.3 Cortical Control during Figure-8 Tracking

Measures of cortical activity and functional connectivity in controls suggest that widespread cortical networks contribute to controlling the arm during a figure-8 tracking task. EEG beta band ERD revealed extensive bilateral desynchronization during the tracking period, including premotor, motor, sensory and parietal cortices. Previous EEG studies examining voluntary thumb, finger, hand, and foot movements report bilateral ERDs for complex tasks and lateralized ERD for simpler movements (Pfurtscheller et al., 1997, 1999; Pfurtscheller & Lopes da Silva, 1999; Pulvermüller et al., 1995). During movements of the entire arm, ERD is present in a large portion of the cortex suggesting that the number of active muscle groups affects ERD (Pfurtscheller et al., 1999). In addition, Pfurtscheller and colleagues (Pfurtscheller et al., 1994) showed ERDs in visual and parietal areas during a visual processing task. In the current study, muscle groups of the entire arm were active during a visuomotor tracking task which likely contributed to the extensive cortical activation.

The patterns of cortical functional connectivity identified with tb-SCORCH indicated that the control group had two nodes with consistent spatial network activity,

located bilaterally in sensorimotor and parietal areas (Figure 4-5A). While the cortical areas outside of the bilateral sensorimotor and parietal regions may have consistent functional connections (e.g. frontal-motor), a majority of the other connections (e.g. frontal-frontal, frontal-visual, etc.) varied across participants resulting in a low spatial correlation of functional connectivity (tb-SCORCH). This implies that the brain applies stronger spatial constraints to functional connectivity patterns of the bilateral sensorimotor and parietal areas' networks than it does to other cortical areas, hinting at the integral role sensorimotor and parietal areas play in a visuomotor tracking task. When looking at the task-based connectivity of a single electrode (e.g., C3, C4) from within the bilateral nodes, connectivity to the opposite sensorimotor and frontal areas appeared to be important to the task. Similar sensorimotor/visual networks have been reported in other studies involving finger and wrist movements where the frontal lobe, sensory cortex, motor cortex, parietal cortex, and occipital lobe function together to control movement (Chen et al., 2003; Leocani et al., 1997; O'Neill et al., 2017; Sukerkar, 2010).

In contrast to the wide-spread cortical activity and connectivity seen in controls, the stroke participants' cortical activity and connectivity were localized to the non-lesioned hemisphere (ipsilateral to paretic arm) during tracking. ERD revealed activity during the tracking period localized to the premotor, motor, sensory and parietal areas of the hemisphere ipsilateral to arm movement. This result supports previous evidence indicating that the non-lesioned hemisphere tends to be more active after a stroke and possibly assumes the role of the damaged tissues (Cicinelli et al., 1997; Delvaux et al., 2003; Johansen-Berg et al., 2002; Platz et al., 2000; Rossini et al., 1998; Wang et al.,

2010). The differences highlighted in Figure 4-3A could indicate the overall effect that stroke lesions have on cortical activity.

When examining patterns of cortical connectivity via tb-SCORCH, the stroke participants had lower values than the controls, except for one node located in the sensorimotor and parietal areas of the non-lesioned hemisphere (Figure 4-5A). The lower functional connectivity seen in stroke survivors may be due to utilization of unique cortical networks, arising from cortical reorganization (Cicinelli et al., 1997; Grefkes & Fink, 2014). When looking at the task-based connectivity of a single electrode (C3, C4) within the bilateral sensorimotor and parietal areas, the lesioned hemisphere's connectivity was altered in stroke while the non-lesioned hemisphere retained a more normal connectivity pattern. These connectivity results are supported by studies that show decreases in functional connectivity throughout the brain, but mainly in the lesioned hemisphere (Crofts et al., 2011; Crofts & Higham, 2009; De Vico Fallani et al., 2009; Tuladhar et al., 2013). Interhemispheric connectivity was also reduced after stroke, which has been reported previously using resting state fMRI and has been shown to correlate strongly with functional outcome (Carter et al., 2009). The patterns of cortical activity and functional connectivity in the stroke group during figure-8 tracking suggest that the non-lesioned hemisphere might contribute more strongly to control of the paretic arm.

4.4.4 Increase in ERD Over Time

ERD increased over time in both the control and stroke groups during sham testing. In controls, increases in cortical activity were localized to bilateral sensory, motor

and parietal areas while in the stroke group, increases were seen mainly in the deficit ROI and frontal cortices of the lesioned hemisphere. These increases in activity over time might be attributed to motor learning. Previous studies examining cortical oscillations during motor tasks have reported increases in alpha and beta band desynchronization (cortical activity) over the sensorimotor cortices during and after learning (Boonstra et al., 2007; Houweling et al., 2008; Meissner et al., 2018; Pollok et al., 2014; Zhuang et al., 1997). Further, cortical activity and size of excitable cortex increases up to the point that a motor task is explicitly learned, after which the activity and size of excitable cortex returns to, or below, baseline levels (Pascual-Leone et al., 1994; Zhuang et al., 1997). The absence of an ERD return to baseline in the current study is interesting given the long duration of the experiment and the fact that participants practiced the task for an extended period before the experiment began. Acquisition of explicit knowledge of the tracking task may have been limited by the fact that our tracking task varied on a trial to trial basis, varying by the start direction of the target (clockwise or counterclockwise).

During the vibration experiments, the increase in ERD over time was not seen in either the control or stroke groups, suggesting that tendon vibration affected the motor learning process. One explanation is that the increase in cortical activity over time is associated with motor memory formation. This idea is supported by studies that have applied transcranial magnetic stimulation above the sensorimotor cortices during and after learning a motor task and found that initial motor learning is not affected, but that memory consolidation of a motor task is lowered under retest conditions (Hadipour-Niktarash et al., 2007; Richardson et al., 2006; Robertson, 2005; Vidoni et al., 2010). It is also possible that vibration facilitated motor learning and allowed the tracking task to be

explicitly learned which, would cause the ERD to return to baseline levels. Applying transcranial alternating current stimulation at 10 and 20Hz above the motor cortex during a serial reaction time task facilitates learning, suggesting that additional input to the cortex facilitates motor learning (Pollok et al., 2015). Motor learning also improves after a vibration sensory attention task, indicating increased learning rates can be obtained by selective modulation of proprioceptive input (Rosenkranz & Rothwell, 2012). While the ERD did return to baseline levels after the application of tendon vibration, the control and stroke groups had differing ERD responses (Figures 4-3B,C) as well as opposite behavioral responses (Figures 4-8B,C) during tendon vibration with tendon vibration disrupting the control group's motor learning; this indicates that the ERD return to baseline was not associated with acquisition of explicit knowledge (at least in controls) and suggest that tendon vibration may be altering cortical activity via a different process.

4.4.5 Effect of Vibration on Cortical Function

The application of tendon vibration during the figure-8 tracking task had different effects on the control and stroke participants. When tendon vibration was applied to controls, cortical activity and connectivity in the TV block did not change when compared to the Pre-TV block. In contrast, when tendon vibration was applied to the stroke participants, cortical activity and connectivity increased in the TV block when compared to the Pre-TV block.

The different responses to tendon vibration between the two groups suggest that the sensory signal was processed differently in each group. The lack of activity change in the control group could result from the brain correctly interpreting the tendon vibration as

noise (i.e. task-irrelevant). Cortical networks are capable of facilitating relevant sensory information while inhibiting unrelated sensory inputs (Alain & Woods, 1994; Corbetta & Shulman, 2002; Desimone & Duncan, 1995; Everling et al., 2002). A consequence of increased sensory noise via tendon vibration during the figure-8 tracking task could be poorer behavioral performance (Burns & Blohm, 2010; Ernst & Banks, 2002; Faisal et al., 2008; van Beers et al., 1996, 1999) which is exactly what was observed in the control group, Figure 4-8C. In a similar way, the increased cortical activity observed in the stroke group in response to tendon vibration could reflect an inability to gate task-irrelevant sensory information (Alain & Woods, 1994; Corbetta & Shulman, 2002; Desimone & Duncan, 1995; Everling et al., 2002). Although people with stroke have deficits gating sensory stimuli (Staines et al., 2002), tracking performance was not disrupted by tendon vibration in the current study. In fact, tendon vibration normalized stroke cortical activity/connectivity and improved behavioral performance, Figures 4-8A,B.

The flow of additional proprioceptive information via tendon vibration may help to boost task-relevant proprioceptive signals of the limb through stochastic resonance, and help the system overcome the sensory deficits typically seen in people with stroke (Connell et al., 2008). Increased cortical activity in the deficit ROI (Figure 4-3B) and to a lesser extent, throughout the lesioned hemisphere (Figure 4-3C) supports this interpretation and is consistent with other studies examining the effects of vibration on the feet, fingers and arm that have shown similar increases in cortical activity (Golaszewski et al., 2006; Radovanovic et al., 2002; Rosenkranz & Rothwell, 2003). Further, increased functional connectivity in the deficit electrode (Figure 4-5B) and throughout the brain (Figure 4-5C) in stroke participants suggests wrist tendon vibration

during a figure-8 tracking task has the capability of normalizing widespread cortical networks that span much farther than the focal site of somatosensory interpretation. This result supports previous findings showing external stimulation (e.g. transcranial direct current stimulation, transcranial magnetic stimulation) can elicit changes in cortical connectivity distant from the stimulation site and improve cortical connectivity in stroke patients (Bestmann et al., 2005; Grefkes et al., 2010; Grefkes & Fink, 2011; Polanía et al., 2011).

4.4.6 Cortical Areas Correlated with Impairment

Whole brain cortical activity and connectivity was positively correlated with upper extremity motor FMA scores in the lesioned hemisphere and negatively correlated with FMA in the non-lesioned hemisphere. These trends suggest that outcomes of stroke improve as the lesioned/non-lesioned hemisphere becomes more/less active or functionally connected, and that more symmetric cortical activity/connectivity patterns result in higher functional outcomes. Shifts from asymmetrical to symmetrical hemispheric cortical organization with training are associated with clinical improvements (Cicinelli et al., 1997; Taub et al., 2011).

Interestingly, cortical activity/connectivity in medial regions of the cortex was most strongly associated with impairment after stroke. The paracentral, posterior cingulate, precuneus and superior parietal gyri are higher order association areas and have been associated with a variety of functions including visuo-spatial imagery, episodic memory, self-processing, consciousness, attention, visuo-motor integration, audio-visual integration and motor control (Cavanna & Trimble, 2006; Culham & Valyear, 2006;

Iacoboni & Zaidel, 2004; Leech & Sharp, 2014; Molholm et al., 2006; Pearson et al., 2011; Wagner et al., 2005). These areas are highly connected and constitute a central hub in the brain's integrative pathways (Hagmann et al., 2008). Functional outcomes after stroke are dependent on lesion location and connectedness of the lesioned area (Honey & Sporns, 2008; Kalinosky, 2016; Kalinosky et al., 2017). Integration areas are likely to be affected after stroke, regardless of lesion location due to their underlying connectedness and the connectedness after stroke appears to play a critical role in recovery of function.

4.4.7 Study Limitations

The current experimental design controlled for several confounding factors, such as motor learning, ordering effects, placebo effects, fatigue and consistent artifact removal. However, other factors may have impacted the observed changes in beta band activity and connectivity including stabilization via trunk muscles, fatigue in lower functioning stroke participants, EEG contamination by muscle activity and exclusion of true EEG signals. During the study, participants were seated in a chair but were not otherwise restrained. Although participants were monitored throughout the experimental sessions for trunk movements, with none noted, the setup may have allowed the control and stroke groups to engage stabilizing trunk muscles differently, eliciting changes in cortical activity not specifically tied to the arm movement. Physical fatigue has also been shown to alter cortical activity (Ng & Raveendran, 2007). While participants were given breaks throughout the experiment to minimize fatigue, a few of the lower functioning stroke participants reported being tired during the experiments. In spite of this, the stroke group's movement kinematics still improved during the stroke-Sham session and there

were similar trends in cortical activity and connectivity between the control-Sham and stroke-Sham sessions, indicating that fatigue played a minimal role. Other potential confounding factors arose in the EEG data processing pipeline. During analysis of the EEG data, AMICA was performed across blocks, sessions, participants and groups to ensure consistent artifact removal. It is possible that the AMICA algorithm did not fully separate signals and artifacts, resulting in the removal of some cortical signals and/or the inclusion of some artifactual components in the subsequent source imaging and analysis. Another possible limitation centers around the choice of reference electrode and the impact of volume conduction on the coherence analysis used to characterize functional connectivity. Coherence is dependent on the reference electrode or referencing scheme (common average, linked mastoids, etc.) (Essl & Rappelsberger, 1998; Nunez et al., 1999; Rappelsberger, 1989). The use of a single electrode as the reference can inflate or deflate coherence values depending on the level of activity at the reference electrode; with higher values at the reference electrode being detrimental to coherence (Zaveri et al., 2000). Rappelsberger (Rappelsberger, 1989) suggests using a reference averaging technique, such as linked earlobes, to better approximate a zero-potential reference and mitigate this issue. While the common average reference provides an alternative averaging technique, the tendency for EEG signals to be synchronized over large areas of the scalp can result in a common average reference remaining high. Coherence is also impacted by volume conduction due to spatial blurring of cortical point sources measured at the scalp. Volume conduction produces significant coherence between EEG electrodes that can extend over distances larger than 8cm (Nunez et al., 1997) even if the cortical regions immediately below the electrodes are not functionally connected. Imaginary

coherence (Nolte et al., 2004) and orthogonalization techniques (Brookes et al., 2012; Hipp et al., 2012) can be used to mitigate this issue. In the current study, we chose to examine task-based coherence (Rappelsberger et al., 1994) which effectively subtracts out the baseline level of coherence, along with the volume conduction effect, from the task period coherence (Chen et al., 2003). While the subtraction approach significantly reduced the impact of the volume conduction artifact on the coherence, it resulted in near zero task-based coherence values for adjacent electrodes due to the dominant effect of volume conduction on nearby electrodes (Figures 4-5 and 4-6). The impact was minimized, however, by comparing the same connections across tasks rather than different connections within tasks.

Lastly, examining the short-term effects of tendon vibration in chronic stroke participants may have failed to illuminate the full repertoire of tendon vibration benefits during arm movements. While the present results suggest that tendon vibration improves cortical activity/connectivity and motor learning rate in chronic stroke participants, tendon vibration did not seem to alter the attainable motor performance level nor sustain cortical activity/connectivity improvements after removal. When long-term training studies apply pure sensory training or electrical stimulation before physical therapy functional outcomes improve when compared to physical therapy alone (Conforto et al., 2007; Hillier & Dunsford, 2006); this suggests that prolonged exposure to tendon vibration in conjunction with therapy may be necessary to sustain cortical improvements as well as generate overall performance increases in the chronic stroke participants. Unlike chronic stroke patients, the central nervous system of acute stroke patients has been recently damaged and is in the process of relearning and reorganizing (Cicinelli et

al., 1997; Delvaux et al., 2003; Rossini et al., 1998; Saur et al., 2006; Wang et al., 2010). Applying tendon vibration during motor control throughout this critical phase may help cortical networks relearn more normal patterns of activity/connectivity and potentially improve attainable motor performance levels.

4.5 Conclusion

The application of vibration to the wrist flexor tendons during hand tracking increased cortical activity and connectivity of the deficit regions in people with stroke. The increases in cortical activity and connectivity with vibration normalized patterns of activity and connectivity. These findings suggest that reactivation of normal cortical networks via tendon vibration may be useful during physical rehabilitation of stroke patients.

CHAPTER 5: SUMMARY OF RESULTS AND FUTURE DIRECTIONS

5.1 Summary

Throughout this dissertation, we examined sensorimotor networks using EEG. Using EEG, with its high temporal resolution, along with source localization procedures and advanced connectivity analysis techniques, we were able to extensively probe the sensorimotor network in stroke survivors and controls. We have provided evidence that suggest sensorimotor networks are involved in the control of arm stability, cortical networks reorganize to more asymmetric, local networks after stroke, and tendon vibration enhances sensorimotor network activity and connectivity during motor control after stroke. This dissertation was among the first studies using EEG to characterize the high-speed temporal dynamics of sensorimotor networks following stroke. This new knowledge has led to a better understanding of how sensorimotor networks function under ordinary circumstances as well as extreme situations such as stroke and revealed previously unknown mechanisms by which tendon vibration improves motor control in stroke survivors, which will lead to better therapeutic approaches. This chapter summarizes the findings previously described throughout the dissertation and provides avenues of future research.

5.1.1 Aim 1: Determine if Cortical Networks Are Involved in Visuomotor Control of Arm Stability

The first objective of this dissertation was to understand how healthy sensorimotor networks function. To accomplish this, we examined sensorimotor networks in controls during upper extremity tasks designed to determine what degree the

sensorimotor network is involved in arm stabilization. The results showed that maintenance of arm position free of perturbations, co-contraction of the arm, volitional arm movements, and stabilization of the arm are associated with different patterns of brain activation and connectivity. Cortical activity in the sensory, motor and visual areas during arm stabilization was similar to that during volitional movement of the arm and was larger than the activity during co-contraction of the arm and an arm hold with no perturbations. Similar cortical activity between volitional arm movements and stabilization of the arm suggested the brain might be generating volitional movement commands to stabilize the arm. On the other hand, stabilization of the arm had a higher level of network connectivity between the sensorimotor and visual regions when compared an arm hold with no perturbations, co-contraction of the arm, and volitional arm movement. The difference in cortical connectivity between tasks might be attributed to an underlying visuomotor error network that utilizes visual error information to update the motor commands of the arm. The comparison of cortical activation and connectivity under different conditions indicates the involvement of cortical networks that contribute to visuomotor control of arm posture.

5.1.2 Aim 2: Characterize the Reorganization of Resting State Cortical Networks After Stroke Using EEG

After normal sensorimotor network function had been characterized in controls, we characterized the baseline (resting state) changes that occur in sensorimotor networks after stroke. The results indicated that the brain displays a shift from dominant alpha/beta band networks towards higher frequency gamma networks after a stroke. Decreases in stroke network cortical activity were found globally for the alpha band and locally above

the lesioned hemisphere for the beta band; both were correlated with functional ability. Asymmetries in stroke network power were also noted for the 15-50Hz frequencies with less power found in the lesioned hemisphere. Brain networks within the alpha and beta bands exhibited less connectivity after stroke while one network in the gamma band displayed increased connectivity after stroke. Stroke related changes in cortical activity and connectivity showed the largest effect in the lesioned hemisphere. These findings suggest that stroke lesions cut pathways within the brain and cause network reorganization into more local, asymmetric networks.

5.1.3 Aim 3: Determine if Cortical Network Mechanisms Underlie Improved Arm Tracking Performance in Chronic Stroke Survivors Due to Wrist Tendon Vibration

Once we had a good understanding of how sensorimotor networks function in controls and how stroke disrupts the baseline state of sensorimotor networks, we examined stroke survivors' sensorimotor networks during a visuomotor tracking task (active state of control) with an emphasis on determining if improvements in motor performance of chronic stroke survivors associated with tendon vibration are due to sensorimotor network mechanisms. We found that the application of vibration to the wrist flexor tendons during hand tracking increased the cortical activity and connectivity of the deficit regions in the stroke group and do not appear to persist after vibration has ended. The increases in stroke cortical activity and connectivity with vibration trend towards normal patterns of activity seen in the neurologically intact group suggesting improved cortical function is associated with enhanced proprioceptive feedback. Even though cortical changes were associated with the application of tendon vibration during

tracking, no improvements in behavioral performance were found to be associated with tendon vibration. The disconnect between the cortical improvements and lack of performance improvements may be due to a motor learning floor effect. These findings suggest that reactivation of normal cortical networks via tendon vibration may be useful during physical rehabilitation of acute stroke patients and during long term physical rehabilitation of chronic stroke patients.

5.2 Integration of Results

Taken separately, each of this dissertation's aims offers a slightly different yet valuable window from which to view the sensorimotor network. However, when information gleaned from all three aims is combined, one appreciates how complex and adaptable the sensorimotor network is and how important the sensorimotor network is to everyday life. While its existence is rarely acknowledged in daily life, its presence is felt in nearly every activity we do throughout the day, including such simple tasks as maintenance of arm posture. Although its presence or lack thereof is often not recognized until something drastically alters functionality, such as stroke, its ability to reorganize after insult prevents a total loss of function. The remarkable ability of the sensorimotor network to reorganize is highlighted when an additional sensory stimulus, such as vibration, is introduced to damaged sensorimotor systems. Even after years of functioning in its adopted, reorganized state, the sensorimotor network quickly shifts back to a state that resembles what is seen before any disruption occurred when additional sensory stimuli are supplied. The ability or even tendency of the sensorimotor network to return to natural patterns with such a simple push suggests how engrained

such natural patterns are in cortical networks and offer a promising method of how to correct dysfunctional cortical network patterns. The ability of outside stimuli to alter or correct dysfunctional patterns of cortical networks lends rationale to cortical modeling studies such as brain controllability that suggests altering activity in certain nodes of the brain via some external stimulus may be able to shift the cortex into different cortical states (Gu et al., 2015; Muldoon et al., 2016). By generating brain controllability models based off large cortical datasets from databases such as the Human Connectome Project (Marcus et al., 2011), it may one day be possible to apply directed stimulation to correct irregular cortical network patterns and function.

5.3 Future Directions

While this dissertation has introduced new important knowledge to the field of neural/neurorehabilitation engineering, there is still an enormous amount of research to be done in order to fully understand the functioning of sensorimotor networks, how stroke alters sensorimotor networks and what therapeutic techniques should be applied to correct the deficits to sensorimotor networks seen post stroke. The following sections highlight avenues of research that have stemmed from this dissertation and seek to answer some of these unanswered questions.

5.3.1 Arm Stabilization

Stabilization of the arm during visuomotor control of arm posture engages cortical control mechanisms that operate in concert with co-contraction of antagonistic muscles and possibly spinal/supraspinal reflex activity to ensure arm stabilization. We

hypothesize that the intermittent voluntary corrections generated by the cortex are the last mechanism recruited to stabilize the arm and are only engaged after co-contraction of antagonistic muscles and spinal/supraspinal reflex activity mechanisms prove insufficient to adequately stabilize the arm. Future studies could test this hypothesis by utilizing multiple tasks with varying degrees of stabilization difficulty to determine the level of stabilization challenge at which cortical activity and connectivity occurs. We expect a graded increase in co-contraction as well as spinal/supraspinal reflex activity up to a critical point, after which cortical networks would be recruited to ensure stability.

In future studies, it would also be interesting to examine how stabilization of the arm changes in various disease populations such multiple sclerosis, myelopathy and stroke. Within these populations, the central and/or peripheral nervous system is damaged resulting in poor motor coordination and stabilization (Conrad et al., 2011a, 2011b, 2015). The mechanism to ensure end point stabilization in these populations may still be intermittent voluntary corrections mediated by a sensorimotor error network, although it may be dysfunctional. Alternatively, control may be relegated to lower level, but functionally intact mechanisms associated with spinal/supraspinal reflexes or co-contraction of antagonistic muscles that may not adequately prevent instability. Previous studies (Conrad et al., 2011a, 2011b, 2015) in people with stroke have shown that the application of tendon vibration improves motor control and endpoint stabilization while not altering spinal reflex activity (Gadhoke, 2011) suggesting that sensory input at the cortical level may be a key factor in arm end point stabilization.

5.3.2 Tendon Vibration

Resting state cortical networks are disrupted after stroke and show a reorganization to more asymmetric, local networks. Understanding the changes that occur to cortical networks after stroke is only the first step in providing effective therapies for stroke rehabilitation. Previous studies in people with stroke have shown that the application of tendon vibration and electrical stimulation improves spasticity, balance control, arm tracking, arm stabilization and hand function (Celnik et al., 2007; Conrad et al., 2011a, 2011b, 2015; Levin & Hui-Chan, 1992; Priplata et al., 2006; Wu et al., 2006). In Aim 3 of this dissertation, we demonstrated how tendon vibration can cause a return to near normal levels of cortical activity and connectivity in stroke survivors during a motor control task. It would be interesting to examine the effect of tendon vibrations in the resting state of stroke survivors to determine if its effect is state dependent (task-based only) or ubiquitous. If the effect of tendon vibration is ubiquitous, it may act to shift the high frequency gamma band resting state networks seen in stroke survivors back to the typical alpha/beta band resting state networks found in controls.

Application of tendon vibration to the wrist forearm flexor tendons during a motor control (figure-8 tracking) task normalizes cortical activity and connectivity in chronic stroke survivors. We hypothesize that applying tendon vibration to stroke survivors during training sessions over an extended period, weeks to months, may result in larger functional improvements compared to training without tendon vibration. The normalization of cortical activity/connectivity with application of tendon vibration would continuously drive the body in a more appropriate fashion, ultimately resulting in better functional performance. Previous studies lend evidence for this hypothesis, showing that

pure sensory training and electrical stimulation before physical therapy sessions can lead to improved functional output after multiple weeks of training (Conforto et al., 2007; Hillier & Dunsford, 2006).

While tendon vibration during motor control normalizes cortical activity and connectivity in chronic stroke survivors during application, normalization of cortical activity and connectivity do not persist after vibration is terminated. Applying tendon vibration to stroke survivors in the acute phase may circumvent this issue. Within the acute stroke group, the central nervous system has been recently damaged and is in the process of relearning and reorganizing (Cicinelli et al., 1997; Delvaux et al., 2003; Rossini et al., 1998; Saur et al., 2006; Wang et al., 2010). Applying tendon vibration during motor control throughout this critical phase of relearning and reorganization may help push cortical networks towards more normal patterns of activation and connectivity. If cortical networks controlling the body after stroke can be normalized in the acute phase, there would be less of a need for cortical reorganization; this could lead to a reduced computational load on extraneous cortical areas used during cortical reorganization and potentially result in faster, better recovery.

It is yet to be seen whether tendon vibration training studies in the chronic stroke population or the application of tendon vibration in the acute stroke phase will lead to long-term improvements in functional outcomes. If improvements in performance cannot be maintained outside of training, a simple wearable vibration device could be designed and fixed to the patient’s arm allowing for improved functional outcomes when performing activities of daily living.

BIBLIOGRAPHY

Abbruzzese, G., Berardelli, A., Rothwell, J. C, Day, B. L., & Marsden, C. D. (1985). Cerebral potentials and electromyographic responses evoked by stretch of wrist muscles in man. *Experimental Brain Research*, *58*(3), 544–551. https://doi.org/10.1007/BF00235870

Akazawa, K., Milner, T. E., & Stein, R. B. (1983). Modulation of reflex EMG and stiffness in response to stretch of human finger muscle. *Journal of Neurophysiology*, *49*(1), 16–27. https://doi.org/10.1152/jn.1983.49.1.16

Alain, C., & Woods, D. L. (1994). Signal clustering modulates auditory cortical activity in humans. *Perception & Psychophysics*, *56*(5), 501–516. https://doi.org/10.3758/BF03206947

Alegre, M., Labarga, A., Gurtubay, I. G., Iriarte, J., Malanda, A., & Artieda, J. (2003). Movement-related changes in cortical oscillatory activity in ballistic, sustained and negative movements. *Experimental Brain Research*, *148*(1), 17–25. https://doi.org/10.1007/s00221-002-1255-x

Alstott, J., Breakspear, M., Hagmann, P., Cammoun, L., & Sporns, O. (2009). Modeling the Impact of Lesions in the Human Brain. *PLoS Computational Biology*, *5*(6). https://doi.org/10.1371/journal.pcbi.1000408

Amans, M. R. (2009). *Proprioceptive Feedback Contributions to the Control of Elbow Extension Movements in Man: Modulating Upper Limb Position Sense via Tendon Vibration*. Marquette University.

Aoki, Y., Ishii, R., Pascual-Marqui, R. D., Canuet, L., Ikeda, S., Hata, M., Imajo, K., Matsuzaki, H., Musha, T., Asada, T., Iwase, M., & Takeda, M. (2015). Detection of EEG-resting state independent networks by eLORETA-ICA method. *Frontiers in Human Neuroscience*, *9*, 1–12. https://doi.org/10.3389/fnhum.2015.00031

Ashe, J., & Georgopoulos, A. P. (1994). Movement Parameters and Neural Activity in Motor Cortex and Area 5. *Cerebral Cortex*, *4*(6), 590–600. https://doi.org/10.1093/cercor/4.6.590

Assenza, G., Zappasodi, F., Pasqualetti, P., Vernieri, F., & Tecchio, F. (2013). A contralesional EEG power increase mediated by interhemispheric disconnection provides negative prognosis in acute stroke. *Restorative Neurology and Neuroscience*, *31*(2), 177–188. https://doi.org/10.3233/RNN-120244

Baillet, S. (2011). Electromagnetic brain mapping using MEG & EEG. *Handbook of Social Neuroscience*, 97–133.

Baillet, S., Mosher, J. C., & Leahy, R. M. (2001). Electromagnetic brain mapping. *IEEE Signal Processing Magazine*, *18*(6), 14–30. https://doi.org/10.1109/79.962275

Baratta, R. V., Solomonow, M., & Zhou, B. H. (1998). Frequency domain-based models of skeletal muscle. *Journal of Electromyography and Kinesiology*, *8*(2), 79–91. https://doi.org/10.1016/S1050-6411(97)00024-2

Barry, R. J., Clarke, A. R., Johnstone, S. J., Magee, C. A., & Rushby, J. A. (2007). EEG differences between eyes-closed and eyes-open resting conditions. *Clinical Neurophysiology*, *118*(12), 2765–2773. https://doi.org/10.1016/j.clinph.2007.07.028

Bassett, D. S., & Bullmore, E. T. (2017). Small-World Brain Networks Revisited. *The Neuroscientist*, *23*(5), 499–516. https://doi.org/10.1177/1073858416667720

Bassett, D. S., & Bullmore, E. (2006). Small-World Brain Networks. *The Neuroscientist*, *12*(6), 512–523. https://doi.org/10.1177/1073858406293182

Beer, R. F., Dewald, J. P. A., & Rymer, W. Z. (2000). Deficits in the coordination of multijoint arm movements in patients with hemiparesis: evidence for disturbed control of limb dynamics. *Experimental Brain Research*, *131*(3), 305–319. https://doi.org/10.1007/s002219900275

Berman, B. D., Horovitz, S. G., Venkataraman, G., & Hallett, M. (2012). Self-modulation of primary motor cortex activity with motor and motor imagery tasks using real-time fMRI-based neurofeedback. *NeuroImage*, *59*(2), 917–925. https://doi.org/10.1016/j.neuroimage.2011.07.035

Bestmann, S., Baudewig, J., Siebner, H. R., Rothwell, J. C., & Frahm, J. (2005). BOLD MRI responses to repetitive TMS over human dorsal premotor cortex. *NeuroImage*, *28*(1), 22–29. https://doi.org/10.1016/j.neuroimage.2005.05.027

Biswal, B., Zerrin Yetkin, F., Haughton, V. M., & Hyde, J. S. (1995). Functional connectivity in the motor cortex of resting human brain using echo-planar mri. *Magnetic Resonance in Medicine*, *34*(4), 537–541. https://doi.org/10.1002/mrm.1910340409

Boettcher, C. E., Ginn, K. A., & Cathers, I. (2008). Standard maximum isometric voluntary contraction tests for normalizing shoulder muscle EMG. *Journal of Orthopaedic Research*, *26*(12), 1591–1597. https://doi.org/10.1002/jor.20675

Bönstrup, M., Schulz, R., Schön, G., Cheng, B., Feldheim, J., Thomalla, G., & Gerloff, C. (2018). Parietofrontal network upregulation after motor stroke. *NeuroImage: Clinical*, *18*(October 2017), 720–729. https://doi.org/10.1016/j.nicl.2018.03.006

Boonstra, T. W., Daffertshofer, A., Breakspear, M., & Beek, P. J. (2007). Multivariate time-frequency analysis of electromagnetic brain activity during bimanual motor

learning. *NeuroImage*, *36*(2), 370–377. https://doi.org/10.1016/j.neuroimage.2007.03.012

Bressler, S. L. (1995). Large-scale cortical networks and cognition. *Brain Research Reviews*, *20*(3), 288–304. https://doi.org/10.1016/0165-0173(94)00016-I

Bridgeman, B. (1995). A review of the role of efference copy in sensory and oculomotor control systems. *Annals of Biomedical Engineering*, *23*(4), 409–422. https://doi.org/10.1007/BF02584441

Brookes, M. J., Woolrich, M., Luckhoo, H., Price, D., Hale, J. R., Stephenson, M. C., Barnes, G. R., Smith, S. M., & Morris, P. G. (2011). Investigating the electrophysiological basis of resting state networks using magnetoencephalography. *Proceedings of the National Academy of Sciences*, *108*(40), 16783–16788. https://doi.org/10.1073/pnas.1112685108

Brookes, M. J., Woolrich, M. W., & Barnes, G. R. (2012). Measuring functional connectivity in MEG: A multivariate approach insensitive to linear source leakage. *NeuroImage*, *63*(2), 910–920. https://doi.org/10.1016/j.neuroimage.2012.03.048

Brunnstrom, S. (1970). *Movement therapy in hemiplegia: a neurophysiological approach*. Harper & Row.

Buchanan, T. S., Rovai, G. P., & Rymer, W. Z. (1989). Strategies for muscle activation during isometric torque generation at the human elbow. *Journal of Neurophysiology*, *62*(6), 1201–1212. https://doi.org/10.1152/jn.1989.62.6.1201

Bullock, T. H., McClune, M. C., Achimowicz, J. Z., Iragui-Madoz, V. J., Duckrow, R. B., & Spencer, S. S. (1995). Temporal fluctuations in coherence of brain waves. *Proceedings of the National Academy of Sciences*, *92*(25), 11568–11572. https://doi.org/10.1073/pnas.92.25.11568

Burke, D., Hagbarth, K.-E., Lofstedt, L., & Wallin, B. G. (1976). the Responses of Human Muscle Spindle Endings. *Journal of Physiology*, *261*, 695–711.

Burns, J. K., & Blohm, G. (2010). Multi-Sensory Weights Depend on Contextual Noise in Reference Frame Transformations. *Frontiers in Human Neuroscience*, *4*(December), 1–15. https://doi.org/10.3389/fnhum.2010.00221

Buzsáki, G., & Draguhn, A. (2004). Neuronal oscillations in cortical networks. *Science (New York, N.Y.)*, *304*(5679), 1926–1929. https://doi.org/10.1126/science.1099745

Calautti, C., Naccarato, M., Jones, P. S., Sharma, N., Day, D. D., Carpenter, A. T., Bullmore, E. T., Warburton, E. A., & Baron, J. C. (2007). The relationship between motor deficit and hemisphere activation balance after stroke: A 3T fMRI study. *NeuroImage*, *34*(1), 322–331. https://doi.org/10.1016/j.neuroimage.2006.08.026

Carey, J. R., Kimberley, T. J., Lewis, S. M., Auerbach, E. J., Dorsey, L., Rundquist, P., & Ugurbil, K. (2002). Analysis of fMRI and finger tracking training in subjects with chronic stroke. *Brain*, *125*(4), 773–788. https://doi.org/10.1093/brain/awf091

Carey, L. M. (1995). Somatosensory Loss after Stroke. *Critical Reviews in Physical and Rehabilitation Medicine*, *7*(1), 51–91. https://doi.org/10.1615/CritRevPhysRehabilMed.v7.i1.40

Carmichael, S. T. (2006). Cellular and molecular mechanisms of neural repair after stroke: Making waves. *Annals of Neurology*, *59*(5), 735–742. https://doi.org/10.1002/ana.20845

Carmichael, S. T. (2008). Themes and Strategies for Studying the Biology of Stroke Recovery in the Poststroke Epoch. *Stroke*, *39*(4), 1380–1388. https://doi.org/10.1161/STROKEAHA.107.499962

Carter, A. R., Astafiev, S. V, Lang, C. E., Connor, L. T., Rengachary, J., Strube, M. J., Pope, D. L. W., Shulman, G. L., & Corbetta, M. (2009). Resting state inter-hemispheric fMRI connectivity predicts performance after stroke. *Annals of Neurology*, *67*(3), NA-NA. https://doi.org/10.1002/ana.21905

Cavanna, A. E., & Trimble, M. R. (2006). The precuneus: A review of its functional anatomy and behavioural correlates. *Brain*, *129*(3), 564–583. https://doi.org/10.1093/brain/awl004

Celnik, P., Hummel, F., Harris-Love, M., Wolk, R., & Cohen, L. G. (2007). Somatosensory Stimulation Enhances the Effects of Training Functional Hand Tasks in Patients With Chronic Stroke. *Archives of Physical Medicine and Rehabilitation*, *88*(11), 1369–1376. https://doi.org/10.1016/j.apmr.2007.08.001

Centers for Disease Control and Prevention (CDC). (2009). Prevalence and most common causes of disability among adults--United States, 2005. *MMWR. Morbidity and Mortality Weekly Report*, *58*(16), 421–426.

Chen, A. C. N., Feng, W., Zhao, H., Yin, Y., & Wang, P. (2008). EEG default mode network in the human brain: Spectral regional field powers. *NeuroImage*, *41*(2), 561–574. https://doi.org/10.1016/j.neuroimage.2007.12.064

Chen, Y., Ding, M., & Scott Kelso, J. A. (2003). Task-related power and coherence changes in neuromagnetic activity during visuomotor coordination. *Experimental Brain Research*, *148*(1), 105–116. https://doi.org/10.1007/s00221-002-1244-0

Cheney, P. D., & Fetz, E. E. (1984). Corticomotoneuronal cells contribute to long latency stretch reflexes in the rhesus monkey. *The Journal of Physiology*, *349*(1), 249–272. https://doi.org/10.1113/jphysiol.1984.sp015155

Cheng, H., Wang, Y., Sheng, J., Kronenberger, W. G., Mathews, V. P., Hummer, T. A., & Saykin, A. J. (2012). Characteristics and variability of structural networks derived from diffusion tensor imaging. *NeuroImage*, *61*(4), 1153–1164. https://doi.org/10.1016/j.neuroimage.2012.03.036

Chollet, F., Dipiero, V., Wise, R. J. S., Brooks, D. J., Dolan, R. J., & Frackowiak, R. S. J. (1991). The functional anatomy of motor recovery after stroke in humans: A study with positron emission tomography. *Annals of Neurology*, *29*(1), 63–71. https://doi.org/10.1002/ana.410290112

Christensen, M. S., Lundbye-Jensen, J., Geertsen, S. S., Petersen, T. H., Paulson, O. B., & Nielsen, J. B. (2007). Premotor cortex modulates somatosensory cortex during voluntary movements without proprioceptive feedback. *Nature Neuroscience*, *10*(4), 417–419. https://doi.org/10.1038/nn1873

Cicinelli, P., Traversa, R., & Rossini, P. (1997). Post-stroke reorganization of brain motor output to the hand: a 2–4 month follow-up with focal magnetic transcranial stimulation. *Electroencephalography and Clinical Neurophysiology/Electromyography and Motor Control*, *105*(6), 438–450. https://doi.org/10.1016/S0924-980X(97)00052-0

Cirstea, M. C., & Levin, M. F. (2000). Compensatory strategies for reaching in stroke. *Brain*, *123*(5), 940–953. https://doi.org/10.1093/brain/123.5.940

Colclough, G. L., Brookes, M. J., Smith, S. M., & Woolrich, M. W. (2015). A symmetric multivariate leakage correction for MEG connectomes. *NeuroImage*, *117*, 439–448. https://doi.org/10.1016/j.neuroimage.2015.03.071

Colclough, G. L., Woolrich, M. W., Tewarie, P. K., Brookes, M. J., Quinn, A. J., & Smith, S. M. (2016). How reliable are MEG resting-state connectivity metrics? *NeuroImage*, *138*, 284–293. https://doi.org/10.1016/j.neuroimage.2016.05.070

Colebatch, J. G., Deiber, M. P., Passingham, R. E., Friston, K. J., & Frackowiak, R. S. J. (1991). Regional cerebral blood flow during voluntary arm and hand movements in human subjects. *Journal of Neurophysiology*, *65*(6), 1392–1401. https://doi.org/10.1152/jn.1991.65.6.1392

Conforto, A. B., Cohen, L. G., Santos, R. L. D., Scaff, M., & Marie, S. K. N. (2007). Effects of somatosensory stimulation on motor function in chronic cortico-subcortical strokes. *Journal of Neurology*, *254*(3), 333–339. https://doi.org/10.1007/s00415-006-0364-z

Connell, L., Lincoln, N., & Radford, K. (2008). Somatosensory impairment after stroke: frequency of different deficits and their recovery. *Clinical Rehabilitation*, *22*(8), 758–767. https://doi.org/10.1177/0269215508090674

Connolly, J. D., Andersen, R. A., & Goodale, M. A. (2003). FMRI evidence for a "parietal reach region" in the human brain. *Experimental Brain Research*, *153*(2), 140–145. https://doi.org/10.1007/s00221-003-1587-1

Conrad, M. O., Gadhoke, B., Scheidt, R. A., & Schmit, B. D. (2015). Effect of Tendon Vibration on Hemiparetic Arm Stability in Unstable Workspaces. *PLOS ONE*, *10*(12), e0144377. https://doi.org/10.1371/journal.pone.0144377

Conrad, M. O., Scheidt, R. A., & Schmit, B. D. (2011a). Effects of wrist tendon vibration on targeted upper-arm movements in poststroke hemiparesis. *Neurorehabilitation and Neural Repair*, *25*(1), 61–70. https://doi.org/10.1177/1545968310378507

Conrad, M. O., Scheidt, R. A., & Schmit, B. D. (2011b). Effects of wrist tendon vibration on arm tracking in people poststroke. *Journal of Neurophysiology*, *106*(3), 1480–1488. https://doi.org/10.1152/jn.00404.2010

Cooper, R., Winter, A., Crow, H., & Walter, W. G. (1965). Comparison of subcortical, cortical and scalp activity using chronically indwelling electrodes in man. *Electroencephalography and Clinical Neurophysiology*, *18*(3), 217–228. https://doi.org/10.1016/0013-4694(65)90088-X

Corbetta, M. (1998). Frontoparietal cortical networks for directing attention and the eye to visual locations: Identical, independent, or overlapping neural systems? *Proceedings of the National Academy of Sciences*, *95*(3), 831–838. https://doi.org/10.1073/pnas.95.3.831

Corbetta, M., & Shulman, G. L. (2002). Control of goal-directed and stimulus-driven attention in the brain. *Nature Reviews. Neuroscience*, *3*(3), 201–215. https://doi.org/10.1038/nrn755

Cordo, P, Gurfinkel, V. S., Bevan, L., & Kerr, G. K. (1995). Proprioceptive consequences of tendon vibration during movement. *Journal of Neurophysiology*, *74*(4), 1675–1688. https://doi.org/10.1152/jn.1995.74.4.1675

Cordo, P., Inglis, J. T., Verschueren, S., Collins, J. J., Merfeld, D. M., Rosenblum, S., Buckley, S., & Moss, F. (1996). Noise in human muscle spindles. *Nature*, *383*(6603), 769–770. https://doi.org/10.1038/383769a0

Correa, A. G., Laciar, E., Patiño, H. D., & Valentinuzzi, M. E. (2007). Artifact removal from EEG signals using adaptive filters in cascade. *Journal of Physics: Conference Series*, *90*(1), 012081. https://doi.org/10.1088/1742-6596/90/1/012081

Crago, P. E., Houk, J. C., & Hasan, Z. (1976). Regulatory actions of human stretch reflex. *Journal of Neurophysiology*, *39*(5), 925–935. https://doi.org/10.1152/jn.1976.39.5.925

Cremoux, S., Tallet, J., Dal Maso, F., Berton, E., & Amarantini, D. (2017). Impaired corticomuscular coherence during isometric elbow flexion contractions in humans with cervical spinal cord injury. *European Journal of Neuroscience*, *46*(4), 1991–2000. https://doi.org/10.1111/ejn.13641

Crofts, J. J., Higham, D. J., Bosnell, R., Jbabdi, S., Matthews, P. M., Behrens, T. E. J., & Johansen-Berg, H. (2011). Network analysis detects changes in the contralesional hemisphere following stroke. *NeuroImage*, *54*(1), 161–169. https://doi.org/10.1016/j.neuroimage.2010.08.032

Crofts, J. J., & Higham, D. J. (2009). A weighted communicability measure applied to complex brain networks. *Journal of the Royal Society Interface*, *6*(33), 411–414. https://doi.org/10.1098/rsif.2008.0484

Culham, J. C., & Valyear, K. F. (2006). Human parietal cortex in action. *Current Opinion in Neurobiology*, *16*(2), 205–212. https://doi.org/10.1016/j.conb.2006.03.005

Damoiseaux, J. S., Rombouts, S. A. R. B., Barkhof, F., Scheltens, P., Stam, C. J., Smith, S. M., & Beckmann, C. F. (2006). Consistent resting-state networks across healthy subjects. *Proceedings of the National Academy of Sciences*, *103*(37), 13848–13853. https://doi.org/10.1073/pnas.0601417103

David, O., Kilner, J. M., & Friston, K. J. (2006). Mechanisms of evoked and induced responses in MEG/EEG. *NeuroImage*, *31*(4), 1580–1591. https://doi.org/10.1016/j.neuroimage.2006.02.034

Dawson, G. D. (1947). Cerebral Responses to Electrical Stimulation of Peripheral Nerve in Man. *Journal of Neurology, Neurosurgery & Psychiatry*, *10*(3), 134–140. https://doi.org/10.1136/jnnp.10.3.134

De Vico Fallani, F., Astolfi, L., Cincotti, F., Mattia, D., la Rocca, D., Maksuti, E., Salinari, S., Babiloni, F., Vegso, B., Kozmann, G., & Nagy, Z. (2009). Evaluation of the Brain Network Organization From EEG Signals: A Preliminary Evidence in Stroke Patient. *The Anatomical Record: Advances in Integrative Anatomy and Evolutionary Biology*, *292*(12), 2023–2031. https://doi.org/10.1002/ar.20965

Delorme, A., & Makeig, S. (2004). EEGLAB: an open sorce toolbox for analysis of single-trail EEG dynamics including independent component anlaysis. *Journal of Neuroscience Methods*, *134*, 9–21. https://doi.org/10.1016/j.jneumeth.2003.10.009

Delorme, A., Palmer, J., Onton, J., Oostenveld, R., & Makeig, S. (2012). Independent EEG sources are dipolar. *PLoS ONE*, *7*(2). https://doi.org/10.1371/journal.pone.0030135

Delvaux, V., Alagona, G., Gérard, P., De Pasqua, V., Pennisi, G., & De Noordhout, A.

M. (2003). Post-stroke reorganization of hand motor area: A 1-year prospective follow-up with focal transcranial magnetic stimulation. *Clinical Neurophysiology*, *114*(7), 1217–1225. https://doi.org/10.1016/S1388-2457(03)00070-1

Demandt, E., Mehring, C., Vogt, K., Schulze-Bonhage, A., Aertsen, A., & Ball, T. (2012). Reaching movement onset- and end-related characteristics of EEG spectral power modulations. *Frontiers in Neuroscience*, *6*(MAY), 1–11. https://doi.org/10.3389/fnins.2012.00065

Denny, M. R., Frisbey, N., & Weaver, J. (1955). Rotary pursuit performance under alternate conditions of distributed and massed practice. *Journal of Experimental Psychology*, *49*(1), 48–54. https://doi.org/10.1037/h0041724

Desikan, R. S., Ségonne, F., Fischl, B., Quinn, B. T., Dickerson, B. C., Blacker, D., Buckner, R. L., Dale, A. M., Maguire, R. P., Hyman, B. T., Albert, M. S., & Killiany, R. J. (2006). An automated labeling system for subdividing the human cerebral cortex on MRI scans into gyral based regions of interest. *NeuroImage*, *31*(3), 968–980. https://doi.org/10.1016/j.neuroimage.2006.01.021

Desimone, R., & Duncan, J. (1995). Neural Mechanisms of Selective Visual Attention. *Annual Review of Neuroscience*, *18*(1), 193–222. https://doi.org/10.1146/annurev.ne.18.030195.001205

Dewald, J. P. A., Pope, P. S., Given, J. D., Buchanan, T. S., & Rymer, W. Z. (1995). Abnormal muscle coactivation patterns during isometric torque generation at the elbow and shoulder in hemiparetic subjects. *Brain*, *118*(2), 495–510. https://doi.org/10.1093/brain/118.2.495

Dong, Y., Dobkin, B. H., Cen, S. Y., Wu, A. D., & Winstein, C. J. (2006). Motor Cortex Activation During Treatment May Predict Therapeutic Gains in Paretic Hand Function After Stroke. *Stroke*, *37*(6), 1552–1555. https://doi.org/10.1161/01.STR.0000221281.69373.4e

Dubovik, S., Pignat, J.-M., Ptak, R., Aboulafia, T., Allet, L., Gillabert, N., Magnin, C., Albert, F., Momjian-Mayor, I., Nahum, L., Lascano, A. M., Michel, C. M., Schnider, A., & Guggisberg, A. G. (2012). The behavioral significance of coherent resting-state oscillations after stroke. *NeuroImage*, *61*(1), 249–257. https://doi.org/10.1016/j.neuroimage.2012.03.024

Dubovik, S., Ptak, R., Aboulafia, T., Magnin, C., Gillabert, N., Allet, L., Pignat, J. M., Schnider, A., & Guggisberg, A. G. (2013). EEG alpha band synchrony predicts cognitive and motor performance in patients with ischemic stroke. *Behavioural Neurology*, *26*(3), 187–189. https://doi.org/10.3233/BEN-2012-129007

Eckhorn, R. (1994). Oscillatory and non-oscillatory synchronizations in the visual cortex and their possible roles in associations of visual features. In J. van Pelt, M. Corner,

& F. Lopes da Silva (Eds.), *Progress in Brain Research* (Vol. 102). Elsevier B.V. https://doi.org/10.1016/S0079-6123(08)60556-7

Eichele, T., Calhoun, V. D., Moosmann, M., Specht, K., Jongsma, M. L. A., Quiroga, R. Q., Nordby, H., & Hugdahl, K. (2008). Unmixing concurrent EEG-fMRI with parallel independent component analysis. *International Journal of Psychophysiology*, *67*(3), 222–234. https://doi.org/10.1016/j.ijpsycho.2007.04.010

Engel, A. K., & Fries, P. (2010). Beta-band oscillations-signalling the status quo? *Current Opinion in Neurobiology*, *20*(2), 156–165. https://doi.org/10.1016/j.conb.2010.02.015

Ernst, M. O., & Banks, M. S. (2002). Humans integrate visual and haptic information in a statistically optimal fashion. *Nature*, *415*(6870), 429–433. https://doi.org/10.1038/415429a

Essl, M., & Rappelsberger, P. (1998). EEG cohererence and reference signals: Experimental results and mathematical explanations. *Medical and Biological Engineering and Computing*, *36*(4), 399–406. https://doi.org/10.1007/BF02523206

Everling, S., Tinsley, C. J., Gaffan, D., & Duncan, J. (2002). Filtering of neural signals by focused attention in the monkey prefrontal cortex. *Nature Neuroscience*, *5*(7), 671–676. https://doi.org/10.1038/nn874

Faisal, A. A., Selen, L. P. J., & Wolpert, D. M. (2008). Noise in the nervous system. *Nature Reviews Neuroscience*, *9*(4), 292–303. https://doi.org/10.1038/nrn2258

Fallon, J. B., & Macefield, V. G. (2007). Vibration sensitivity of human muscle spindles and golgi tendon organs. *Muscle and Nerve*, *36*(1), 21–29. https://doi.org/10.1002/mus.20796

Fang, Y., Yue, G. H., Hrovat, K., Sahgal, V., & Daly, J. J. (2007). Abnormal cognitive planning and movement smoothness control for a complex shoulder/elbow motor task in stroke survivors. *Journal of the Neurological Sciences*, *256*(1–2), 21–29. https://doi.org/10.1016/j.jns.2007.01.078

Feinberg, I. (1978). Efference Copy and Corollary Discharge: Implications for Thinking and Its Disorders*. *Schizophrenia Bulletin*, *4*(4), 636–640. https://doi.org/10.1093/schbul/4.4.636

Feldman, A. G. (1986). Once More on the Equilibrium-Point Hypothesis (λ Model) for Motor Control. *Journal of Motor Behavior*, *18*(1), 17–54. https://doi.org/10.1080/00222895.1986.10735369

Filimon, F., Nelson, J. D., Huang, R.-S., & Sereno, M. I. (2009). Multiple Parietal Reach Regions in Humans: Cortical Representations for Visual and Proprioceptive

Feedback during On-Line Reaching. *Journal of Neuroscience*, *29*(9), 2961–2971. https://doi.org/10.1523/JNEUROSCI.3211-08.2009

Flash, T., & Hogan, N. (1985). The coordination of arm movements: an experimentally confirmed mathematical model. *The Journal of Neuroscience*, *5*(7), 1688–1703. https://doi.org/4020415

Foley, J. M., & Meyer, R. A. (1993). Energy cost of twitch and tetanic contractions of rat muscle estimatedin situ by gated31P NMR. *NMR in Biomedicine*, *6*(1), 32–38. https://doi.org/10.1002/nbm.1940060106

Formaggio, E., Storti, S. F., Boscolo Galazzo, I., Gandolfi, M., Geroin, C., Smania, N., Spezia, L., Waldner, A., Fiaschi, A., & Manganotti, P. (2013). Modulation of event-related desynchronization in robot-assisted hand performance: Brain oscillatory changes in active, passive and imagined movements. *Journal of NeuroEngineering and Rehabilitation*, *10*(1), 1. https://doi.org/10.1186/1743-0003-10-24

Fortier, P. A., Kalaska, J. F., & Smith, A. M. (1989). Cerebellar neuronal activity related to whole-arm reaching movements in the monkey. *Journal of Neurophysiology*, *62*(1), 198–211. https://doi.org/10.1152/jn.1989.62.1.198

Franklin, D. W., Burdet, E., Osu, R., Kawato, M., & Milner, T. E. (2003a). Functional significance of stiffness in adaptation of multijoint arm movements to stable and unstable dynamics. *Experimental Brain Research*, *151*(2), 145–157. https://doi.org/10.1007/s00221-003-1443-3

Franklin, D. W., Osu, R., Burdet, E., Kawato, M., & Milner, T. E. (2003b). Adaptation to Stable and Unstable Dynamics Achieved By Combined Impedance Control and Inverse Dynamics Model. *Journal of Neurophysiology*, *90*(5), 3270–3282. https://doi.org/10.1152/jn.01112.2002

Franklin, D. W., So, U., Kawato, M., & Milner, T. E. (2004). Impedance Control Balances Stability With Metabolically Costly Muscle Activation. *Journal of Neurophysiology*, *92*(5), 3097–3105. https://doi.org/10.1152/jn.00364.2004

Fugl-Meyer, A. R., Jääskö, L., Leyman, I., Olsson, S., & Steglind, S. (1975). The post-stroke hemiplegic patient. 1. a method for evaluation of physical performance. *Scandinavian Journal of Rehabilitation Medicine*, *7*(1), 13–31.

Gadhoke, B. (2011). *Role of tendon vibration in multijoint reflex coupling in the hemiparetic arm post stroke*. Marquette University.

Gale, A., Coles, M., & Boyd, E. (1971). Variation in visual input and the occipital EEG: II. *Psychonomic Science*, *23*(1), 99–100. https://doi.org/10.3758/BF03336026

Gale, A., Dunkin, N., & Coles, M. (1969). Variation in visual input and the occipital

EEG. *Psychonomic Science*, *14*(6), 262–263. https://doi.org/10.3758/BF03329113

Gauthier, G. M., & Robinson, D. A. (1975). Adaptation of the human vestibuloocular reflex to magnifying lenses. *Brain Research*, *92*(2), 331–335. https://doi.org/10.1016/0006-8993(75)90279-6

Ghez, C., & Shinoda, Y. (1978). Spinal mechanisms of the functional stretch reflex. *Experimental Brain Research*, *32*(1), 55–68. https://doi.org/10.1007/BF00237390

Giblin, D. R. (2006). Somatosensory Evoked Potentials in Healthy Subjects and in Patients with Lesions of the Nervous System. *Annals of the New York Academy of Sciences*, *112*(1), 93–142. https://doi.org/10.1111/j.1749-6632.1964.tb26744.x

Gilbertson, T. (2005). Existing Motor State Is Favored at the Expense of New Movement during 13-35 Hz Oscillatory Synchrony in the Human Corticospinal System. *Journal of Neuroscience*, *25*(34), 7771–7779. https://doi.org/10.1523/JNEUROSCI.1762-05.2005

Golaszewski, S. M., Siedentopf, C. M., Koppelstaetter, F., Fend, M., Ischebeck, A., Gonzalez-Felipe, V., Haala, I., Struhal, W., Mottaghy, F. M., Gallasch, E., Felber, S. R., & Gerstenbrand, F. (2006). Human brain structures related to plantar vibrotactile stimulation: A functional magnetic resonance imaging study. *NeuroImage*, *29*(3), 923–929. https://doi.org/10.1016/j.neuroimage.2005.08.052

Goldman, R., Stern, J., Engel, J., & Cohen, M. (2002). Simultaneous EEG and fMRI of the alpha rhythm. *NeuroReport*, *23*(1), 2487–2492. https://doi.org/10.1097/01.wnr.0000047685.08940.d0

Gordon, J., Ghilardi, M. F., & Ghez, C. (1995). Impairments of reaching movements in patients without proprioception. I. Spatial errors. *Journal of Neurophysiology*, *73*(1), 347–360. https://doi.org/10.1152/jn.1995.73.1.347

Gourab, K., & Schmit, B. D. (2010). Changes in movement-related β-band EEG signals in human spinal cord injury. *Clinical Neurophysiology*, *121*(12), 2017–2023. https://doi.org/10.1016/j.clinph.2010.05.012

Gracies, J. M. (2005). Pathophysiology of spastic paresis. II: Emergence of muscle overactivity. *Muscle and Nerve*, *31*(5), 552–571. https://doi.org/10.1002/mus.20285

Gramfort, A., Papadopoulo, T., Olivi, E., & Clerc, M. (2010). OpenMEEG: Opensource software for quasistatic bioelectromagnetics. *BioMedical Engineering Online*, *9*, 1–20. https://doi.org/10.1186/1475-925X-9-45

Grech, R., Cassar, T., Muscat, J., Camilleri, K. P., Fabri, S. G., Zervakis, M., Xanthopoulos, P., Sakkalis, V., & Vanrumste, B. (2008). Review on solving the inverse problem in EEG source analysis. *Journal of NeuroEngineering and*

Rehabilitation, *5*, 1–33. https://doi.org/10.1186/1743-0003-5-25

Grefkes, C., & Fink, G. R. (2011). Reorganization of cerebral networks after stroke: New insights from neuroimaging with connectivity approaches. *Brain*, *134*(5), 1264–1276. https://doi.org/10.1093/brain/awr033

Grefkes, C., & Fink, G. R. (2014). Connectivity-based approaches in stroke and recovery of function. *The Lancet Neurology*, *13*(2), 206–216. https://doi.org/10.1016/S1474-4422(13)70264-3

Grefkes, C., Nowak, D. A., Eickhoff, S. B., Dafotakis, M., Küst, J., Karbe, H., & Fink, G. R. (2008). Cortical connectivity after subcortical stroke assessed with functional magnetic resonance imaging. *Annals of Neurology*, *63*(2), 236–246. https://doi.org/10.1002/ana.21228

Grefkes, C., Nowak, D. A., Wang, L. E., Dafotakis, M., Eickhoff, S. B., & Fink, G. R. (2010). Modulating cortical connectivity in stroke patients by rTMS assessed with fMRI and dynamic causal modeling. *NeuroImage*, *50*(1), 233–242. https://doi.org/10.1016/j.neuroimage.2009.12.029

Gribble, P. L., Mullin, L. I., Cothros, N., & Mattar, A. (2003). Role of Cocontraction in Arm Movement Accuracy. *Journal of Neurophysiology*, *89*(5), 2396–2405. https://doi.org/10.1152/jn.01020.2002

Gu, S., Pasqualetti, F., Cieslak, M., Telesford, Q. K., Yu, A. B., Kahn, A. E., Medaglia, J. D., Vettel, J. M., Miller, M. B., Grafton, S. T., & Bassett, D. S. (2015). Controllability of structural brain networks. *Nature Communications*, *6*(1), 8414. https://doi.org/10.1038/ncomms9414

Guzzetta, A., Staudt, M., Petacchi, E., Ehlers, J., Erb, M., Wilke, M., Krägeloh-Mann, I., & Cioni, G. (2007). Brain representation of active and passive hand movements in children. *Pediatric Research*, *61*(4), 485–490. https://doi.org/10.1203/pdr.0b013e3180332c2e

Gwin, J. T., & Ferris, D. P. (2012). An EEG-based study of discrete isometric and isotonic human lower limb muscle contractions. *Journal of NeuroEngineering and Rehabilitation*, *9*(1), 1–11. https://doi.org/10.1186/1743-0003-9-35

Hadipour-Niktarash, A., Lee, C. K., Desmond, J. E., & Shadmehr, R. (2007). Impairment of Retention But Not Acquisition of a Visuomotor Skill Through Time-Dependent Disruption of Primary Motor Cortex. *Journal of Neuroscience*, *27*(49), 13413–13419. https://doi.org/10.1523/jneurosci.2570-07.2007

Hagmann, P., Cammoun, L., Gigandet, X., Meuli, R., Honey, C. J., Van Wedeen, J., & Sporns, O. (2008). Mapping the structural core of human cerebral cortex. *PLoS Biology*, *6*(7), 1479–1493. https://doi.org/10.1371/journal.pbio.0060159

Hämäläinen, M. S., & Ilmoniemi, R. J. (1994). Interpreting magnetic fields of the brain: minimum norm estimates. *Medical & Biological Engineering & Computing*, *32*(1), 35–42. https://doi.org/10.1007/BF02512476

Hari, R., & Salmelin, R. (1997). Human cortical oscillations: A neuromagnetic view through the skull. *Trends in Neurosciences*, *20*(1), 44–49. https://doi.org/10.1016/S0166-2236(96)10065-5

Hasan, Z. (2005). The Human Motor Control System's Response to Mechanical Perturbation: Should It, Can It and Does It Ensure Stability? *Journal of Motor Behavior*, *37*(6), 484–493. https://doi.org/10.3200/JMBR.37.6.484-493

Hidler, J. M., & Rymer, W. Z. (1999). A simulation study of reflex instability in spasticity: Origins of clonus. *IEEE Transactions on Rehabilitation Engineering*, *7*(3), 327–340. https://doi.org/10.1109/86.788469

Hillier, S., & Dunsford, A. (2006). A pilot study of sensory retraining for the hemiparetic foot post-stroke. *International Journal of Rehabilitation Research*, *29*(3), 237–242. https://doi.org/10.1097/01.mrr.0000210052.32539.22

Hincapié, A. S., Kujala, J., Mattout, J., Pascarella, A., Daligault, S., Delpuech, C., Mery, D., Cosmelli, D., & Jerbi, K. (2017). The impact of MEG source reconstruction method on source-space connectivity estimation: A comparison between minimum-norm solution and beamforming. *NeuroImage*, *156*(April), 29–42. https://doi.org/10.1016/j.neuroimage.2017.04.038

Hipp, J. F., Hawellek, D. J., Corbetta, M., Siegel, M., & Engel, A. K. (2012). Large-scale cortical correlation structure of spontaneous oscillatory activity. *Nature Neuroscience*, *15*(6), 884–890. https://doi.org/10.1038/nn.3101

Hof, A. L. (1998). In vivo measurement of the series elasticity release curve of human triceps surae muscle. *Journal of Biomechanics*, *31*(9), 793–800. https://doi.org/10.1016/S0021-9290(98)00062-1

Hogan, M. C., Kurdak, S. S., & Arthur, P. G. (1996). Effect of gradual reduction in O2 delivery on intracellular homeostasis in contracting skeletal muscle. *Journal of Applied Physiology*, *80*(4), 1313–1321. https://doi.org/10.1152/jappl.1996.80.4.1313

Hogan, N. (1984). Adaptive Control of Mechanical Impedance by Coactivation of Antagonist Muscles. *IEEE Transactions on Automatic Control*, *AC-29*(8), 681–690.

Honey, C. J., & Sporns, O. (2008). Dynamical consequences of lesions in cortical networks. *Human Brain Mapping*, *29*(7), 802–809. https://doi.org/10.1002/hbm.20579

Houk, J. C., Fagg, A. H., & Barto, A. G. (2000). Fractional Power Damping Model of

Joint Motion. In M. L. Latash (Ed.), *Progress in motor control: structure-function relations in voluntary movements* (pp. 147–178).

Houweling, S., Daffertshofer, A., van Dijk, B. W., & Beek, P. J. (2008). Neural changes induced by learning a challenging perceptual-motor task. *NeuroImage*, *41*(4), 1395–1407. https://doi.org/10.1016/j.neuroimage.2008.03.023

Huang, H., & Ding, M. (2016). Linking Functional Connectivity and Structural Connectivity Quantitatively: A Comparison of Methods. *Brain Connectivity*, *6*(2), 99–108. https://doi.org/10.1089/brain.2015.0382

Hyngstrom, A., Onushko, T., Chua, M., & Schmit, B. D. (2010). Abnormal Volitional Hip Torque Phasing and Hip Impairments in Gait Post Stroke. *Journal of Neurophysiology*, *103*(3), 1557–1568. https://doi.org/10.1152/jn.00528.2009

Hyvärinen, A., & Oja, E. (2000). Independent component analysis: algorithms and applications. *Neural Networks*, *13*(4–5), 411–430. https://doi.org/10.1016/S0893-6080(00)00026-5

Iacoboni, M., & Zaidel, E. (2004). Interhemispheric visuo-motor integration in humans: The role of the superior parietal cortex. *Neuropsychologia*, *42*(4), 419–425. https://doi.org/10.1016/j.neuropsychologia.2003.10.007

Indovina, I., & Sanes, J. N. (2001). On Somatotopic Representation Centers for Finger Movements in Human Primary Motor Cortex and Supplementary Motor Area. *NeuroImage*, *13*(6), 1027–1034. https://doi.org/10.1006/nimg.2001.0776

Inman, C. S., James, G. A., Hamann, S., Rajendra, J. K., Pagnoni, G., & Butler, A. J. (2012). Altered resting-state effective connectivity of fronto-parietal motor control systems on the primary motor network following stroke. *NeuroImage*, *59*(1), 227–237. https://doi.org/10.1016/j.neuroimage.2011.07.083

James, G. A., Lu, Z.-L., VanMeter, J. W., Sathian, K., Hu, X. P., & Butler, A. J. (2009). Changes in Resting State Effective Connectivity in the Motor Network Following Rehabilitation of Upper Extremity Poststroke Paresis. *Topics in Stroke Rehabilitation*, *16*(4), 270–281. https://doi.org/10.1310/tsr1604-270

Jasper, H., & Penfield, W. (1949). Electrocorticograms in man: Effect of voluntary movement upon the electrical activity of the precentral gyrus. *Archiv for Psychiatrie Und Nervenkrankheiten*, *183*(1–2), 163–174. https://doi.org/10.1007/BF01062488

Jervis, B. W., Coelho, M., & Morgan, G. W. (1989). Effect on EEG responses of removing ocular artefacts by proportional EOG subtraction. *Medical & Biological Engineering & Computing*, *27*(5), 484–490. https://doi.org/10.1007/BF02441466

Johansen-Berg, H., Rushworth, M. F. S., Bogdanovic, M. D., Kischka, U., Wimalaratna,

S., & Matthews, P. M. (2002). The role of ipsilateral premotor cortex in hand movement after stroke. *Proceedings of the National Academy of Sciences*, *99*(22), 14518–14523. https://doi.org/10.1073/pnas.222536799

Kalaska, J. F., Scott, S. H., Cisek, P., & Sergio, L. E. (1997). Cortical control of reaching movements. *Curr.Opin.Neurobiol.*, *7*(0959-4388 (Print)), 849–859. https://doi.org/10.1016/S0959-4388(97)80146-8

Kalinosky, B. (2016). *Structural-functional brain connectivity underlying integrative sensorimotor function after stroke.* (Issue May). Marquette University.

Kalinosky, B. T., Berrios Barillas, R., & Schmit, B. D. (2017). Structurofunctional resting-state networks correlate with motor function in chronic stroke. *NeuroImage: Clinical*, *16*(July), 610–623. https://doi.org/10.1016/j.nicl.2017.07.002

Kamper, D. G., McKenna-Cole, A. N., Kahn, L. E., & Reinkensmeyer, D. J. (2002). Alterations in reaching after stroke and their relation to movement direction and impairment severity. *Archives of Physical Medicine and Rehabilitation*, *83*(5), 702–707. https://doi.org/10.1053/apmr.2002.32446

Karamzadeh, N., Medvedev, A., Azari, A., Gandjbakhche, A., & Najafizadeh, L. (2013). Capturing dynamic patterns of task-based functional connectivity with EEG. *NeuroImage*, *66*, 311–317. https://doi.org/10.1016/j.neuroimage.2012.10.032

Kawano, T., Hattori, N., Uno, Y., Kitajo, K., Hatakenaka, M., Yagura, H., Fujimoto, H., Yoshioka, T., Nagasako, M., Otomune, H., & Miyai, I. (2017). Large-Scale Phase Synchrony Reflects Clinical Status After Stroke: An EEG Study. *Neurorehabilitation and Neural Repair*, *31*(6), 561–570. https://doi.org/10.1177/1545968317697031

Kilavik, B. E., Zaepffel, M., Brovelli, A., MacKay, W. A., & Riehle, A. (2013). The ups and downs of beta oscillations in sensorimotor cortex. *Experimental Neurology*, *245*, 15–26. https://doi.org/10.1016/j.expneurol.2012.09.014

Koenig, T., Studer, D., Hubl, D., Melie, L., & Strik, W. . (2005). Brain connectivity at different time-scales measured with EEG. *Philosophical Transactions of the Royal Society B: Biological Sciences*, *360*(1457), 1015–1024. https://doi.org/10.1098/rstb.2005.1649

Kopell, N., Ermentrout, G. B., Whittington, M. A., & Traub, R. D. (2000). Gamma rhythms and beta rhythms have different synchronization properties. *Proceedings of the National Academy of Sciences*, *97*(4), 1867–1872. https://doi.org/10.1073/pnas.97.4.1867

Köpruner, V., & Pfurtscheller, G. (1984). Multiparametric asymmetry score (MAS) — distinction between normal and ischaemic brains. *Electroencephalography and*

Clinical Neurophysiology, *57*(4), 343–346. https://doi.org/10.1016/0013-4694(84)90157-3

Kornhuber, H. H., & Deecke, L. (2016). Brain potential changes in voluntary and passive movements in humans: readiness potential and reafferent potentials. *Pflügers Archiv - European Journal of Physiology*, *468*(7), 1115–1124. https://doi.org/10.1007/s00424-016-1852-3

Koshland, G. F., Hasan, Z., & Gerilovsky, L. (1991). Activity of wrist muscles elicited during imposed or voluntary movements about the elbow joint. *Journal of Motor Behavior*, *23*(2), 91–100. https://doi.org/10.1080/00222895.1991.9942026

Krakauer, J. W., & Shadmehr, R. (2006). Consolidation of motor memory. *Trends in Neurosciences*, *29*(1), 58–64. https://doi.org/10.1016/j.tins.2005.10.003

Kurtzer, I. L., Pruszynski, J. A., & Scott, S. H. (2008). Long-Latency Reflexes of the Human Arm Reflect an Internal Model of Limb Dynamics. *Current Biology*, *18*(6), 449–453. https://doi.org/10.1016/j.cub.2008.02.053

Kybic, J., Clerc, M., Abboud, T., Faugeras, O., Keriven, R., & Papadopoulo, T. (2005). A common formalism for the integral formulations of the forward EEG problem. *IEEE Transactions on Medical Imaging*, *24*(1), 12–28. https://doi.org/10.1109/TMI.2004.837363

Lacquaniti, F., & Soechting, J. F. (1984). Behavior of the stretch reflex in a multi-jointed limb. *Brain Research*, *311*(1), 161–166. https://doi.org/10.1016/0006-8993(84)91411-2

Lacquaniti, F., & Soechting, J. F. (1986). EMG responses to load perturbations of the upper limb: effect of dynamic coupling between shoulder and elbow motion. *Experimental Brain Research*, *61*(3). https://doi.org/10.1007/BF00237573

Lance, J. W. (1980). The control of muscle tone, reflexes, and movement: Robert Wartenbeg Lecture. *Neurology*, *30*(12), 1303–1303. https://doi.org/10.1212/WNL.30.12.1303

Lange, G., Waked, W., Kirshblum, S., & DeLuca, J. (2000). Organizational strategy influence on visual memory performance after stroke: Cortical/subcortical and left/right hemisphere contrasts. *Archives of Physical Medicine and Rehabilitation*, *81*(1), 89–94. https://doi.org/10.1016/S0003-9993(00)90227-2

Latash, M. L. (2000). The organization of quick corrections within a two-joint synergy in conditions of unexpected blocking and release of a fast movement. *Clinical Neurophysiology*, *111*(6), 975–987. https://doi.org/10.1016/S1388-2457(00)00263-7

Latash, M. L., Levin, M. F., Scholz, J. P., & Schöner, G. (2010). Motor control theories

and their applications. *Medicina (Kaunas, …*, *46*(6), 382–392. https://doi.org/10.1016/j.bbi.2008.05.010

Lee, J. J., & Schmit, B. D. (2018). Effect of sensory attenuation on cortical movement-related oscillations. *Journal of Neurophysiology*, *119*(3), 971–978. https://doi.org/10.1152/jn.00171.2017

Leech, R., & Sharp, D. J. (2014). The role of the posterior cingulate cortex in cognition and disease. *Brain*, *137*(1), 12–32. https://doi.org/10.1093/brain/awt162

Leocani, L., Toro, C., Manganotti, P., Zhuang, P., & Hallett, M. (1997). Event-related coherence and event-related desynchronization/synchronization in the 10 Hz and 20 Hz EEG during self- paced movements. *Electroencephalography and Clinical Neurophysiology - Evoked Potentials*, *104*(3), 199–206. https://doi.org/10.1016/S0168-5597(96)96051-7

Levin, M. F., & Hui-Chan, C. W. Y. (1992). Relief of hemiparetic spasticity by TENS is associated with improvement in reflex and voluntary motor functions. *Electroencephalography and Clinical Neurophysiology/ Evoked Potentials*, *85*(2), 131–142. https://doi.org/10.1016/0168-5597(92)90079-Q

Liepert, J., Hamzei, F., & Weiller, C. (2000). Motor cortex disinhibition of the unaffected hemisphere after acute stroke. *Muscle & Nerve*, *23*(11), 1761–1763. https://doi.org/10.1002/1097-4598(200011)23:11<1761::AID-MUS14>3.0.CO;2-M

Logothetis, N. K. (2002). The neural basis of the blood-oxygen-level-dependent functional magnetic resonance imaging signal. *Philosophical Transactions of the Royal Society B: Biological Sciences*, *357*(1424), 1003–1037. https://doi.org/10.1098/rstb.2002.1114

Logothetis, N. K. (2003). The underpinnings of the BOLD functional magnetic resonance imaging signal. *Journal of Neuroscience*, *23*(10), 3963–3971. https://doi.org/10.1523/jneurosci.23-10-03963.2003

Lopes da Silva, F. (2013). EEG and MEG: Relevance to Neuroscience. *Neuron*, *80*(5), 1112–1128. https://doi.org/10.1016/j.neuron.2013.10.017

Loram, I. D., & Lakie, M. (2002). Human balancing of an inverted pendulum: Position control by small, ballistic-like, throw and catch movements. *Journal of Physiology*, *540*(3), 1111–1124. https://doi.org/10.1113/jphysiol.2001.013077

Lotze, M., Erb, M., Flor, H., Huelsmann, E., Godde, B., & Grodd, W. (2000). fMRI Evaluation of Somatotopic Representation in Human Primary Motor Cortex. *NeuroImage*, *11*(5), 473–481. https://doi.org/10.1006/nimg.2000.0556

Luck, S. J., & Kappenman, E. S. (2011). *The Oxford Handbook of event-related potential*

components. Oxford University Press.

Mahjoory, K., Nikulin, V. V., Botrel, L., Linkenkaer-Hansen, K., Fato, M. M., & Haufe, S. (2017). Consistency of EEG source localization and connectivity estimates. *NeuroImage*, *152*, 590–601. https://doi.org/10.1016/j.neuroimage.2017.02.076

Makeig, S., Debener, S., Onton, J., & Delorme, A. (2004). Mining event-related brain dynamics. *Trends in Cognitive Sciences*, *8*(5), 204–210. https://doi.org/10.1016/j.tics.2004.03.008

Mann, C. A., Sterman, M. B., & Kaiser, D. A. (1996). Suppression of EEG rhythmic frequencies during somato-motor and visuo-motor behavior. *International Journal of Psychophysiology*, *23*(1–2), 1–7. https://doi.org/10.1016/0167-8760(96)00036-0

Mantini, D., Perrucci, M. G., Del Gratta, C., Romani, G. L, Corbetta, M. (2007). Electrophysiological signatures of resting state networks in the human brain. *Proceedings of the National Academy of Sciences*, *104*(32), 13170. http://doi.org/10.1073/pnas.0700668104

Marcus, D. S., Harwell, J., Olsen, T., Hodge, M., Glasser, M. F., Prior, F., Jenkinson, M., Laumann, T., Curtiss, S. W., & Van Essen, D. C. (2011). Informatics and Data Mining Tools and Strategies for the Human Connectome Project. *Frontiers in Neuroinformatics*, *5*(June), 1–12. https://doi.org/10.3389/fninf.2011.00004

Marsden, C. D., Rothwell, J. C., & Day, B. L. (1983). Long-latencey automatic responses to muscle stretch in man: origin and function. *Advances in Neurology*, *39*, 509–539.

Mazer, B. L., Sofer, S., Korner-Bitensky, N., & Gelinas, I. (2001). Use of the UFOV to Evaluate and Retrain Visual Attention Skills in Clients With Stroke: A Pilot Study. *American Journal of Occupational Therapy*, *55*(5), 552–557. https://doi.org/10.5014/ajot.55.5.552

Mazoyer, B., Zago, L., Mellet, E., Bricogne, S., Etard, O., Houdé, O., Crivello, F., Joliot, M., Petit, L., & Tzourio-Mazoyer, N. (2001). Cortical networks for working memory and executive functions sustain the conscious resting state in man. *Brain Research Bulletin*, *54*(3), 287–298. https://doi.org/10.1016/S0361-9230(00)00437-8

McFarland, D. J., Miner, L. A., Vaughan, T. M., & Wolpaw, J. R. (2000). Mu and beta rhythm topographies during motor imagery and actual movements. *Brain Topography*, *12*(3), 177–186. https://doi.org/10.1023/A:1023437823106

Meissner, S. N., Krause, V., Südmeyer, M., Hartmann, C. J., & Pollok, B. (2018). The significance of brain oscillations in motor sequence learning: Insights from Parkinson's disease. *NeuroImage: Clinical*, *20*(August), 448–457. https://doi.org/10.1016/j.nicl.2018.08.009

Michel, C. M., Murray, M. M., Lantz, G., Gonzalez, S., Spinelli, L., & Grave de Peralta, R. (2004). EEG source imaging. *Clinical Neurophysiology*, *115*(10), 2195–2222. https://doi.org/10.1016/j.clinph.2004.06.001

Milner, T., Cloutier, C., Leger, A., & Franklin, D. (1995). Inability to activate muscles maximally during cocontraction and the effect on joint stiffness. *Experimental Brain Research*, *107*(2), 293–305. https://doi.org/10.1007/BF00230049

Mintzopoulos, D., Astrakas, L. G., Khanicheh, A., Konstas, A. A., Singhal, A., Moskowitz, M. A., Rosen, B. R., & Tzika, A. A. (2009). Connectivity alterations assessed by combining fMRI and MR-compatible hand robots in chronic stroke. *NeuroImage*, *47*, T90–T97. https://doi.org/10.1016/j.neuroimage.2009.03.007

Misulis, K., & Head, T. (2003). *Essentials of Clinical Neurophysiology* (Third). Elsevier.

Mognon, A., Jovicich, J., Bruzzone, L., & Buiatti, M. (2011). ADJUST: An automatic EEG artifact detector based on the joint use of spatial and temporal features. *Psychophysiology*, *48*(2), 229–240. https://doi.org/10.1111/j.1469-8986.2010.01061.x

Molholm, S., Sehatpour, P., Mehta, A. D., Shpaner, M., Gomez-Ramirez, M., Ortigue, S., Dyke, J. P., Schwartz, T. H., & Foxe, J. J. (2006). Audio-Visual Multisensory Integration in Superior Parietal Lobule Revealed by Human Intracranial Recordings. *Journal of Neurophysiology*, *96*(2), 721–729. https://doi.org/10.1152/jn.00285.2006

Morasso, P. G. P., & Sanguineti, V. (2002). Ankle muscle stiffness alone cannot stabilize balance during quiet standing. *Journal of Neurophysiology*, *88*(4), 2157–2162. https://doi.org/10.1152/jn.00719.2001

Morasso, P. G., & Schieppati, M. (1999). Can muscle stiffness alone stabilize upright standing? *Journal of Neurophysiology*, *82*(3), 1622–1626. https://doi.org/10.1152/jn.1999.82.3.1622

Mortimer, J. A., Webster, D. D., & Dukich, T. G. (1981). Changes in short and long latency stretch responses during the transition from posture to movement. *Brain Research*, *229*(2), 337–351. https://doi.org/10.1016/0006-8993(81)90998-7

Mozaffarian, D., Benjamin, E. J., Go, A. S., Arnett, D. K., Blaha, M. J., Cushman, M., Das, S. R., de Ferranti, S., Després, J.-P., Fullerton, H. J., Howard, V. J., Huffman, M. D., Isasi, C. R., Jiménez, M. C., Judd, S. E., Kissela, B. M., Lichtman, J. H., Lisabeth, L. D., Liu, S., … Turner, M. B. (2015). Heart Disease and Stroke Statistics—2016 Update. In *Circulation* (Vol. 133, Issue 4). https://doi.org/10.1161/cir.0000000000000350

Muellbacher, W., Ziemann, U., Wissel, J., Dang, N., Kofler, M., Facchini, S., Boroojerdi, B., Poewe, W., & Hallett, M. (2002). Early consolidation in human primary motor

cortex. *Nature*, *415*(6872), 640–644. https://doi.org/10.1038/nature712

Muldoon, S. F., Pasqualetti, F., Gu, S., Cieslak, M., Grafton, S. T., Vettel, J. M., & Bassett, D. S. (2016). Stimulation-Based Control of Dynamic Brain Networks. *PLOS Computational Biology*, *12*(9), e1005076. https://doi.org/10.1371/journal.pcbi.1005076

Murakami, S., & Okada, Y. (2006). Contributions of principal neocortical neurons to magnetoencephalography and electroencephalography signals. *The Journal of Physiology*, *575*(3), 925–936. https://doi.org/10.1113/jphysiol.2006.105379

Mutha, P. K., Boulinguez, P., & Sainburg, R. L. (2008). Visual modulation of proprioceptive reflexes during movement. *Brain Research*, *1246*, 54–69. https://doi.org/10.1016/j.brainres.2008.09.061

Newell, A., & Rosenbloom, P. S. (1981). Mechanisms of Skill Aquisition and the Law of Practice. In J. R. Anderson (Ed.), *Cognitive skills and their acquisition* (pp. 1–55). Erlbaum.

Ng, S. C., & Raveendran, P. (2007). EEG Peak Alpha Frequency as an Indicator for Physical Fatigue. In T. Jarm, P. Kramar, & A. Zupanic (Eds.), *11th Mediterranean Conference on Medical and Biomedical Engineering and Computing* (pp. 517–520). Springer-Verlag Berlin Heidelberg. https://doi.org/10.1007/978-3-540-73044-6_132

Nolte, G., Bai, O., Wheaton, L., Mari, Z., Vorbach, S., & Hallett, M. (2004). Identifying true brain interaction from EEG data using the imaginary part of coherency. *Clinical Neurophysiology*, *115*(10), 2292–2307. https://doi.org/10.1016/j.clinph.2004.04.029

Nolte, G., Ziehe, A., Nikulin, V. V., Schlögl, A., Krämer, N., Brismar, T., & Müller, K. R. (2008). Robustly estimating the flow direction of information in complex physical systems. *Physical Review Letters*, *100*(23), 1–4. https://doi.org/10.1103/PhysRevLett.100.234101

Nunez, P. (1995). *Neocortical Dynamics and Human EEG Rhythms*. Oxford University Press.

Nunez, P. L. (2000). Toward a quantitative description of large-scale neocortical dynamic function and EEG. *Behavioral and Brain Sciences*, *23*(3), 371–398. https://doi.org/10.1017/S0140525X00003253

Nunez, P. L., Silberstein, R. B., Shi, Z., Carpenter, M. R., Srinivasan, R., Tucker, D. M., Doran, S. M., Cadusch, P. J., & Wijesinghe, R. S. (1999). EEG coherency II: experimental comparisons of multiple measures. *Clinical Neurophysiology*, *110*(3), 469–486. https://doi.org/10.1016/S1388-2457(98)00043-1

Nunez, P. L., & Srinivasan, R. (2006). *Electric fields of the brain: The neuophysics of*

EEG (Second). Oxford University Press.

Nunez, P. L., Srinivasan, R., Westdorp, A. F., Wijesinghe, R. S., Tucker, D. M., Silberstein, R. B., & Cadusch, P. J. (1997). EEG coherency: I: statistics, reference elctrode, volume conduction, Laplacians, cortical imaging, and interpretation at multiple scales. *Electroencephalography and Clinical Neurophysiology*, *103*(5), 499–515. https://doi.org/10.1016/S0013-4694(97)00066-7

O'Neill, G. C., Tewarie, P. K., Colclough, G. L., Gascoyne, L. E., Hunt, B. A. E., Morris, P. G., Woolrich, M. W., & Brookes, M. J. (2017). Measurement of dynamic task related functional networks using MEG. *NeuroImage*, *146*. https://doi.org/10.1016/j.neuroimage.2016.08.061

Oostenveld, R., Fries, P., Maris, E., & Schoffelen, J. M. (2011). FieldTrip: Open source software for advanced analysis of MEG, EEG, and invasive electrophysiological data. *Computational Intelligence and Neuroscience*, *2011*. https://doi.org/10.1155/2011/156869

Palmer, J. A., Makeig, S., Kreutz-Delgado, K., & Rao, B. D. (2008). Newton method for the ICA mixture model. *IEEE International Conference on Acoustics, Speech and Signal Processing*, 1805–1808. https://doi.org/10.1109/ICASSP.2008.4517982

Pascual-Leone, A., Grafman, J., & Hallett, M. (1994). Modulation of cortical motor output maps during development of implicit and explicit knowledge. *Science*, *263*(5151), 1287–1289. https://doi.org/10.1126/science.8122113

Patel, A. T., Duncan, P. W., Lai, S. M., & Studenski, S. (2000). The relation between impairments and functional outcomes poststroke. *Archives of Physical Medicine and Rehabilitation*, *81*(10), 1357–1363. https://doi.org/10.1053/apmr.2000.9397

Pearson, J. M., Heilbronner, S. R., Barack, D. L., Hayden, B. Y., & Platt, M. L. (2011). Posterior cingulate cortex: adapting behavior to a changing world. *Trends in Cognitive Sciences*, *15*(4), 143–151. https://doi.org/10.1016/j.tics.2011.02.002

Pellegrino, G., Tomasevic, L., Tombini, M., Assenza, G., Bravi, M., Sterzi, S., Giacobbe, V., Zollo, L., Guglielmelli, E., Cavallo, G., Vernieri, F., & Tecchio, F. (2012). Inter-hemispheric coupling changes associate with motor improvements after robotic stroke rehabilitation. *Restorative Neurology and Neuroscience*, *30*(6), 497–510. https://doi.org/10.3233/RNN-2012-120227

Penfield, W., & Boldrey, E. (1937). Somatic Motor and Sensory Representation in Man. *Brain*, 389–443. https://doi.org/10.1093/brain/60.4.389

Pfluger, E. (1853). *Die Sensoriscen Functionen des Rückenmarks bei Wirbelttieren*.

Pfurtscheller, G., & Lopes da Silva, F. (1999). Functional Meaning of Event-related

Desynchronization End Sunchronization (ERS). In G Pfurtscheller & F. Lopes da Silva (Eds.), *Event-Related Desynchronization Handbook of Electroencephalography and Clinical Neurophysiology, vol 6* (pp. 51–66). Elsevier.

Pfurtscheller, G., Neuper, C., Andrew, C., & Edlinger, G. (1997). Foot and hand area mu rhythms. *International Journal of Psychophysiology*, *26*(1–3), 121–135. https://doi.org/10.1016/S0167-8760(97)00760-5

Pfurtscheller, G., Neuper, C., & Mohl, W. (1994). Event-related desynchronization (ERD) during visual processing. *International Journal of Psychophysiology*, *16*(2–3), 147–153. https://doi.org/10.1016/0167-8760(89)90041-X

Pfurtscheller, G., Pichler-Zalaudek, K., & Neuper, C. (1999). ERD and ERS in voluntary movement of different limbs. In G. Pfurtscheller & F. Lopes da Silva (Eds.), *Event-Related Desynchronization Handbook of Electroencephalography and Clinical Neurophysiology, vol 6* (Issue 6, pp. 245–268). Elsevier.

Pfurtscheller, G., Stancák, A., & Neuper, C. (1996). Post-movement beta synchronization. A correlate of an idling motor area? *Electroencephalography and Clinical Neurophysiology*, *98*(4), 281–293. https://doi.org/10.1016/0013-4694(95)00258-8

Pfurtscheller, G, & Lopes da Silva, F. H. (1999). Event-related EEG / MEG synchronization and desynchronization : basic principles. *Clinical Neurophysiology*, *110*, 1842–1857. https://doi.org/10.1016/S1388-2457(99)00141-8

Pfurtscheller, G., Zalaudek, K., & Neuper, C. (1998). Event-related beta synchronization after wrist, finger and thumb movement. *Electroencephalography and Clinical Neurophysiology - Electromyography and Motor Control*, *109*(2), 154–160. https://doi.org/10.1016/S0924-980X(97)00070-2

Platz, T., Kim, I., Pintschovious, H., Winter, T., Kieselback, A., Villringer, K., Kurth, R., & Mauritz, K. (2000). Multimodal EEG analysis in man suggests impairment-specific changes in movement-related electric brain activity after stroke. *Brain*, *123*(12), 2475–2490. https://doi.org/10.1093/brain/123.12.2475

Pogosyan, A., Gaynor, L. D., Eusebio, A., & Brown, P. (2009). Boosting Cortical Activity at Beta-Band Frequencies Slows Movement in Humans. *Current Biology*, *19*(19), 1637–1641. https://doi.org/10.1016/j.cub.2009.07.074

Polanía, R., Nitsche, M. A., & Paulus, W. (2011). Modulating functional connectivity patterns and topological functional organization of the human brain with transcranial direct current stimulation. *Human Brain Mapping*, *32*(8), 1236–1249. https://doi.org/10.1002/hbm.21104

Pollok, B., Latz, D., Krause, V., Butz, M., & Schnitzler, A. (2014). Changes of motor-

cortical oscillations associated with motor learning. *Neuroscience*, *275*, 47–53. https://doi.org/10.1016/j.neuroscience.2014.06.008

Pollok, B., Boysen, A. C., & Krause, V. (2015). The effect of transcranial alternating current stimulation (tACS) at alpha and beta frequency on motor learning. *Behavioural Brain Research*, *293*, 234–240. https://doi.org/10.1016/j.bbr.2015.07.049

Priplata, A. A., Niemi, J. B., Harry, J. D., Lipsitz, L. A., & Collins, J. J. (2003). Vibrating insoles and balance control in elderly people. *Lancet*, *362*(9390), 1123–1124. https://doi.org/10.1016/S0140-6736(03)14470-4

Priplata, A. A., Patritti, B. L., Niemi, J. B., Hughes, R., Gravelle, D. C., Lipsitz, L. A., Veves, A., Stein, J., Bonato, P., & Collins, J. J. (2006). Noise-enhanced balance control in patients with diabetes and patients with stroke. *Annals of Neurology*, *59*(1), 4–12. https://doi.org/10.1002/ana.20670

Pruszynski, J. A., Kurtzer, I., & Scott, S. H. (2011a). The long-latency reflex is composed of at least two functionally independent processes. *Journal of Neurophysiology*, *106*(1), 449–459. https://doi.org/10.1152/jn.01052.2010

Pruszynski, J. A., Kurtzer, I., & Scott, S. H. (2008). Rapid Motor Responses Are Appropriately Tuned to the Metrics of a Visuospatial Task. *Journal of Neurophysiology*, *100*(1), 224–238. https://doi.org/10.1152/jn.90262.2008

Pruszynski, J A., Kurtzer, I., Nashed, J. Y., Omrani, M., Brouwer, B., Scott, S. H. (2011b). Primary motor cortex underlies sensory integration for fast feedback control. *Nature*, *478*(7369), 387–391. https://doi.org/10.1038/nature10436

Puce, A., & Hämäläinen, M. S. (2017). A review of issues related to data acquisition and analysis in EEG/MEG studies. *Brain Sciences*, *7*(6). https://doi.org/10.3390/brainsci7060058

Pulvermüller, F., Lutzenberger, W., Preißl, H., & Birbaumer, N. (1995). Motor programming in both hemispheres: an EEG study of the human brain. *Neuroscience Letters*, *190*(1), 5–8. https://doi.org/10.1016/0304-3940(95)11486-G

Qin, Y., Xu, P., & Yao, D. (2010). A comparative study of different references for EEG default mode network: The use of the infinity reference. *Clinical Neurophysiology*, *121*(12), 1981–1991. https://doi.org/10.1016/j.clinph.2010.03.056

Rachman, S., & Grassi, J. (1965). Reminiscence, Inhibition and Consolidation. *British Journal of Psychology*, *56*(2–3), 157–162. https://doi.org/10.1111/j.2044-8295.1965.tb00955.x

Radovanovic, S., Korotkov, A., Ljubisavljevic, M., Lyskov, E., Thunberg, J., Kataeva,

G., Danko, S., Roudas, M., Pakhomov, S., Medvedev, S., & Johansson, H. (2002). Comparison of brain activity during different types of proprioceptive inputs: A positron emission tomography study. *Experimental Brain Research*, *143*(3), 276–285. https://doi.org/10.1007/s00221-001-0994-4

Raichle, M. E., MacLeod, A. M., Snyder, A. Z., Powers, W. J., Gusnard, D. A., & Shulman, G. L. (2001). A default mode of brain function. *Proceedings of the National Academy of Sciences*, *98*(2), 676–682. https://doi.org/10.1073/pnas.98.2.676

Raichle, M. E. (2015). The Brain's Default Mode Network. *Annual Review of Neuroscience*, *38*(1), 433–447. https://doi.org/10.1146/annurev-neuro-071013-014030

Rappelsberger, P., Lacroix, D., & Petsche, H. (1993). Amplitude and coherence mapping: Its application in psycho- and patho-physiological studies. In M. Rother & U. Zwiener (Eds.), *Quantitative EEG analysis : clinical utility and new methods* (pp. 179–186).

Rappelsberger, P, Pfurtscheller, G., & Filz, O. (1994). Calculation of event-related coherence--a new method to study short- lasting coupling between brain areas. *Brain Topogr*, *7*(2), 121–127. https://doi.org/10.1007/BF01186770

Rappelsberger, P. (1989). The reference problem and mapping of coherence: A simulation study. *Brain Topography*, *2*(1–2), 63–72. https://doi.org/10.1007/BF01128844

Richardson, A. G., Overduin, S. A., Valero-Cabre, A., Padoa-Schioppa, C., Pascual-Leone, A., Bizzi, E., & Press, D. Z. (2006). Disruption of Primary Motor Cortex before Learning Impairs Memory of Movement Dynamics. *Journal of Neuroscience*, *26*(48), 12466–12470. https://doi.org/10.1523/jneurosci.1139-06.2006

Robertson, E. M. (2005). Off-Line Learning and the Primary Motor Cortex. *Journal of Neuroscience*, *25*(27), 6372–6378. https://doi.org/10.1523/jneurosci.1851-05.2005

Roll, J. P., Vedel, J. P., & Ribot, E. (1989). Alteration of proprioceptive messages induced by tendon vibration in man: a microneurographic study. *Experimental Brain Research*, *76*(1). https://doi.org/10.1007/BF00253639

Rosazza, C., & Minati, L. (2011). Resting-state brain networks: Literature review and clinical applications. *Neurological Sciences*, *32*(5), 773–785. https://doi.org/10.1007/s10072-011-0636-y

Rosenkranz, K., & Rothwell, J. C. (2012). Modulation of Proprioceptive Integration in the Motor Cortex Shapes Human Motor Learning. *Journal of Neuroscience*, *32*(26), 9000–9006. https://doi.org/10.1523/jneurosci.0120-12.2012

Rosenkranz, K., & Rothwell, J. C. (2003). Differential effect of muscle vibration on intracortical inhibitory circuits in humans. *Journal of Physiology*, *551*(2), 649–660. https://doi.org/10.1113/jphysiol.2003.043752

Rossini, P. M., Caltagirone, C., Castriota-Scanderbeg, A., Cicinelli, P., Del Gratta, C., Demartin, M., Pizzella, V., Traversa, R., & Romani, G. L. (1998). Hand motor cortical area reorganization in stroke: a study with fMRI, MEG and TCS maps. *NeuroReport*, *9*(9), 2141–2146. https://doi.org/10.1097/00001756-199806220-00043

Rossiter, H. E., Boudrias, M.-H., & Ward, N. S. (2014). Do movement-related beta oscillations change after stroke? *Journal of Neurophysiology*, *112*(9), 2053–2058. https://doi.org/10.1152/jn.00345.2014

Sainburg, R. L. (2002). Evidence for a dynamic-dominance hypothesis of handedness. *Experimental Brain Research*, *142*(2), 241–258. https://doi.org/10.1007/s00221-001-0913-8

Sainburg, R. L. (2005). Handedness: Differential specializations for control of trajectory and position. *Exercise and Sport Sciences Reviews*, *33*(4), 206–213. https://doi.org/10.1097/00003677-200510000-00010

Sakkalis, V. (2011). Review of advanced techniques for the estimation of brain connectivity measured with EEG/MEG. *Computers in Biology and Medicine*, *41*(12), 1110–1117. https://doi.org/10.1016/j.compbiomed.2011.06.020

Sanei, S., & Chambers, J. A. (2007). EEG Signal Processing. In *Chemistry & biodiversity* (Vol. 1). https://doi.org/10.1002/9780470511923

Sarlegna, F. R., & Sainburg, R. L. (2007). The effect of target modality on visual and proprioceptive contributions to the control of movement distance. *Experimental Brain Research*, *176*(2), 267–280. https://doi.org/10.1007/s00221-006-0613-5

Saur, D., Lange, R., Baumgaertner, A., Schraknepper, V., Willmes, K., Rijntjes, M., & Weiller, C. (2006). Dynamics of language reorganization after stroke. *Brain*, *129*(6), 1371–1384. https://doi.org/10.1093/brain/awl090

Scheeringa, R., Bastiaansen, M. C. M., Petersson, K. M., Oostenveld, R., Norris, D. G., & Hagoort, P. (2008). Frontal theta EEG activity correlates negatively with the default mode network in resting state. *International Journal of Psychophysiology*, *67*(3), 242–251. https://doi.org/10.1016/j.ijpsycho.2007.05.017

Scheeringa, R., Petersson, K. M., Kleinschmidt, A., Jensen, O., & Bastiaansen, M. C. m. (2012). EEG Alpha Power Modulation of fMRI Resting-State Connectivity. *Brain Connectivity*, *2*(5), 254–264. https://doi.org/10.1089/brain.2012.0088

Scheidt, R. A., & Ghez, C. (2007). Separate Adaptive Mechanisms for Controlling Trajectory and Final Position in Reaching. *Journal of Neurophysiology*, *98*(6), 3600–3613. https://doi.org/10.1152/jn.00121.2007

Scheidt, R. A., & Stoeckmann, T. (2007). Reach Adaptation and Final Position Control Amid Environmental Uncertainty After Stroke. *Journal of Neurophysiology*, *97*(4), 2824–2836. https://doi.org/10.1152/jn.00870.2006

Schieber, M. H. (2001). Constraints on Somatotopic Organization in the Primary Motor Cortex. *Journal of Neurophysiology*, *86*(5), 2125–2143. https://doi.org/10.1152/jn.2001.86.5.2125

Schoffelen, J. M., & Gross, J. (2009). Source connectivity analysis with MEG and EEG. *Human Brain Mapping*, *30*(6), 1857–1865. https://doi.org/10.1002/hbm.20745

Schott, G. D. (1993). Penfield's homunculus: a note on cerebral cartography. *Journal of Neurology, Neurosurgery & Psychiatry*, *56*(4), 329–333. https://doi.org/10.1136/jnnp.56.4.329

Semmes, J., Weinstein, S., Ghent, L., & Teuber, H. (1960). *Somatosensory Changes after Penetrating Brain Wounds in Man*. Harvard University Press.

Shadmehr, R., Smith, M. A., & Krakauer, J. W. (2010). Error Correction, Sensory Prediction, and Adaptation in Motor Control. *Annual Review of Neuroscience*, *33*(1), 89–108. https://doi.org/10.1146/annurev-neuro-060909-153135

Sharma, N., Baron, J.-C., & Rowe, J. B. (2009). Motor imagery after stroke: Relating outcome to motor network connectivity. *Annals of Neurology*, *66*(5), 604–616. https://doi.org/10.1002/ana.21810

Shemmell, J., An, J. H., & Perreault, E. J. (2009). The Differential Role of Motor Cortex in Stretch Reflex Modulation Induced by Changes in Environmental Mechanics and Verbal Instruction. *Journal of Neuroscience*, *29*(42), 13255–13263. https://doi.org/10.1523/JNEUROSCI.0892-09.2009

Siegel, M., Donner, T. H., & Engel, A. K. (2012). Spectral fingerprints of large-scale neuronal interactions. *Nature Reviews Neuroscience*, *13*(2), 121–134. https://doi.org/10.1038/nrn3137

Sih, B. L., & Stuhmiller, J. H. (2003). The Metabolic Cost of Force Generation. *Medicine & Science in Sports & Exercise*, *35*(4), 623–629. https://doi.org/10.1249/01.MSS.0000058435.67376.49

Singer, W. (1995). Visual Feature Integration and the Temporal Correlation Hypothesis. *Annual Review of Neuroscience*, *18*(1), 555–586. https://doi.org/10.1146/annurev.neuro.18.1.555

Singh, M., & Karpovich, P. V. (1966). Isotonic and isometric forces of forearm flexors and extensors. *Journal of Applied Physiology*, *21*(4), 1435–1437. https://doi.org/10.1152/jappl.1966.21.4.1435

Snoddy, G. S. (1926). Learning and stability: a psychophysiological analysis of a case of motor learning with clinical applications. *Journal of Applied Psychology*, *10*(1), 1–36. https://doi.org/10.1037/h0075814

Snyder, D. B., Beardsley, S. A., & Schmit, B. D. (2019). Role of the cortex in visuomotor control of arm stability. *Journal of Neurophysiology*, *122*(5), 2156–2172. https://doi.org/10.1152/jn.00003.2019

Sober, S. J., & Sabes, P. N. (2005). Flexible strategies for sensory integration during motor planning. *Nature Neuroscience*, *8*(4), 490–497. https://doi.org/10.1038/nn1427

Soechting, J. F., Dufresne, J. R., & Lacquaniti, F. (1981). Time-varying properties of myotatic response in man during some simple motor tasks. *Journal of Neurophysiology*, *46*(6), 1226–1243. https://doi.org/10.1152/jn.1981.46.6.1226

Spieser, L., Meziane, H. B., & Bonnard, M. (2010). Cortical mechanisms underlying stretch reflex adaptation to intention: A combined EEG–TMS study. *NeuroImage*, *52*(1), 316–325. https://doi.org/10.1016/j.neuroimage.2010.04.020

Staines, W. R., Black, S. E., Graham, S. J., & McIlroy, W. E. (2002). Somatosensory gating and recovery from stroke involving the thalamus. *Stroke*, *33*(11), 2642–2651. https://doi.org/10.1161/01.STR.0000032552.40405.40

Stam, C. J., de Haan, W., Daffertshofer, A., Jones, B. F., Manshanden, I., van Cappellen van Walsum, A. M., Montez, T., Verbunt, J. P. A., de Munck, J. C., van Dijk, B. W., Berendse, H. W., & Scheltens, P. (2009). Graph theoretical analysis of magnetoencephalographic functional connectivity in Alzheimer's disease. *Brain*, *132*(1), 213–224. https://doi.org/10.1093/brain/awn262

Stein, P. S. G., & Grossman, M. L. (1980). Central Program for Scratch Reflex in Turtle. *Journal of Comparitve Physiology*, *140*(4), 287–294.

Stępień, M., Conradi, J., Waterstraat, G., Hohlefeld, F. U., Curio, G., & Nikulin, V. V. (2011). Event-related desynchronization of sensorimotor EEG rhythms in hemiparetic patients with acute stroke. *Neuroscience Letters*, *488*(1), 17–21. https://doi.org/10.1016/j.neulet.2010.10.072

Steriade, M., Gloor, P., Llinás, R. R., Lopes da Silva, F. H., & Mesulam, M. M. (1990). Basic mechanisms of cerebral rhythmic activities. In *Electroencephalography and Clinical Neurophysiology* (Vol. 76, Issue 6, pp. 481–508).

https://doi.org/10.1016/0013-4694(90)90001-Z

Stone, J. (2004). *Independent Component Analysis: A Tutorial Introduction*. Massachusetts Institute of Technology.

Straathof, M., Sinke, M. R. T., Dijkhuizen, R. M., & Otte, W. M. (2019). A systematic review on the quantitative relationship between structural and functional network connectivity strength in mammalian brains. *Journal of Cerebral Blood Flow & Metabolism*, *39*(2), 189–209. https://doi.org/10.1177/0271678X18809547

Stratton, S. M., Liu, Y.-T., Hong, S. L., Mayer-Kress, G., & Newell, K. M. (2007). Snoddy (1926) Revisited: Time Scales of Motor Learning. *Journal of Motor Behavior*, *39*(6), 503–515. https://doi.org/10.3200/JMBR.39.6.503-516

Strens, L. H. A., Asselman, P., Pogosyan, A., Loukas, C., Thompson, A. J., & Brown, P. (2004). Corticocortical coupling in chronic stroke: Its relevance to recovery. *Neurology*, *63*(3), 475–484. https://doi.org/10.1212/01.WNL.0000133010.69694.F8

Sukerkar, P. (2010). *EEG source localization of visual and proprioceptive error processing during visually-guided target tracking with the wrist.* (Issue December). Marquette University.

Suminski, A. J., Rao, S. M., Mosier, K. M., & Scheidt, R. A. (2007). Neural and Electromyographic Correlates of Wrist Posture Control. *Journal of Neurophysiology*, *97*(2), 1527–1545. https://doi.org/10.1152/jn.01160.2006

Sun, F. T., Miller, L. M., & D'Esposito, M. (2004). Measuring interregional functional connectivity using coherence and partial coherence analyses of fMRI data. *NeuroImage*, *21*(2), 647–658. https://doi.org/10.1016/j.neuroimage.2003.09.056

Swann, N., Tandon, N., Canolty, R., Ellmore, T. M., McEvoy, L. K., Dreyer, S., DiSano, M., & Aron, A. R. (2009). Intracranial EEG Reveals a Time- and Frequency-Specific Role for the Right Inferior Frontal Gyrus and Primary Motor Cortex in Stopping Initiated Responses. *Journal of Neuroscience*, *29*(40), 12675–12685. https://doi.org/10.1523/JNEUROSCI.3359-09.2009

Tadel, F., Baillet, S., Mosher, J. C., Pantazis, D., & Leahy, R. M. (2011). Brainstorm: A user-friendly application for MEG/EEG analysis. *Computational Intelligence and Neuroscience, 2011*. https://doi.org/10.1155/2011/879716

Taub, E., Weiller, C., Liepert, J., Bauder, H., & Miltner, W. H. R. (2011). Treatment-Induced Cortical Reorganization After Stroke in Humans. *Stroke, 31*(6), 1210–1216. https://doi.org/10.1161/01.str.31.6.1210

Todorov, E., & Jordan, M. I. (2002). Optimal feedback control as a theory of motor coordination. *Nature Neuroscience*, *5*(11), 1226–1235.

https://doi.org/10.1038/nn963

Tracey, D. J., Walmsley, B., & Brinkman, J. (1980). “Long-loop” reflexes can be obtained in spinal monkeys. *Neuroscience Letters*, *18*(1), 59–65. https://doi.org/10.1016/0304-3940(80)90213-X

Trombly, C. A. (1992). Deficits of Reaching in Subjects With Left Hemiparesis: A Pilot Study. *American Journal of Occupational Therapy*, *46*(10), 887–897. https://doi.org/10.5014/ajot.46.10.887

Tuladhar, A. M., Snaphaan, L., Shumskaya, E., Rijpkema, M., Fernandez, G., Norris, D. G., & de Leeuw, F. E. (2013). Default Mode Network Connectivity in Stroke Patients. *PLoS ONE*, *8*(6). https://doi.org/10.1371/journal.pone.0066556

Tyler, A. E., & Hutton, R. S. (1986). Was Sherrington right about co-contractions? *Brain Research*, *370*(1), 171–175. https://doi.org/10.1016/0006-8993(86)91119-4

Tyson, S. F., Hanley, M., Chillala, J., Selley, A. B., & Tallis, R. C. (2008). Sensory loss in hospital-admitted people with stroke: Characteristics, associated factors, and relationship with function. *Neurorehabilitation and Neural Repair*, *22*(2), 166–172. https://doi.org/10.1177/1545968307305523

Tzourio-Mazoyer, N., Landeau, B., Papathanassiou, D., Crivello, F., Etard, O., Delcroix, N., Mazoyer, B., & Joliot, M. (2002). Automated Anatomical Labeling of Activations in SPM Using a Macroscopic Anatomical Parcellation of the MNI MRI Single-Subject Brain. *NeuroImage*, *15*(1), 273–289. https://doi.org/10.1006/nimg.2001.0978

van Beers, R. J., Sittig, A. C., & Gon, J. J. D. van der. (1999). Integration of Proprioceptive and Visual Position-Information: An Experimentally Supported Model. *Journal of Neurophysiology*, *81*(3), 1355–1364. https://doi.org/10.1152/jn.1999.81.3.1355

van Beers, R. J., Sittig, A. C., & van der Gon Denier, J. J. (1996). How humans combine simultaneous proprioceptive and visual position information. *Experimental Brain Research*, *111*(2), 253–261. https://doi.org/10.1007/BF00227302

Vatta, F., Meneghini, F., Esposito, F., Mininel, S., & Di Salle, F. (2010). Realistic and Spherical Head Modeling for EEG Forward Problem Solution: A Comparative Cortex-Based Analysis. *Computational Intelligence and Neuroscience*, *2010*, 1–11. https://doi.org/10.1155/2010/972060

Vestling, M., Tufvesson, B., & Iwarsson, S. (2003). Indicators for return to work after stroke and the importance of work for subjective well-being and life satisfaction. *Journal of Rehabilitation Medicine*, *35*(3), 127–131. https://doi.org/10.1080/16501970310010475

Vidoni, E. D., Acerra, N. E., Dao, E., Meehan, S. K., & Boyd, L. A. (2010). Role of the primary somatosensory cortex in motor learning: An rTMS study. *Neurobiology of Learning and Memory*, *93*(4), 532–539. https://doi.org/10.1016/j.nlm.2010.01.011

von Stein, A., Chiang, C., & Konig, P. (2000). Top-down processing mediated by interareal synchronization. *Proceedings of the National Academy of Sciences*, *97*(26), 14748–14753. https://doi.org/10.1073/pnas.97.26.14748

von Stein, Astrid, & Sarnthein, J. (2000). Different frequencies for different scales of cortical integration: from local gamma to long range alpha/theta synchronization. *International Journal of Psychophysiology*, *38*(3), 301–313. https://doi.org/10.1016/S0167-8760(00)00172-0

Wagner, A. D., Shannon, B. J., Kahn, I., & Buckner, R. L. (2005). Parietal lobe contributions to episodic memory retrieval. *Trends in Cognitive Sciences*, *9*(9), 445–453. https://doi.org/10.1016/j.tics.2005.07.001

Wang, L., Guo, X. Sun, J. Jin, Z., & Tong S. (2012). Cortical networks of hemianopia stroke patients: A graph theoretical analysis of EEG signals at resting state. *2012 Annual International Conference of the IEEE Engineering in Medicine and Biology Society*, 49–52. https://doi.org/10.1109/EMBC.2012.6345868

Wang, L., Yu, C., Chen, H., Qin, W., He, Y., Fan, F., Zhang, Y., Wang, M., Li, K., Zang, Y., Woodward, T. S., & Zhu, C. (2010). Dynamic functional reorganization of the motor execution network after stroke. *Brain*, *133*(4), 1224–1238. https://doi.org/10.1093/brain/awq043

Ward, N. S. (2003). Neural correlates of motor recovery after stroke: a longitudinal fMRI study. *Brain*, *126*(11), 2476–2496. https://doi.org/10.1093/brain/awg245

Ward, N. S., Brown, M. M., Thompson, A. J., & Frackowiak, R. S. J. (2003). Neural correlates of outcome after stroke: a cross-sectional fMRI study. *Brain*, *126*(6), 1430–1448. https://doi.org/10.1093/brain/awg145

Ward, N. S, Newton, J. M., Swayne, O. B. C., Lee, L., Frackowiak, R. S. J., Thompson, A. J., Greenwood, R. J., & Rothwell, J. C. (2007). The relationship between brain activity and peak grip force is modulated by corticospinal system integrity after subcortical stroke. *European Journal of Neuroscience*, *25*(6), 1865–1873. https://doi.org/10.1111/j.1460-9568.2007.05434.x

Weiller, C., Jüptner, M., Fellows, S., Rijntjes, M., Leonhardt, G., Kiebel, S., Müller, S., Diener, H. C., & Thilmann, A. F. (1996). Brain Representation of Active and Passive Movements. *NeuroImage*, *4*(2), 105–110. https://doi.org/10.1006/nimg.1996.0034

Weiller, C., Chollet, F., Friston, K. J., Wise, R. J. S., & Frackowiak, R. S. J. (1992). Functional reorganization of the brain in recovery from striatocapsular infarction in man. *Annals of Neurology*, *31*(5), 463–472. https://doi.org/10.1002/ana.410310502

Weiller, C., Ramsay, S. C., Wise, R. J. S., Friston, K. J., & Frackwiak, R. S. J. (1993). Individual patterns of functional reorganization in the human cerebral cortex after capsular infraction. *Annals of Neurology*, *33*(2), 181–189. https://doi.org/10.1002/ana.410330208

Welch, P. (1967). The use of fast Fourier transform for the estimation of power spectra: A method based on time averaging over short, modified periodograms. *IEEE Transactions on Audio and Electroacoustics*, *15*(2), 70–73. https://doi.org/10.1109/TAU.1967.1161901

Wierzbicka, M. M., & Wiegner, A. W. (1996). Accuracy of motor responses in subjects with and without control of antagonist muscle. *Journal of Neurophysiology*, *75*(6), 2533–2541. https://doi.org/10.1152/jn.1996.75.6.2533

Wierzbicka, M. M., & Wiegner, A. W. (1992). Effects of weak antagonist on fast elbow flexion movements in man. *Experimental Brain Research*, *91*(3), 509–519. http://doi.org/10.1007/BF00227847

Winkler, I., Haufe, S., & Tangermann, M. (2011). Automatic Classification of Artifactual ICA-Components for Artifact Removal in EEG Signals. *Behavioral and Brain Functions*, *7*(1), 30. https://doi.org/10.1186/1744-9081-7-30

Wittenberg, G. F., Bastian, A. J., Dromerick, A. W., Thach, W. T., & Powers, W. J. (2000). Mirror Movements Complicate Interpretation of Cerebral Activation Changes during Recovery from Subcortical Infarction. *Neurorehabilitation and Neural Repair*, *14*(3), 213–221. https://doi.org/10.1177/154596830001400307

Wu, C. W., Seo, H. J., & Cohen, L. G. (2006). Influence of electric somatosensory stimulation on paretic-hand function in chronic stroke. *Archives of Physical Medicine and Rehabilitation*, *87*(3), 351–357. https://doi.org/10.1016/j.apmr.2005.11.019

Wu, J., Quinlan, E. B., Dodakian, L., McKenzie, A., Kathuria, N., Zhou, R. J., Augsburger, R., See, J., Le, V. H., Srinivasan, R., & Cramer, S. C. (2015). Connectivity measures are robust biomarkers of cortical function and plasticity after stroke. *Brain*, *138*(8), 2359–2369. https://doi.org/10.1093/brain/awv156

Xia, M., Wang, J., & He, Y. (2013). BrainNet Viewer: A Network Visualization Tool for Human Brain Connectomics. *PLoS ONE*, *8*(7), e68910. https://doi.org/10.1371/journal.pone.0068910

Yuan, H., Liu, T., Szarkowski, R., Rios, C., Ashe, J., & He, B. (2010). Negative

covariation between task-related responses in alpha/beta-band activity and BOLD in human sensorimotor cortex: An EEG and fMRI study of motor imagery and movements. *NeuroImage*, *49*(3), 2596–2606. https://doi.org/10.1016/j.neuroimage.2009.10.028

Zalesky, A., Fornito, A., & Bullmore, E. T. (2010). Network-based statistic: Identifying differences in brain networks. *NeuroImage*, *53*(4), 1197–1207. https://doi.org/10.1016/j.neuroimage.2010.06.041

Zaveri, H. P., Duckrow, R. B., & Spencer, S. S. (2000). The effect of a scalp reference signal on coherence measurements of intracranial electroencephalograms. *Clinical Neurophysiology*, *111*(7), 1293–1299. https://doi.org/10.1016/S1388-2457(00)00321-7

Zhou, B., & Wong, W. H. (2011). A bootstrap-based non-parametric ANOVA method with applications to factorial microarray data. *Statistica Sinica*, *21*(2), 495–514.

Zhu, J., Jin, Y., Wang, K., Zhou, Y., Feng, Y., Yu, M., & Jin, X. (2015). Frequency-Dependent Changes in the Regional Amplitude and Synchronization of Resting-State Functional MRI in Stroke. *PLOS ONE*, *10*(4), e0123850. https://doi.org/10.1371/journal.pone.0123850

Zhuang, P., Toro, C., Grafman, J., Manganotti, P., Leocani, L., & Hallett, M. (1997). Event-related desynchronization (ERD) in the alpha frequency during development of implicit and explicit learning. *Electroencephalography and Clinical Neurophysiology*, *102*(4), 374–381. https://doi.org/10.1016/S0013-4694(96)96030-7

APPENDIX A: MANIPULANDUM

Design

The specific hypotheses to be addressed in this study required a method of measuring hand position in space while being able to apply perturbations to the hand. Since EEG is highly susceptible to electromagnetic noise and was to be recorded while performing the experiments, a system had to be designed and built that would minimize electrical interference. To achieve this, a passive manipulandum system was developed to track hand position in three-dimensional space, Figure A-1. The device was constructed using 2.5x2.5cm extruded aluminum (80/20 Inc., Columbia City, Indiana) and contained a manipulandum with three rotational joints to allow unrestricted movement in the horizontal plane and one translational joint to allow movement in the vertical direction. Each joint was equipped with an optical encoder to capture the three-dimensional location of the hand (Rotational Joint 1: CS15-2500, Celesco Transducer Products, Inc., Chatsworth, CA; Rotational Joint 2: CS15-2500, Celesco Transducer Products, Inc., Chatsworth, CA; Rotational Joint 3: HS35-5000, BEI Sensors, Goleta, CA; Translational Joint: SE1-50, Celesco Transducer Products Inc., Chatsworth, CA). While seated at the device, the participant's forearm was secured to an Ultra High Molecular Weight Polyethylene tray (43cm x 11cm) located at the end of the manipulandum. A load cell (not depicted) was located under the tray and used to measure force (Force Transducer: LC203-500, OMEGA Engineering Inc., Norwalk, CT). The device has the option to provide variable arm support to the participant via a weight stack that can be attached to a pulley system located at the translational joint. However, for the experiments described in

this dissertation, the translational joint was fixed preventing movements in the vertical direction. Perturbations to the position of the arm can be generated by mounting magnets on the arm support tray and base of the passive manipulandum frame; perturbation strength can be altered by adjusting the distance between the two magnets. An opaque screen (86.5cm x 68.5cm) was mounted above the device's manipulandum onto which experimental information was displayed using a projector. The device was integrated with LabVIEW 2010 SP1 (National Instruments Corporation, Austin, Texas) to record sensor output and generate the experimental display.

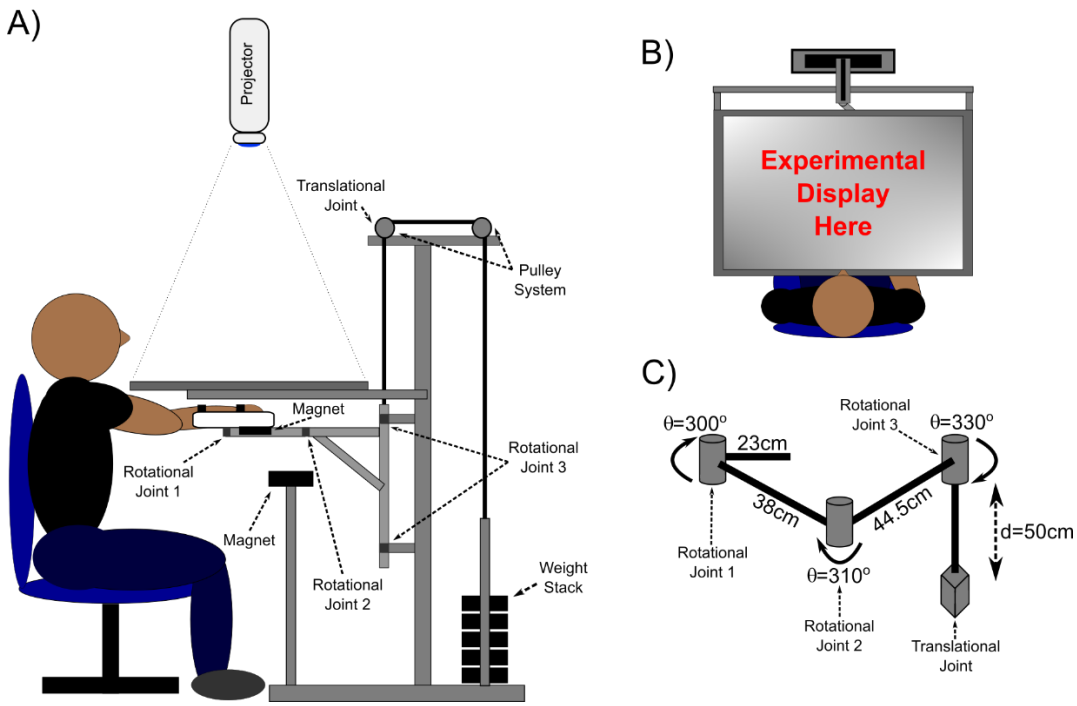

Figure A-1: Diagram of Manipulandum. Illustration of the passive manipulandum system as seen from the side (A) and from above (B) with a detailed description of the manipulandum (C). The projector is used to display experimental information generated with LabVIEW on the opaque screen located above the participants arm. The rotational joints and translational joint are equipped with optical encoders to allow for calculation of hand position in three-dimensional space. Magnets can be mounted on the passive manipulandum to generate force fields. Varying levels of arm support can be supplied by way of the weight stack.

Recording Device Output

In order to read the sensor output into LabVIEW, a National Instruments USB-6229 DAQ board (National Instruments Corporation, Austin, Texas) was used. The encoder data from rotational joints 1 and 2 were read into LabVIEW as angular encoder data using the 2 counter channels available on the DAQ. The encoder data from rotational joint 3 was converted into a 16-bit binary count using a counting circuit and read into LabVIEW as 16 lines of digital input. The encoder data from the translational joint was converted into a voltage (using a binary counting circuit, digital to analog converter circuit, and amplifier circuit) and read into LabVIEW as a single line of analog input. The load cell data was amplified and then read into LabVIEW using a single line of analog input. Data was read into LabVIEW in this fashion due to the limitations of the DAQ board (only 2 angular encoder counter channels) and the inability for LabVIEW to simultaneously record data from multiple DAQ boards. As well as recording sensor output from the device the DAQ board also has the capability of recording other analog signals (e.g. EMG). Calibration curves for the translational joint linear encoder data and load cell data are shown in Figure A-2.

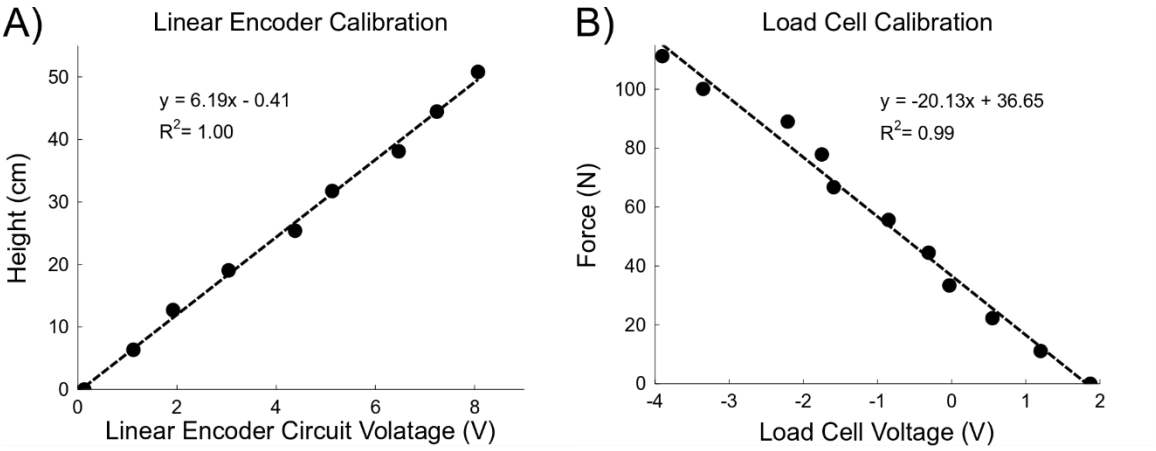

Figure A-2: Calibration Curves. Calibration curves for the translational joint linear encoder data (A) and load cell data (B). The translational joint was moved through its entire range of motion with 0cm and 50cm representing the lowest and highest points along its path, respectively. The load cell was tested within its compression range by adding weights to the arm tray. The load cell's tension range was not calibrated; however, the load cell does have a linear relationship between voltage and force which can be extended into this range.

LabVIEW

Along with reading in the device's sensor data and various other analog data required during an experiment, LabVIEW was also used to generate the experimental scenes/instructions displayed to the participant using the projector, synchronize multiple systems (e.g. EEG) throughout the experiment and save any experimental data for later processing. The LabVIEW code used in conjunction with the device was broken up into two programs. The first LabVIEW program, 'main' program, was located on the experimenter's computer, accepted experimenter input (e.g. number of trials, condition type, etc.) and displayed experimental information (e.g. current trial, device sensor information, etc.) to the experimenter. The 'main' program was broken up into three sections: 1) continuously reads data acquired by the DAQ board, converts all rotational joint data to angles, calculates three-dimensional hand position based off of joint angles

and translational joint displacement and generates any dynamic task requirements (e.g. visual perturbations to hand position, moving target locations, feedback of EMG data, etc.) 2) determines the order of the experimental conditions to display (e.g. baseline, stabilization period, tracing period, vibration on/off, etc.), the timing between conditions and generates a synchronization pulse sent to one of the DAQ board's digital output channels 3) saves experimental data (hand position, target location, experimental condition, etc.) to a text file at the end of an experimental run. The second LabVIEW program was a sub VI that accepted experimental information from the 'main' program (e.g. hand location, condition, etc.) and generated the scenes that were displayed to the participant through the projector.

APPENDIX B: TENDON VIBRATOR

In order to apply vibrations to the forearm flexor tendons during experiments, a custom-made tendon vibrator was constructed similar to the design illustrated in Aman's masters thesis (Amans, 2009). The vibrator consisted of 5g offset mass (cold-finished CA360 brass) that rotated about the shaft of a DC-micromotor (1319T012SR, Faulhaber Group, Clearwater, FL) and was enclosed in a hollow Teflon rod (3cm x 1.9cm). To minimize the effect of electromagnetic noise from the vibrator on EEG data, the vibrator and was encased by a thin aluminum sheet that was electrically grounded and concealed in electrical tape, Figure B-1A. The weight of the electrically grounded vibrator was approximately 23g. The frequency of vibration was adjusted by altering the voltage sent to the device using a motion controller (MCDC3006S, Faulhaber Group, Clearwater, FL) interfaced with LabVIEW through a serial port. After adding the 5g offset mass to the shaft of the motor, a calibration curve was computed to determine the true frequency of motor operation depending on the motion controller commands, Figure B-1B.

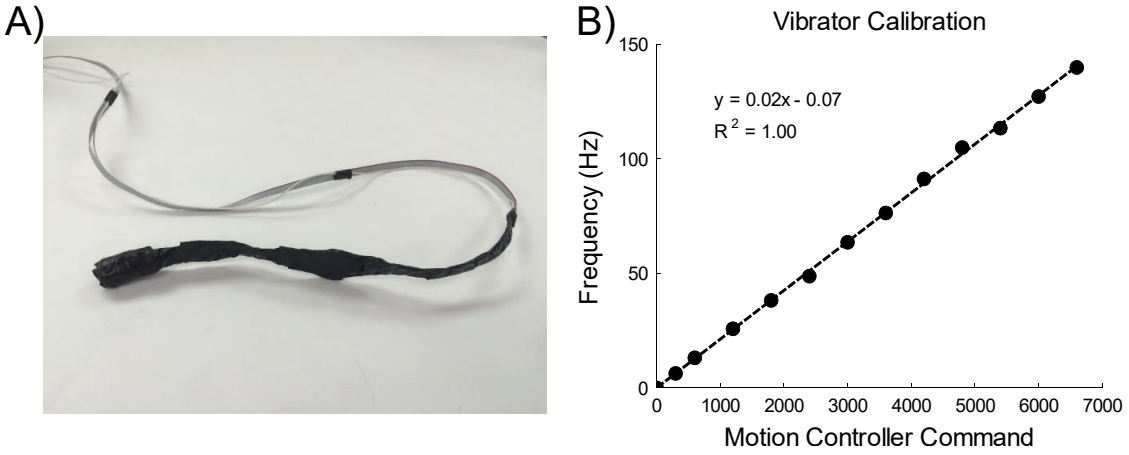

Figure B-1: Tendon Vibrator. A) Tendon vibrator encased by a thin aluminum sheet that was electrically grounded and concealed in electrical tape. B) Calibration curve for the motion controller and tendon vibrator setup. Revolutions per minute of the DC-micromotor with the 5g offset mass was recorded using a tachometer.

APPENDIX C: INDEPENDENT COMPONENT ANALYSIS

Independent component analysis (ICA) is blind source separation technique that attempts to decompose data into statistically independent components (Puce & Hämäläinen, 2017). When boiled down, ICA is basically solving for a mixing matrix, $\boldsymbol{A}$, in equation C.1,

$$\boldsymbol{x} = \boldsymbol{A}\boldsymbol{s} \qquad \text{(C.1)}$$

where $\boldsymbol{x}$ is a matrix of observations and $\boldsymbol{s}$ is a matrix of independent components. Once $\boldsymbol{A}$ is known, it can be inverted to create an unmixing matrix, $\boldsymbol{W}$, and used to calculate the independent sources, $\boldsymbol{s}$, using equation C.2.

$$\boldsymbol{s} = \boldsymbol{W}\boldsymbol{x} \qquad \text{(C.2)}$$

To solve ICA equations C.1 and C.2, ICA algorithms try to maximize the independence of the underlying components (sources) by examining the kurtosis, negentropy, mutual information or likelihood estimation of sources with two main assumptions: underlying sources are independent and sources have non-gaussian distributions (Hyvärinen & Oja, 2000). The type of data and the way in which the data is introduced to the ICA algorithm has implications on the resulting properties of independent components (e.g. temporally independent, spatially independent, spatiotemporally independent, etc.) and how they are interpreted (Brookes et al., 2011; Eichele et al., 2008; Hyvärinen & Oja, 2000; O'Neill et al., 2017).

In the case of this dissertation, EEG data were separated into signal and artefactual temporally independent components using an Adaptive Mixture Independent Component Analysis (Palmer et al., 2008). Representative examples of EEG source components (Figure C-1), eye related components (Figure C-2), EMG components

(Figure C-3) and electrical noise components (Figure C-4) were identified by distinct characteristics and shown below (Delorme et al., 2012; Makeig et al., 2004; Mognon et al., 2011; Puce & Hämäläinen, 2017). Figures C-1, C-2, C-3, and C-4 were generated using ICA component data from Aim 1. Aim 1 examined young healthy adults and consisted of point-to-point reach/stabilization tasks with 40 trials. Each trial was epoched so that it consisted of a baseline period (-3 to 0s before target presentation) and target acquisition/stabilization period (0-6s after target presentation. When the target was presented, participants moved their hand as quickly and accurately as possible from the home position to the target location. For a more detailed description of the task, please refer to methods section in Aim 1.

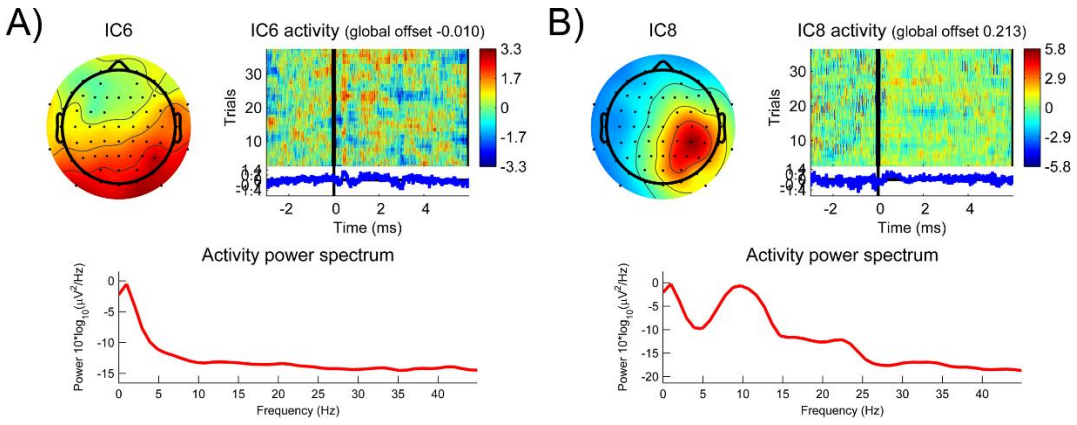

Figure C-1: Typical EEG Source Components. A) ICA component most likely related to the EEG evoked response. An ERP can be seen in the average of the component activity over trials. B) ICA component most likely related to the EEG induced response. Source power is larger in the baseline period (-3s to 0s) than after the cue to move (0s to 6s). ICA components representing EEG sources typically have smooth spatial topographies (can be dipolar in nature) with larger activity over central regions of the scalp. Activity across trials is usually distributed equally with no single trial dominating the component. Peaks in the frequency spectrums are seen in the Alpha (8-12Hz) and Beta (12-30Hz) bands. Top Left: Topography plot of the components, represents the column of the mixing matrix associated with the component; Top Right: Trial wise component voltage with component ERP underneath; Bottom: power spectrum of component.

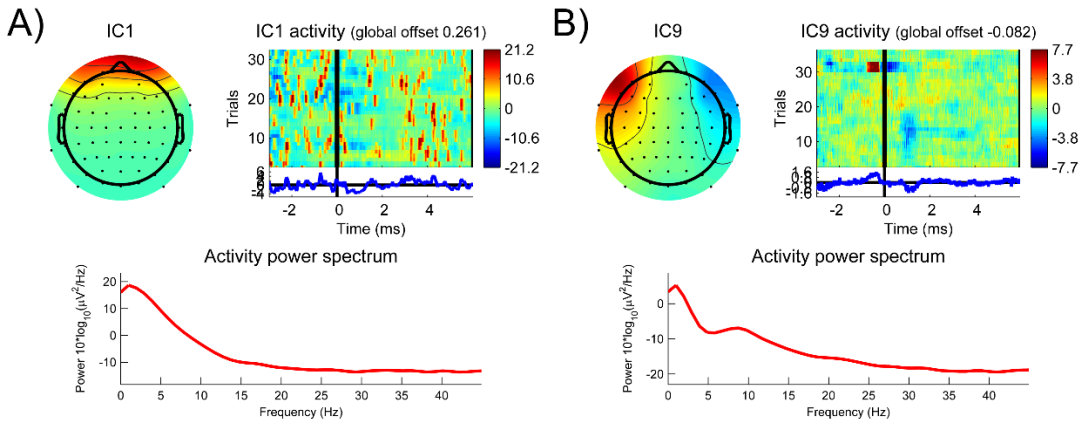

Figure C-2: Typical Eye Related Components. A) ICA component most likely related to eye blinks. Spatial activity located in the frontal region with large spikes in component activity seen at various times across trials. B) ICA component most likely related to lateral EOG. Dipolar spatial activity located in the frontal region with only a few trials dominating the activity in the component. ICA components representing eye artefacts typically have smooth spatial topographies (can be dipolar in nature) with large activity located near the frontal regions. Activity across trials is usually sporadic and only a few trials may dominate the component activity. Frequency spectrums tend to show an exponential decrease in power from the lower frequencies to the higher frequencies. Top Left: Topography plot of the components, represents the column of the mixing matrix associated with the component; Top Right: Trial wise component voltage with component ERP underneath; Bottom: power spectrum of component.

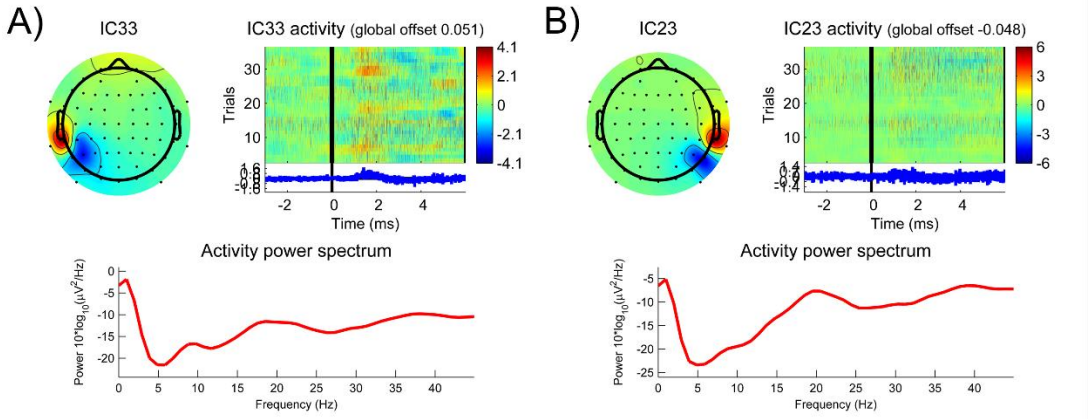

Figure C-3: Typical EMG Source Components. ICA components most likely related to left (A) and right (B) EMG. Frequency band power is unusually large in the higher frequency bands. ICA components representing EMG artefacts typically have smooth spatial topographies (can be dipolar in nature) with larger activity over the periphery. Activity can be distributed equally across trials if the component represents a muscle consistently activated during the task, but activity can also be large in only a few trials indicating a stray movement during the experiment. The frequency spectrums tend to

have high power in the higher frequency bands breaking the traditional 1/f curve seen in EEG data. Top Left: Topography plot of the components, represents the column of the mixing matrix associated with the component; Top Right: Trial wise component voltage with component ERP underneath; Bottom: power spectrum of component.

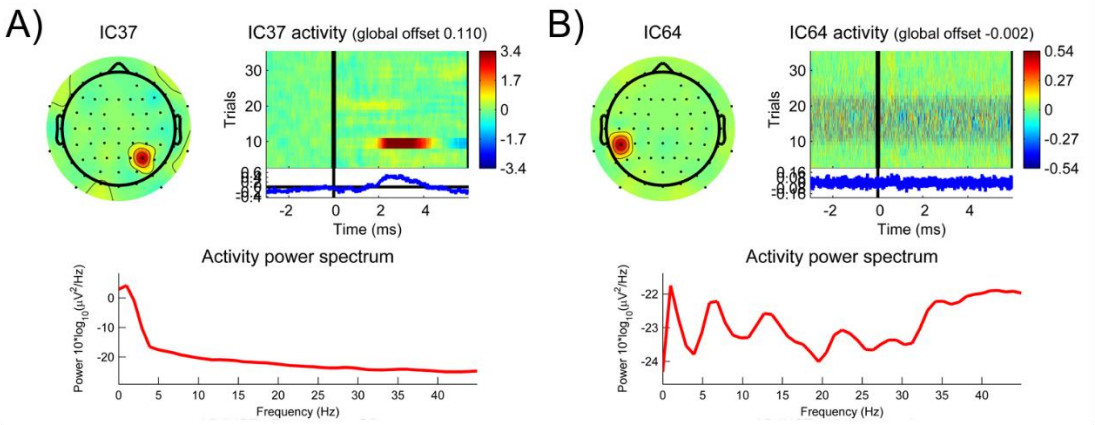

Figure C-4: Typical Electrode Noise Components. A) ICA component most likely related to electrode movement. The spatial topography indicates the component is localized to one electrode with component activity being dominated by only a few trials. B) ICA component most likely related to a noisy electrode. The spatial topography indicates the component is localized to one electrode with the frequency spectrum indicating no clear pattern of EEG activity. ICA components representing electrode artefacts typically have spatial topographies localized to one electrode. Activity across trials can either be dominated by a few trials if movement is the culprit or distributed across trials if the electrode impedance is high. The frequency spectrums can seem random and meaningless or show an exponential decrease depending on the resulting type of electrode artefact. Top Left: Topography plot of the components, represents the column of the mixing matrix associated with the component; Top Right: Trial wise component voltage with component ERP underneath; Bottom: power spectrum of component.

APPENDIX D: SPATIALLY CORRELATED COHERENCE

Spatially correlated coherence (SCORCH) is a metric we developed to quantify spatial patterns of coherence. Although coherence is listed in the name, other measures of connectivity could be used in place of coherence. The need for a new metric arose when we realized that examining the connectivity (coherence) between numerous regions (matrix: number of regions by number of regions) was difficult to display and interpret at face value with each region consisting of a unique connectivity profile (map). When SCORCH is applied to a data set, it reduces the connectivity matrix (number of regions by number of regions) to a vector (number of regions by 1) summarizing how each region's connectivity profile relates (correlates) to some predefined gold standard connectivity profile.

For this dissertation, specifically Aim 3 data, task-based coherence (connectivity) of 65 channel EEG data were analyzed. In this case, SCORCH quantified how well a participant's single-electrode connectivity map matched the ground truth connectivity map for that electrode (see following). Aim 3 data was used in the following example calculation of a single control participant's SCORCH, Figure D-1. Aim 3 examined stroke survivors and an age matched control group as they performed figure-8 tracking tasks. During the figure-8 tracking tasks, a target moved in a figure-8 pattern formed by 2 virtual side-by-side circles. As the target moved, participants were instructed to follow the target, attempting to keep the cursor in the center of the target. For a more detailed description of the task, please refer to methods section in Aim 2.

The first step in calculating SCORCH was to generate a ground truth data set. The ground truth data set was calculated by averaging the connectivity across control

participants (matrix size: 65x65). We then spatially correlated each single-electrode connectivity map (65x1 array for each electrode) with the respective single-electrode connectivity map from the ground truth connectivity matrix defined across control participants. This resulted in a SCORCH array (65x1) with a single correlation coefficient value for each single-electrode connectivity map. An electrode displaying a high value of SCORCH indicates that its global connectivity topography (i.e. network connectivity pattern) resembles that seen in the ground truth data set whereas a low value of SCORCH would imply the opposite.

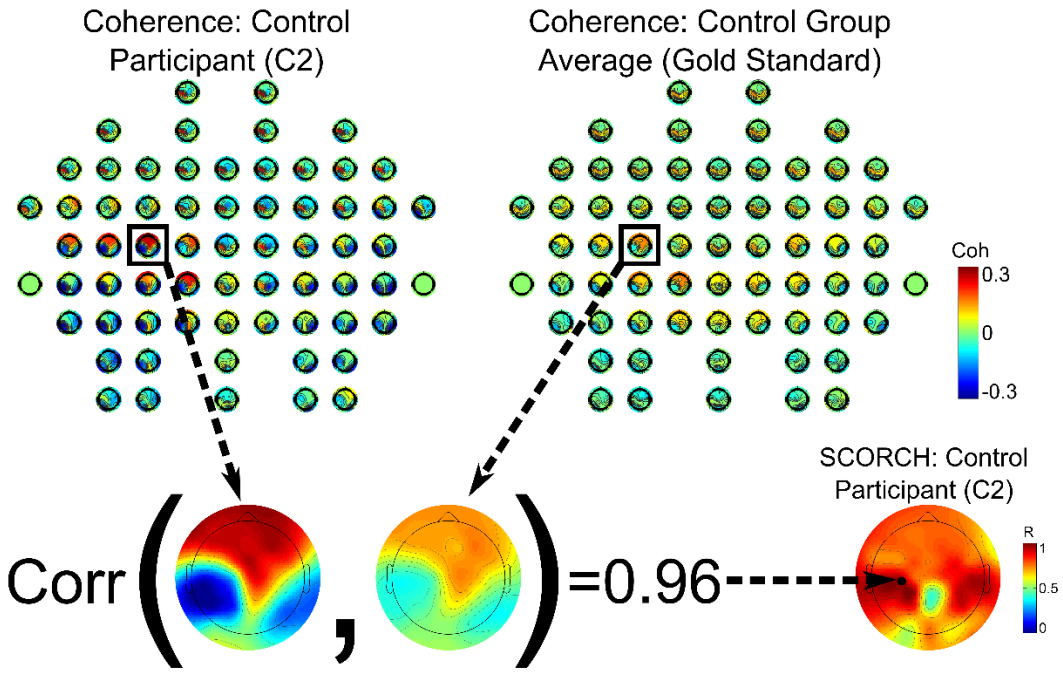

Figure D-1: Spatially Correlated Coherence Work-Flow. Diagram of spatially correlated coherence (SCORCH) calculation for a representative control participant from Aim 2. Coherence maps for a control participant (C2) and control group average (gold standard) display the EEG electrode cap layout with electrode coherence topographies located at each electrode location. The top of the electrode cap layouts and electrode coherence topographies represent the frontal regions of the scalp whereas the left side represents the left side of the scalp. Single electrode coherence topography maps were extracted from the control participant and the gold standard electrode layouts and correlated. The resulting correlation coefficient was stored, and the process was repeated for all electrode locations.